Reviews of Geophysics

REVIEW ARTICLE
10.1029/2019RG000695

Hydraulic Fracturing-Induced Seismicity

Ryan Schultz[1], Robert J. Skoumal[2], Michael R. Brudzinski[3], Dave Eaton[4], Brian Baptie[5], and William Ellsworth[1]

[1]Department of Geophysics, Stanford University, Stanford, CA, USA, [2]U.S. Geological Survey, Moffett Field, CA, USA, [3]Department of Geology and Environmental Earth Science, Miami University, Oxford, OH, USA, [4]Department of Geoscience, University of Calgary, Calgary, Alberta, Canada, [5]British Geological Survey, Edinburgh, UK

Key Points:
- Induced seismicity caused by hydraulic fracturing has been recognized in basins around the world
- Common themes are observed in disparate cases of hydraulic fracturing-induced seismicity
- A better understanding of the commonalities will yield better recognition of cases and management of hazards/risks

Correspondence to:
R. Schultz,
rjs10@stanford.edu

Citation:
Schultz, R., Skoumal, R. J., Brudzinski, M. R., Eaton, D., Baptie, B., & Ellsworth, W. (2020). Hydraulic fracturing-induced seismicity. *Reviews of Geophysics*, *58*, e2019RG000695. https://doi.org/10.1029/2019RG000695

Received 19 MAR 2020
Accepted 9 JUN 2020
Accepted article online 12 JUN 2020

Abstract Hydraulic fracturing (HF) is a technique that is used for extracting petroleum resources from impermeable host rocks. In this process, fluid injected under high pressure causes fractures to propagate. This technique has been transformative for the hydrocarbon industry, unlocking otherwise stranded resources; however, environmental concerns make HF controversial. One concern is HF-induced seismicity, since fluids driven under high pressure also have the potential to reactivate faults. Controversy has inevitably followed these HF-induced earthquakes, with economic and human losses from ground shaking at one extreme and moratoriums on resource development at the other. Here, we review the state of knowledge of this category of induced seismicity. We first cover essential background information on HF along with an overview of published induced earthquake cases to date. Expanding on this, we synthesize the common themes and interpret the origin of these commonalities, which include recurrent earthquake swarms, proximity to well bore, rapid response to stimulation, and a paucity of reported cases. Next, we discuss the unanswered questions that naturally arise from these commonalities, leading to potential research themes: consistent recognition of cases, proposed triggering mechanisms, geologically susceptible conditions, identification of operational controls, effective mitigation efforts, and science-informed regulatory management. HF-induced seismicity provides a unique opportunity to better understand and manage earthquake rupture processes; overall, understanding HF-induced earthquakes is important in order to avoid extreme reactions in either direction.

Plain Language Summary Earthquakes can be induced by a number of anthropogenic sources. One category of induced earthquake is caused by hydraulic fracturing (HF)—a technique used by industry to produce petroleum from normally impermeable rocks. The widespread use of HF has resulted in a significant increase in induced earthquakes. In this paper, we provide a review of all the reported cases of HF-induced earthquakes: in Canada, the United States, the United Kingdom, and China. Some of these cases are exceptional, having events as large as 5.7 M_L or earthquakes triggered up to 1.5 km away. That said, there are common themes that are repeated in all of the cases: similar waveforms, swarm-like sequences, proximity to HF stimulation in time and space, and that only the small minority of HF wells induced earthquakes. Likely, these common themes are related to the physics of HF stimulation and the geology of the target formations. Many of the proposed interpretations are still open-ended research areas, such as consistent recognition of cases, proposed triggering mechanisms, geologically susceptible conditions, identification of operational controls, effective mitigation efforts, and science-informed regulatory management. Overall, a better understanding of these earthquakes will allow for adequately balanced management of their risks.

1. Background

In the past, fine-grained organic-rich sediments were regarded by the petroleum industry as only hydrocarbon source rocks; their low permeability renders these types of rocks uneconomical as a hydrocarbon reservoir (see the glossary for a definition of terms). Instead, conventional oil and gas operations have targeted higher permeability hydrocarbon reservoirs, trapped by less permeable geological structures. However, the advent of hydraulic fracturing (HF) has made it possible to economically produce hydrocarbons directly from these low-permeability formations, unlocking their vast reserves (U.S. Energy Information Administration, 2013). During HF stimulation, fluid is pumped into the subsurface at high pressure, increasing pore pressure until it exceeds the fracture gradient (Figure 1). After this point, hydraulic fractures and shear failures propagate throughout the rock matrix (Detournay, 2016; Hubbert & Willis, 1972;

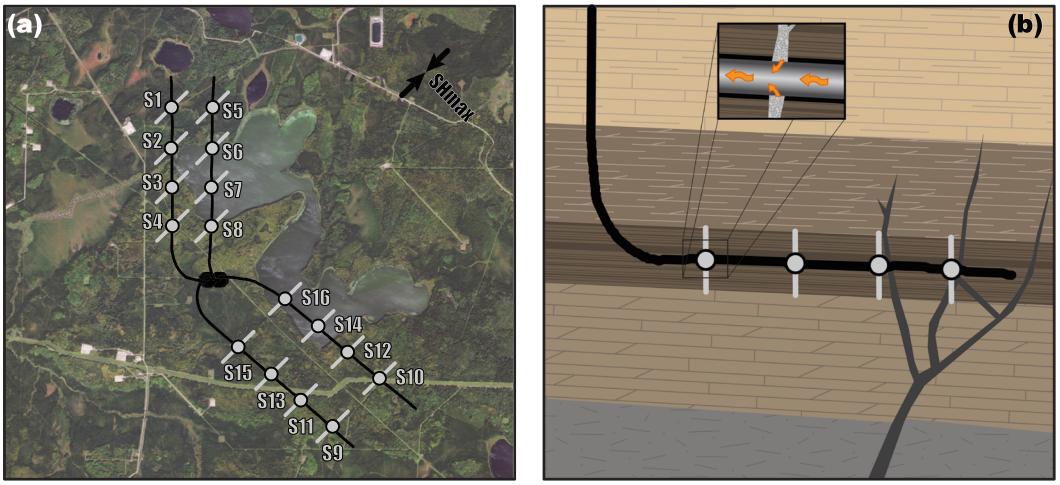

Figure 1. Schematic diagram of a hypothetical HF operation. (a) Map view of a four-well (black lines) pad with 16 completed stages (gray vectors); the northern wells were stimulated sequentially from "toe" to "heel" (see text annotations), while the southern wells use a "zipper frack" completion schema. (b) Cross-sectional view showing a well lateral (black line) and four-stage stimulations (gray vectors) that fractured the target formation (darkest brown strata); only the two furthest right stages are hydraulically connected to a basement rooted fault (dark gray lines). Inset diagram shows hydrocarbons (orange arrows) entering the perforated wellbore (black/gray cylinder), via fractures in the target formation.

King, 2010). The intention of this process is to create a permeable fracture network that facilitates fluid migration into the well bore (Gale et al., 2014; Rinaldi & Rutqvist, 2019). Since the initial hydraulic well stimulation test in Kansas during 1947 (Montgomery & Smith, 2010), HF technologies have become more sophisticated. Technological developments have included horizontal drilling (King, 2010), slickwater fracturing (Palisch et al., 2010), the inclusion of chemical additives, proppant design (Liang et al., 2016), completion schema (Rafiee et al., 2012), and optimization of completion productivity (Gale et al., 2014; Lecampion et al., 2015; Weng et al., 2011).

While HF has driven considerable economic growth, there have also been concerns regarding the environmental challenges associated with this technique (Campbell et al., 2020): including groundwater contamination (Myers, 2012), overuse of freshwater (Chen & Carter, 2016), and management of produced brines (Gregory et al., 2011). Commonly, brine management has focused on disposal into subsurface formations. It has been well documented that subsurface disposal has the potential to induce earthquakes (Ellsworth, 2013; Healy et al., 1968). In fact, various anthropogenic activities have the ability to cause induced earthquakes (Foulger et al., 2017; Grigoli et al., 2017; Keranen & Weingarten, 2018; McGarr et al., 2002; Nicholson & Wesson, 1990, 1992). Underground mining, deep artificial water reservoirs, oil and gas extraction, geothermal power generation, and wastewater disposal have all resulted in cases of induced seismicity. As elaborated in this review, induced earthquakes have also been documented as being caused directly by HF stage stimulation (e.g., Atkinson et al., 2020).

In this review paper, we present a comprehensive overview of the history of HF-induced earthquakes (Figure 2). We summarize our understanding of this category of earthquake: documented cases (section 2), findings from previous studies, common themes observed throughout these cases (section 3), and their implications for triggering and management (section 4). For convenience to the reader, we have organized the writing within subsections to be independent of the others (or to clearly reference prerequisite subsections).

2. Summary of Documented Cases

The objective of HF stimulation is to enhance the flow of fluids through impermeable strata (King, 2010). This process causes tensile failures and shearing along natural fractures (Rinaldi & Rutqvist, 2019). Under normal circumstances, HF stimulation is accompanied by small-scale fracture events, which are often termed "microseismic" due to their small magnitudes ($Mw < 0$) (Eaton et al., 2018; Li, Tan, et al., 2019;

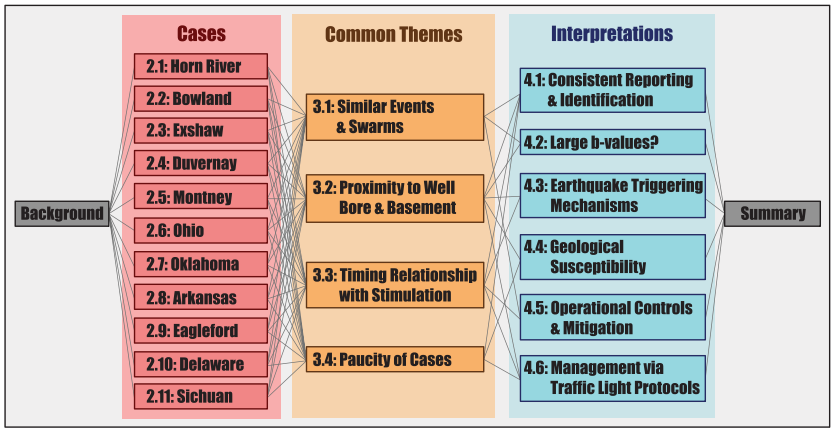

Figure 2. The learned architecture of hydraulic fracturing-induced seismicity. This figure is a graphical table of contents for our review paper; sections are represented as layers, individual subsections are represented as neurons, and subsection interdependencies are linked lines.There is full connectivity between the subsections within sections 2 (Cases) and 3 (Common Themes). There is limited connectivity between the subsections within sections 3 (Common Themes) and 4 (Interpretations).

Warpinski et al., 2012). However, there has been a growing interest in characterizing exceptional cases in which HF causes reactivation of preexisting faults, resulting in induced seismicity (Atkinson et al., 2020; Davies et al., 2013). In this situation, HF tips the frictional balance between the effective normal and shear stresses on a fault toward the failure condition, similar to other injection-related induced earthquakes (Healy et al., 1968; Segall & Lu, 2015). A few exceptional cases were recognized early in the development of unconventional hydrocarbons, usually during microseismic monitoring (Kanamori & Hauksson, 1992; Maxwell et al., 2009; Nicholson & Wesson, 1990; Wolhart et al., 2006).

The following subsections focus on documented cases of HF-induced seismicity, as of this writing (Figure 3). We summarize cases by their host basins, covering aspects related to the geology of the target formation, HF development, documented cases of HF fault activation, the findings of all relevant studies, and regulatory requirements. Sections are ordered chronologically, as individual cases of HF-induced earthquakes became well recognized. We note that there are likely cases of seismogenic HF plays that are currently undocumented.

2.1. The Muskwa Shale in the Horn River Basin, Canada

The first documented case of multiple earthquakes induced by HF occurred in the Horn River Basin, which straddles the border between the Northwest Territories and British Columbia (BC), in northwestern Canada (Figure 4a). The western boundary of the Horn River Basin is marked by the Bovie Fault, a fault system with

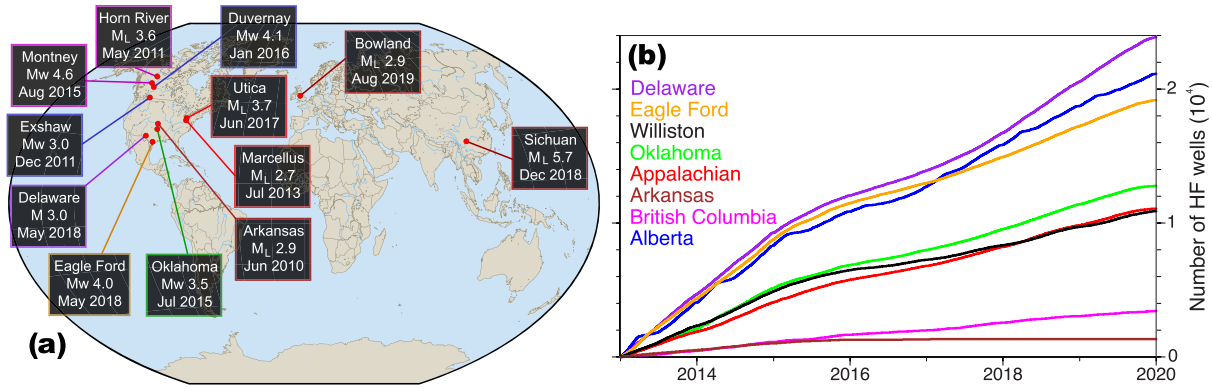

Figure 3. Global cases of reported HF-induced seismicity. (a) Cases of well-recognized seismogenic HF plays (red circles) are annotated with their play name and their largest documented earthquake. (b) Cumulative number of HF wells completed within a basin or political area (colored lines). Data for this panel are from FracFocus (www.fracfocus.org), an industry self-reporting database that is known to be incomplete.

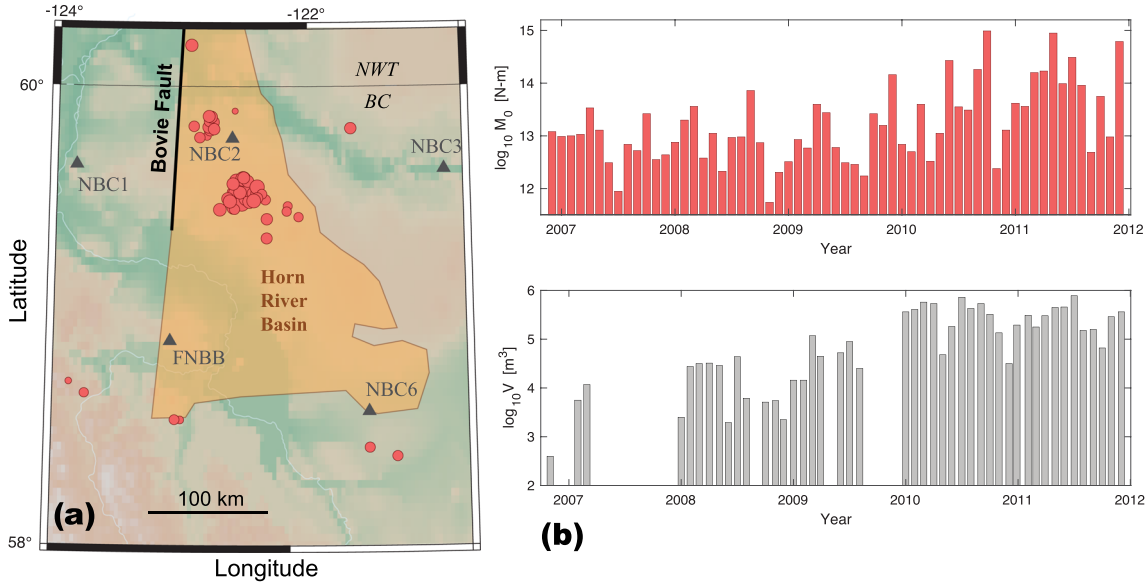

Figure 4. Locations and timings of Horn River Basin HF-induced events. (a) Regional map of the Horn River Basin (orange area) showing seismicity (red circles) detected to the end of 2016. Triangles show broadband seismograph stations, of which only FNBB was operational during shale gas development that peaked in 2011. Events detected by Farahbod, Kao, Walker, and Cassidy (2015) using the single-station method are not plotted. (b) Time series of cumulative monthly seismic moment (M_0) and monthly injected volume for all operations in the HRB. See Farahbod, Kao, Cassidy, and Walker (2015) and Farahbod, Kao, Walker, and Cassidy (2015) for more details.

complex history of tectonic activity (MacLean & Morrow, 2004). The Horn River Basin hosts the Middle-Late Devonian Horn River Group, composed of three organic-rich shale units (Evie, Otter Park, and Muskwa Formations) with a net thickness >300 m (British Columbia Oil and Gas Commission, BC OGC, 2012). With an estimated marketable dry gas resource of more than 70 trillion cubic feet (2.0×10^{12} m^3) (Johnson et al., 2011), the Horn River Basin represents one of the largest shale gas plays in North America. Industry operations to assess and develop the shale gas resources within the Horn River Basin commenced in November 2006 and peaked in 2011 but have since been suspended, largely due to the low North American prices for dry gas and the great distance of the Horn River Basin from markets. The Horn River Basin is notable for being the first global resource play with a multitude of documented cases of seismicity induced by HF (BC OGC, 2012).

An investigation by the BC Oil and Gas Commission (2012) documented 38 seismic events up to 3.8 M_L that were detected within the Horn River Basin by the Canadian National Seismograph Network, from 2009–2011. Seismicity catalogs derived from local seismograph arrays operated by industry contained more than 200 induced events associated with HF operations during the same time period (BC OGC, 2012). Although the national earthquake catalog contained only a single Horn River Basin event (15 February 2004, 2.4 M_L) before the start of shale gas development, subsequent analysis showed that the paucity of reported seismicity was partly due to the previously sparse seismograph network coverage (Farahbod, Kao, Walker, & Cassidy, 2015). By applying a single-station location method to continuous data from the Station FNBB during a predevelopment 1-year time interval, Farahbod, Kao, Walker, and Cassidy (2015) detected 24 events with magnitudes ranging from 1.8–2.9 M_L. Their entire catalog yielded an overall b value of 1.21 (a parameter that defines the proportion of small to large events), including both predevelopment (background) seismicity and induced seismicity. Farahbod, Kao, Cassidy, and Walker (2015) found that total injected volume from HF had a greater effect than injection pressure on the pattern of local seismicity. They also found that relatively large seismic moment release (>10^{14} Nm) within the Horn River Basin occurred only when monthly injected volume exceeded ~150,000 m^3, summed over all operations in the basin (Figure 4b). As a regulatory response, additional broadband stations were installed within the newly created Northern British Columbia (NBC) seismograph network (Figure 4a). Partly due to a decline of development in the Horn River Basin since 2011, no further regulatory controls on HF-induced earthquakes were enacted in this basin.

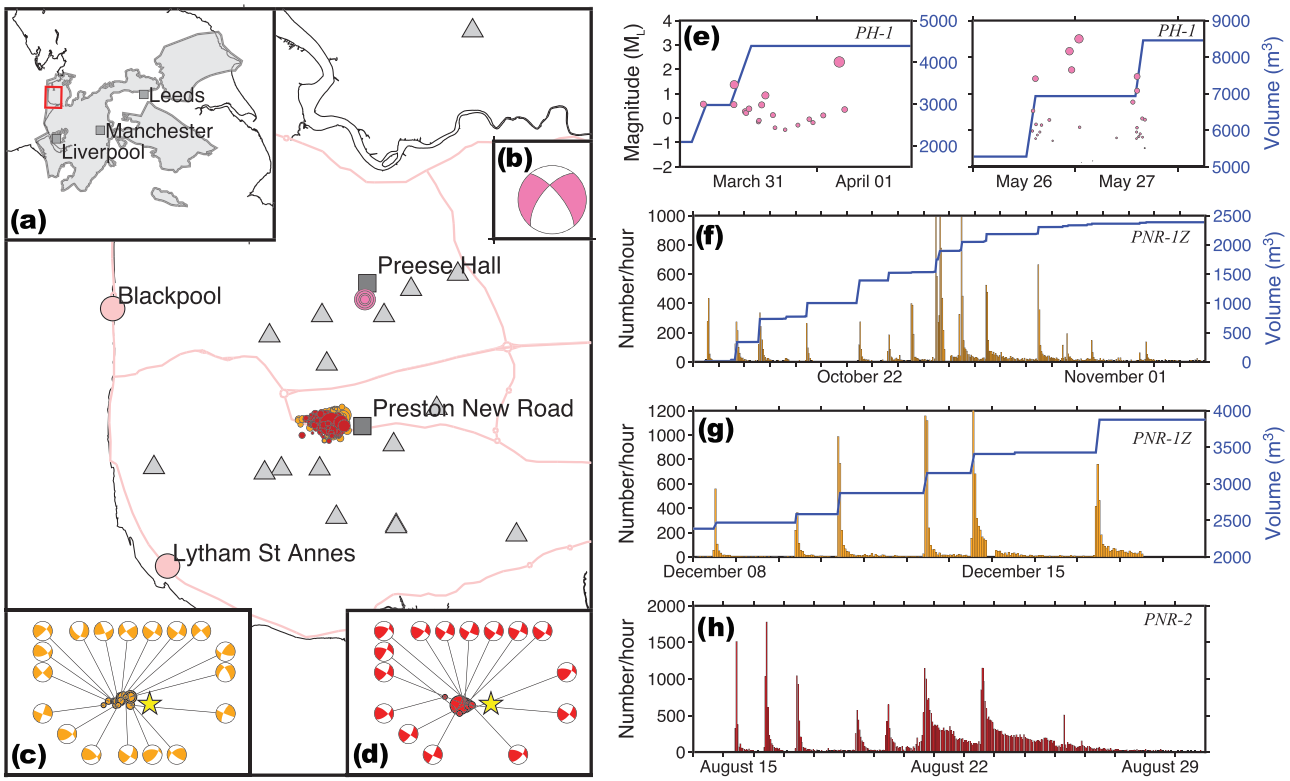

Figure 5. Map of HF-induced earthquakes in the United Kingdom. (a) Seismicity recorded during operations at Preese Hall in 2011 (pink circles) and at Preston New Road in 2018 (orange circles) and 2019 (red circles). Locations of Preese Hall (PH-1) and Preston New Road sites (PNR-1Z and PNR-2) are shown by gray squares, and gray triangles show locations of surface seismometers. The shaded area in the inset depicts regions of shale gas across North England. Red rectangle shows area of larger map. (b) The focal mechanisms for the magnitude −0.2 M_L event at Preese Hall on 2 August 2011 (Clarke et al., 2014). (c and d) Focal mechanisms calculated for selected events during operations at Preston New Road in 2018 and 2019, respectively. (e) HF stage completion volume (blue line) and induced seismicity (pink circles) for HF Stages 2, 4, and 5 at Preese Hall, Blackpool (PH-1). (f–h) HF stage completion volume (blue lines) and histograms of the number of events per hour recorded by downhole microseismic arrays during operations in PNR-1Z in October 2018, PNR-1Z in December 2018, and PNR-2 in August 2019.

2.2. The Bowland Shale in the United Kingdom

Marine shales were deposited in a complex series of tectonically active basins during the Carboniferous (ca.347–318 Ma). These depositions have resulted in the Bowland-Hodder shale gas play across a large area of central Britain (Andrews, 2013). Shale thicknesses are up to 5,000 m in the Bowland, Blacon, Gainsborough, Widmerpool, Edale, and Cleveland basins (Figure 5) and contain sufficient organic matter to generate considerable amounts of hydrocarbons. While a large in-place volume of gas has been identified in the shales beneath central Britain, the recoverable amount remains unknown. To date, there have only been three HF wells completed in the United Kingdom.

In 2011, HF of the first dedicated shale gas well in the United Kingdom, Preese Hall 1 (PH-1) near Blackpool, Lancashire, led to felt seismicity (Clarke et al., 2014), the suspension of HF operations, and inquiries into induced seismicity and associated risks (de Pater & Baisch, 2011; Royal Society and Royal Academy of Engineering, 2012). The largest seismic event, on 1 April 2011, had a magnitude of 2.3 M_L and was felt locally at an intensity of 4 EMS (European Macroseismic Scale; Grünthal, 1998). de Pater and Baisch (2011) concluded that the earthquake activity was caused by fluid injection directly into a nearby fault zone, which reduced the effective normal stress on the fault and causing it to fail repeatedly in a series of small earthquakes. Clarke et al. (2014) identified a possible causative fault following a detailed 3-D seismic reflection study and also used waveform cross correlation (e.g., Shelly et al., 2013) to show the strong similarity between events and to infer locations and mechanisms (Figure 5b). The seismicity starts soon after the operations begin and continues for some hours after operations stop (Figure 5e). In Stages 2 and 4 the

largest earthquakes occurred approximately 10 hr after the start of injection, while the well was shut-in and under high pressure. No seismicity was observed during Stages 1 and 3, and only very weak seismicity occurred during Stage 5. de Pater and Baisch (2011) attribute the lack of seismicity in Stage 3 to the smaller pumped volume and the use of flowback (fluid returned to the surface within a specified period of time after HF has stopped). The pumped volume in Stage 5 was similar to Stages 2 and 4, but there was also flowback.

Subsequently, the U.K. Department for Energy and Climate Change (DECC, 2013) published regulations for HF that contained specific measures for mitigating induced seismicity, including using a traffic light protocol to control whether injection can proceed. This traffic light protocol requires operators to suspend HF operations, reduce pressure, and monitor earthquakes if an event larger than 0.5 M_L occurs during operations.

In late 2018, HF of the Bowland Shale was carried out at the Preston New Road 1Z horizontal well (PNR-1Z), approximately 4 km south of Preese Hall. The PNR-1Z well targets the Bowland shale at a depth of approximately 2,300 m and runs approximately east-west for 700 m horizontally through the unit. A total of 16 stages was stimulated between 16 October and 17 December 2018 with a maximum (per stage) injected volume of 431 m^3. No HF was carried out between 3 November and 4 December, the period when flowback from the well took place.

Operations in the PNR-1Z well were accompanied by seismicity (Clarke et al., 2019) that was recorded by both a dense network of surface sensors and by a downhole geophone array in the adjacent PNR-2 well. The largest event had a magnitude of 1.6 M_L and was felt by a small number of people near the epicenter. Seismicity is observed to move from west to east, corresponding to different stages of operations. Focal mechanisms (Figure 5c) show predominantly strike-slip faulting along near vertical NW-SE or NE-SW planes, which is consistent with observed mechanisms for most tectonic earthquakes in the British Isles (Baptie, 2010). Event rates increase when injection starts and decays rapidly after injection stops but there is considerable variation in event rates between individual stages of operations, with some showing relatively high activity rates (Figures 5f and 5g). Stages close to the heel (east) end of the horizontal well show higher levels of seismicity than those at the toe (west) end, despite similar stimulation volumes.

HF operations in the PNR-2 well at Preston New Road, Lancashire, started on 15 August 2019 and were also accompanied by seismicity. The horizontal PNR-2 well runs roughly parallel to the PNR-1Z well that was stimulated in October–December 2018 and is offset by approximately 200 m. The largest of these events was 2.9 M_L and occurred on 26 August 2019 at 07:30 UTC, almost 72 hr after a HF stage on 23 August. Seismicity is again observed to move from west to east, corresponding to different stages of operations with similar focal mechanisms to PNR-1z (Figure 5d).

Figure 5h shows the seismicity rate as a function of time, during the completion of PNR-2 in August 2019. Full operational parameters were not available at time of writing; however, the published Hydraulic Fracture Plan states that the approach was similar to PNR-1Z, with a planned maximum injected volume of 765 m^3 in any single stage. The events initially show strong temporal association with HF stages, as there are relatively few events outside these periods—suggesting that the event rates decay rapidly with time after stimulation stops. After 21 August 2019, the event rate decays more slowly with time and a number of larger trailing events are observed outside of periods of operation. The last stage was stimulated on 23 August 2019, with trailing events continuing to occur in the following few days: a 2.1 M_L event on 22:01 (UTC) 24 August 2019 (~40 hr after the last HF stage) and a 2.9 M_L on 26 August 2019, 07:30 UTC (~72 hr after the last HF stage). The latter is the largest HF-related earthquake recorded in the United Kingdom to date, and it was strongly felt at distances of up to a few kilometers from the epicenter with maximum intensities of 6 EMS. This led to a premature end to operations in the PNR-2 well with only 7 (out of 47 HF) stages completed. The U.K. government subsequently announced an immediate moratorium on HF, due to the possibility of unacceptable impacts on local communities.

2.3. The Wabamun/Exshaw/Banff Formation in the Alberta Basin, Canada

In southern Alberta, Canada, the Big Valley and Stettler carbonates, Exshaw dolomitic siltstones, and Banff shales collectively comprise an unconventional oil resource (Zaitlin et al., 2010). These Devonian-Mississippian aged formations have been recognized as a source rock for heavy oil and bitumen and are stratigraphically equivalent to the Bakken Formation in North Dakota, which has undergone widespread development. Rokosh et al. (2012) estimate median quantities of in-place oil within the Exshaw at

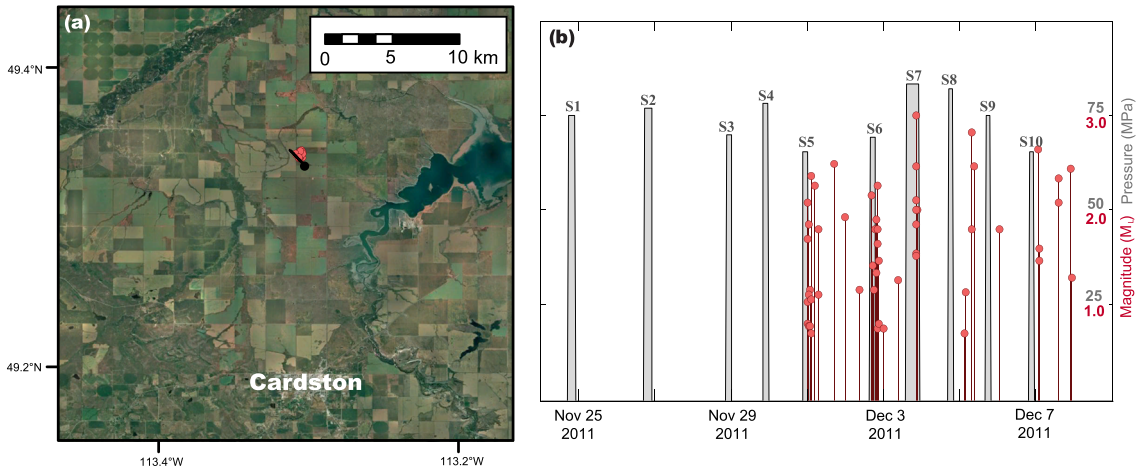

Figure 6. Locations and timings of Exshaw HF-induced events. (a) Regional map of the Exshaw well (black tadpole) alongside locations earthquakes (red circles). (b) Time series of the earthquake magnitudes (red circles) and individual stage completions (gray area). See Schultz, Mei, et al. (2015) for more details.

24.8 billion barrels (4.0×10^9 m^3). This formation was not well developed by industry, as only ~40 horizontal wells were drilled (Galloway et al., 2018). This section focuses on a single horizontal well completed in December 2011 in the Ninastoko Field, developed to exploit the Exshaw shale oil. This well was completed in 10 stages, with an average volume of 716 m^3 per stage (Schultz, Mei, et al., 2015).

More than 60 small earthquakes (up to 3.0 M_L) with similar waveforms were detected from December 2011 to March 2012 north of Cardston, Alberta (Figure 6). This area had no prior documented seismic activity of comparable magnitude or frequency. The timing of these earthquakes followed the fifth stage of stimulation, and it was concluded that they were induced by the contemporaneous HF well completion (Schultz, Mei, et al., 2015). Further study (Galloway et al., 2018) demonstrated the presence of a basement-rooted fault that intersected the target formation. Evidence of paleokarst and collapse brecciation at the stimulation level (near the reactivated fault) indicated a permeable conduit that could allow pore pressure to rapidly diffuse down into the crystalline basement, where the earthquakes occurred (Galloway et al., 2018). To date, this is the only documented case of HF-induced earthquakes in this play. The development of the Exshaw Formation as an unconventional play was soon abandoned, as it was deemed to be uneconomical. Due to this, no regulation was developed to manage HF-induced earthquakes in this area.

2.4. The Duvernay Formation in the Alberta Basin, Canada

The Late Devonian Duvernay Formation is an organic-rich, fine-grained carbonaceous unit that is stratigraphically equivalent to the Muskwa Formation in the Horn River Basin (Switzer et al., 1994). Multiple depositional cycles occurred over a large area (Figure 7), coeval with the growth and development of extensive carbonate reef complexes of the Leduc Formation (Stoakes, 1980). The Leduc and other reef complexes in Alberta are interpreted to have nucleated along paleobathymetric highs that separated reefs from the surrounding shale subbasins (Eaton et al., 1995). Like the Montney Formation, the Duvernay Formation contains vast hydrocarbons resources, with median estimates of shale-hosted oil and natural gas liquid volumes at 61.7 and 11.3 billion barrels (9.8 and 1.8×10^9 m^3), respectively (Rokosh et al., 2012). Initial development of the Duvernay resource play began in 2010, with the first reported cases of induced seismicity in 2013 occurring near Fox Creek, Alberta (Schultz, Stern, et al., 2015; Schultz et al., 2017). To date, there have been more than 1,000 HF wells completed in the Duvernay Formation from 2010–2020 (Schultz & Pawley, 2019). Typical stage, well, and pad completions use volumes of ~1,500, ~20,000, and ~50,000 m^3, respectively (Schultz et al., 2018).

Central Alberta has experienced numerous cases of induced seismicity (Stern et al., 2013) related to secondary hydrocarbon recovery starting in the 1970s (Baranova et al., 1999; Wetmiller, 1986) and wastewater disposal starting in the 1990s (Schultz et al., 2014). Earthquakes induced by HF in the Duvernay play are some of the most well-studied cases worldwide (Figure 7). Using regional seismograph networks (Schultz

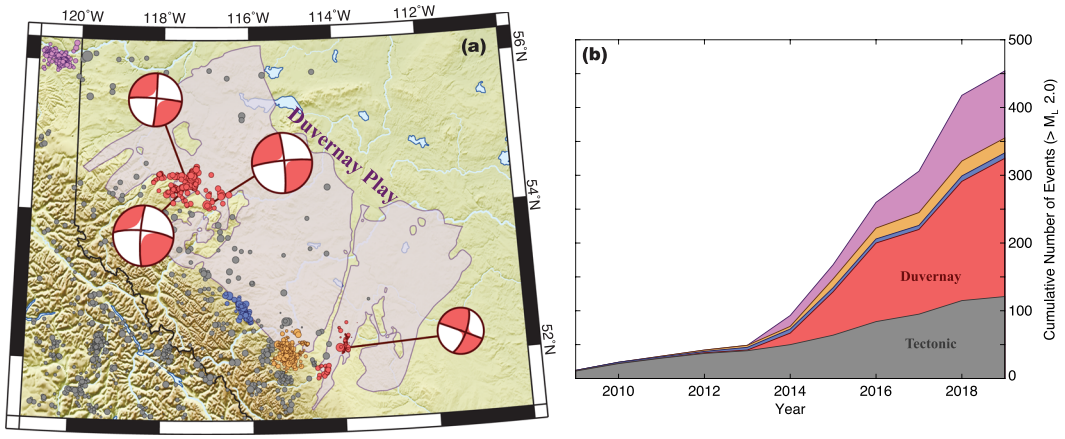

Figure 7. Locations and timings of Duvernay HF-induced events. (a) Regional map of the Duvernay Formation (light purple area) alongside earthquakes (circles). Likely tectonic earthquakes are colored gray, disposal induced are blue (Schultz et al., 2014), secondary recovery induced are orange (Wetmiller, 1986), Montney HF induced are purple, and Duvernay HF induced are red. Focal mechanisms of the four largest events are shown, from left to right: 12 January 2016, 4.1 *Mw*; 23 January 2015, 3.6 *Mw*; 13 June 2015, 3.9 *Mw*; and 4 March 2019 3.7 *Mw*. (b) Time series of the cumulative number of events above the detection threshold (filled area), color coordinated with the left panel. See Schultz et al. (2017) and Schultz and Wang (2020) for more details.

et al., 2017; Wang et al., 2017) and local arrays (Bao & Eaton, 2016; Eaton et al., 2018), seismological studies of induced seismicity in the Duvernay play consistently show that induced events exhibit strong spatiotemporal association with nearby HF operations, with dominantly strike-slip focal mechanisms (R. Wang et al., 2016, 2017, 2018; Zhang et al., 2016). The focal depths of induced events are systematically shallower than natural seismicity (Zhang et al., 2016) and, over a broad area, the rate of induced seismicity surpasses the rate of tectonic earthquakes (Atkinson et al., 2016)—appreciably changing the seismic hazard in the region (Ghofrani et al., 2019; Schultz & Nanometrics, 2019).

These induced earthquakes have been interpreted as reactivation of basement-rooted transtensional strike-slip faults (R. Wang et al., 2017), which is consistent with fault inferences from 3-D reflection seismic data (Chopra et al., 2017; Corlett et al., 2018; Eaton et al., 2018) and the present-day tectonic stress field (Shen, Schmitt, & Haug, 2019; Shen, Schmitt, & Schultz, 2019; H. Zhang, Eaton, et al., 2019). Notably, foreshock microseismicity detected using a dense local network appears to show fault activation processes leading up to the mainshock (Eyre, Eaton, Zecevic, et al., 2019), including inferred aseismic slip (Eyre, Eaton, Garagash, et al., 2019). HF-induced seismicity in this region exhibits variable persistence, with activity in some clusters continuing for at least several months after the mainshock (Bao & Eaton, 2016; Schultz et al., 2017). Faults in this region have been inferred to be near critically stressed (i.e., in a state of incipient failure), due to inferred dynamic triggering from teleseismic surface waves (B. Wang et al., 2015, 2019).

Moment tensor analysis indicates that minor non-double-couple source components of induced events could be linked to tensile fracture growth, multiple intersecting fractures, dilatant jogs created at the overlapping areas of multiple fractures, or nonplanar preexisting faults (R. Wang et al., 2018; Zhang et al., 2016). Studies on these events have been diverse, covering topics related to crustal anisotropy (T. Li, Gu, et al., 2019), stress drop (Clerc et al., 2016; Holmgren et al., 2019, 2020), ground motions (Atkinson & Assatourians, 2017; Kaski & Atkinson, 2017; Rodríguez-Pradilla & Eaton, 2019), and site amplification (Farrugia et al., 2017, 2018). Ongoing analysis of these events has included incorporating them in processed ground motion databases, for use in earthquake hazard studies (Assatourians & Atkinson, 2020). Initially, the induced events were restricted in their spatial location to the Kaybob portion of the Duvernay play but have followed drilling development more than 300 km away into the East Shale Basin portion of the Duvernay, near Red Deer (Schultz & Wang, 2020).

Statistical analysis comparing HF operational parameters and seismicity response shows that operations that injected larger completion volumes ($>10^4$ m^3) tended to be more seismogenic, and that the productivity of induced earthquakes scales linearly with stimulation volume in susceptible areas (Schultz et al., 2018).

Corroborating work showed that induced events in Alberta related to Duvernay HF, wastewater disposal (Schultz et al., 2014), and secondary recovery (Baranova et al., 1999; Wetmiller, 1986), preferentially occur in locations close to the margins of a near-basement carbonate reef platform (Ghofrani & Atkinson, 2016; Schultz et al., 2016)—a potential proxy indicator of faults that host fluid flow (G. R. Davies & Smith, 2006). In some areas that are undergoing rapid development, the Duvernay is overpressured (i.e., pore pressure significantly above hydrostatic), and there is evidence to suggest that the susceptibility to induced seismicity is greater in overpressured zones (Eaton & Schultz, 2018). A recent analysis using machine learning methods indicates that proximity of the injection zone to basement, in situ stress, formation overpressure, proximity to fossil reef margins, lithium concentration (indicative of basement fluids and therefore fault conduits), and rate of natural seismicity are among the strongest predictors of geological susceptibility to induced seismicity in the Duvernay play (Pawley et al., 2018; Schultz & Pawley, 2019).

Following one of the first widely felt events in the Kaybob area (23 January 2015 M_L 4.4), the provincial regulator enacted a traffic light protocol with thresholds set at 4.0 M_L and 2.0 M_L for red and yellow lights, respectively (Alberta Energy Regulator, AER, 2015). Under this regulatory order, operators are required to perform a preoperation hazard assessment, independently monitor nearby events above the yellow light magnitude level, self-report, and enact mitigation strategies following any yellow light earthquakes within 5 km, and immediately suspend operations after a red light (Kao, Visser, et al., 2018; Shipman et al., 2018). Following the first widely felt event in the East Shale Basin of the Duvernay Formation (4 March 2019, 4.2 M_L), the provincial regulator enacted another traffic light protocol with thresholds set at 3.0 M_L and 1.0 M_L for red and yellow lights, respectively (AER, 2019). In response to the ongoing earthquakes in Alberta and a greater need for understanding their mechanisms, the Scientific Induced Seismicity Monitoring Network (SCISMN) was established as a platform for publicly sharing and disseminating industry waveform data collected for regulatory mandates (Schultz, Yusifbayov, & Shipman, 2020).

2.5. The Montney Formation in the Western Canada Sedimentary Basin, Canada

The Montney Formation is a Lower to Middle Triassic, siltstone-dominated clastic unit with a subsurface extent of approximately 130,000 km^2, spanning the border between BC and Alberta in western Canada (Figure 8). It was deposited in an open shelf marine environment and forms a westward thickening wedge, exceeding 300 m in thickness (Edwards et al., 1994). Prior to 2005, conventional oil and gas extraction focused on localized, high permeability sandstone units deposited in a shallow marine environment, whereas subsequent development deployed horizontal drilling and HF methods to develop the vast unconventional resource play (BC OGC, 2014a). Estimates of natural gas (449 trillion cubic feet, 12.7×10^{12} m^3), natural gas liquids (14.5 billion barrels, 2.3×10^9 m^3) and oil (1.1 billion barrels, 0.2×10^9 m^3) indicate that the Montney Formation is potentially one of the most productive resource plays in North America (National Energy Board, 2013). There have been more than 7,000 HF wells completed in the Montney Formation from 2007–2020 (from geoSCOUT). As unconventional oil and gas development in the Horn River Basin progressed and caused HF-induced earthquakes (Figure 4), the installation of eight new seismograph stations in northern BC enhanced seismicity monitoring within the northern Montney play. An investigation by the provincial regulator (BC OGC, 2014b) showed that, over a period from August 2013 to October 2014, 231 seismic events ranging from 2.4–4.4 M_L were attributed to oil and gas operations in the Montney. Of these, 38 events were inferred to be induced by wastewater disposal, while 193 were linked to HF operations based on a spatiotemporal association filter. The onset of Montney Induced Seismicity resulted in a significant change in regional seismicity rate (Figure 8).

Figure 8a shows a map of seismicity for the period October 2006 to September 2017, based on a compilation of catalogs in BC (Babaie Mahani et al., 2017, 2019; Babaie Mahani & Kao, 2018; Visser et al., 2017) and Alberta (Stern et al., 2013). As indicated by numbered labels, the seismicity distribution during this period is characterized by conspicuous clusters that include induced seismicity within the Horn River Basin (1), northern Montney (2), Kiskatinaw area (3), and Fox Creek area (5). One cluster (4) is associated with blasting for coal mining. Since the Fox Creek cluster is linked to development of the deeper Duvernay zone (section 2.4), it is clear that virtually all of Montney induced seismicity is spatially limited to the BC portion of this resource play. Two prominent zones of seismicity in BC, the northern Montney (Babaie Mahani et al., 2017) and the Kiskatinaw area (Yu et al., 2019), are characterized by distinct patterns of activity (BC OGC, 2014b). In particular, the northern Montney area is characterized by a b value of ~1.0–1.3 and a

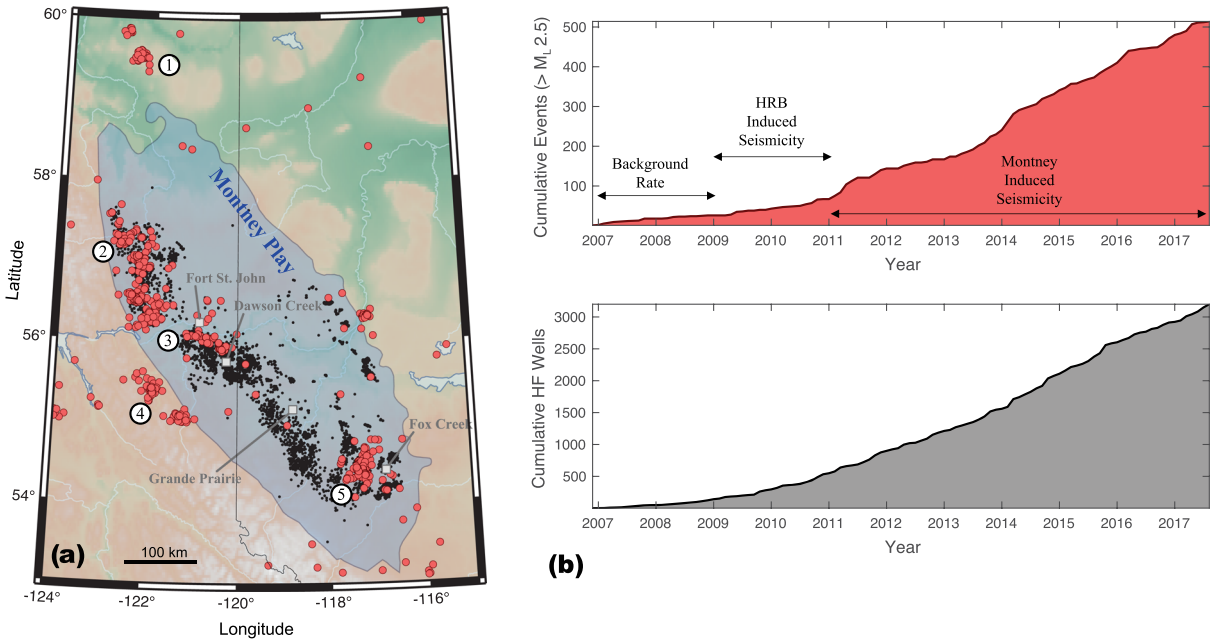

Figure 8. Locations and timings of Montney HF-induced events. (a) Map of showing seismicity (red circles), HF wells (black dots) completed in the Montney Formation (blue area), alongside labeled municipalities, and the Alberta BC border (black line). Larger seismicity ($M_L \geq 2.5$) plotted in this map covers the time period from October 2006 to September 2017 and is taken from earthquake catalogs provided by AER and BC OGC. Numbers indicate seismicity clusters: 1 = Horn River Basin (HRB), 2= northern Montney, 3 = Kiskatinaw, 4 = quarries, and 5 = Fox Creek (Duvernay). (b) Graphs showing cumulative seismicity in BC (upper panel) and horizontal HF wells in the Montney Formation in BC (lower panel). The cumulative seismicity graph indicates apparent changes in seismicity rate corresponding from background rate to development of the HRB and then development of the Montney play. Hydraulically fractured wells in the Montney (BC) show a relatively steady rate starting in 2010.

time lag of up to 2 days following the end of HF operations, while the Kiskatinaw area south of Fort St. John has a *b* value of ~1.5 (indicative of a greater proportion of low-magnitude events), and seismicity tends to occur during or immediately following injection (Babaie Mahani et al., 2017; BC OGC, 2014b; Igonin et al., 2018). The largest event (27 August 2015, 4.6 *Mw*) was observed in the northern Montney area (Babaie Mahani et al., 2017, 2019). In both regions of Montney, induced earthquakes tend to show reverse and strike-slip mechanisms (Babaie Mahani et al., 2020).

In response to increased levels of seismicity, the provincial regulator (B.C. Oil and Gas Commission) introduced new permit conditions in 2016 that required ground motion monitoring, reporting of ground motions within 30 days after operations, and suspension of HF in the event of an induced earthquake above 4.0 M_L within 5 km of operations (Kao, Visser, et al., 2018). In 2018, the regulator issued a Special Project Order for the Kiskatinaw region, with additional conditions that included notifying nearby residents, deploying an accelerometer within three km of the common drilling pad, and reduction of the magnitude threshold to 3.0 M_L for suspension of operations.

2.6. The Utica and Marcellus Shales in the Appalachian Basin, United States

In the northern Appalachian Basin in the eastern United States, the organic-rich Ordovician Point Pleasant-Utica Shale and Middle Devonian Marcellus Shale are some of the most developed unconventional plays in the world and represent a significant component in the United States energy market (e.g., Carr et al., 2013). The Appalachian Basin is currently the largest natural gas producing area in the United States with over 18,000 cubic feet/day (500 m^3/day) in 2019 (Energy Information Administration, EIA, 2019a). The Marcellus and Point Pleasant Utica extend from New York to Kentucky, with prospective areas of 190,000 and 220,000 km^2, proven reserves of 135 and 24 trillion cubic feet (3.8 and 0.7 × 10^{12} m^3) of natural gas, and 345 and 210 million barrels (54.8 and 33.4 × 10^6 m^3) of oil, respectively (EIA, 2019c). The Marcellus Shale consists primarily of shale and lesser amounts of bentonite, limestone, and siltstone overlying the Middle Devonian Mahantango Formation with a thickness up to 300 m, while the Utica and

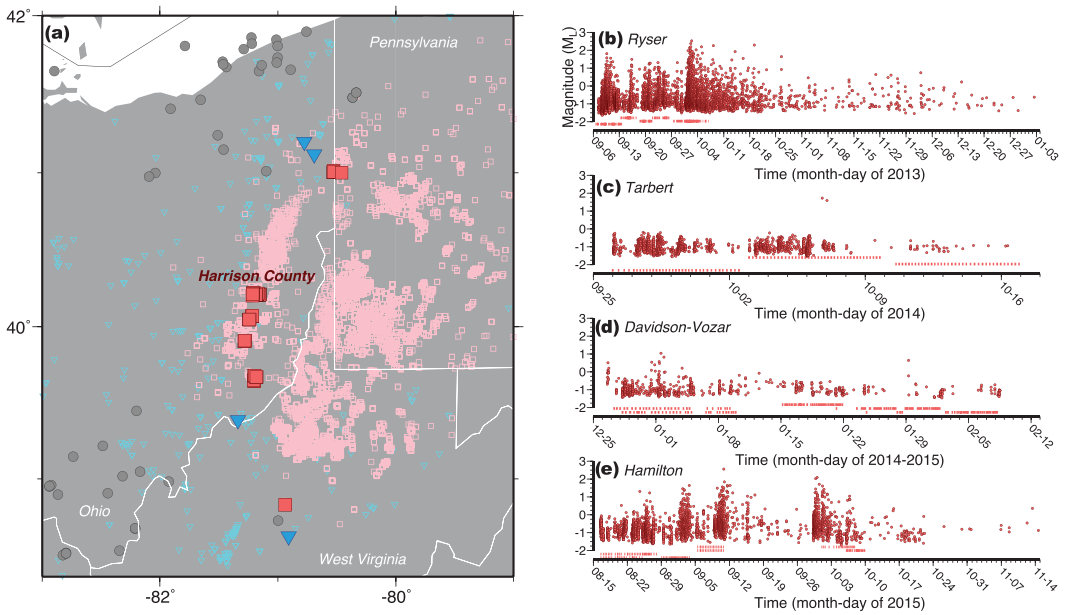

Figure 9. Locations and timings of Appalachian Basin HF-induced events. (a) Map showing the location sequences of cataloged ($M > 2.0$) seismicity in Ohio and neighboring states from 2010–2017. Blue triangles show earthquake sequences induced by wastewater disposal, while red squares are HF induced; pink squares and cyan triangles show the remaining horizontal and wastewater disposal wells in the area, respectively. Circles are earthquakes of probably natural origin. (b–e) Temporal distribution of HF-induced seismicity for four cases in Harrison County (Kozłowska et al., 2018), showing magnitudes of seismic events (red circles) together with timings of HF stage stimulations (red bars). Figure modified from Brudzinski & Kozlowska, (2019) and Skoumal et al. (2015b).

underlying Point Pleasant Formation are calcareous, organic-rich shales that overly the Trenton Limestone with a combined thickness up to 100 m. A rapid increase in drilling HF wells targeting the Marcellus began in 2009, with the Utica drilling accelerating since 2011. To date, there have been more than 11,000 HF wells completed in the Appalachian Basin (www.fracfocus.org). This coincided with a significant increase in seismicity rate linked to two processes: wastewater disposal and HF (Figure 9a) (Brudzinski & Kozłowska, 2019). For example, wastewater disposal near Youngstown was responsible for inducing a 3.9 *Mw* earthquake (W. Y. Kim, 2013; Skoumal et al., 2014). The seismicity here has not been as pervasive as other areas of North America, such that the cases have been typically isolated and provided opportunities to study the seismogenic process in detail.

The observed seismicity is concentrated in a corridor that extends north-south in eastern Ohio, westernmost Pennsylvania and into central West Virginia (Figure 9a), perhaps due to differences in operational targets and geological variations. Ohio appears to have a higher prevalence of seismicity induced by wastewater disposal than surrounding states, likely influenced by the relatively large number of wells disposing of fluids in proximity to the Precambrian basement in the state (Skoumal, Brudzinski, & Currie, 2018). Ohio also has an order of magnitude higher prevalence of seismicity induced by HF than surrounding states, and prior work has suggested this is due to the targeting of the deeper Utica-Point Pleasant Shale formation in Ohio that is closer to basement rocks than the Marcellus Shale formation in West Virginia or Pennsylvania (Homman, 2015; Skoumal, Brudzinski, & Currie, 2018). So far, the only case to occur in neighboring Pennsylvania was in 2016, when operators targeted the Utica instead of the Marcellus. This is similar to a set of Utica wells in Poland Township, Ohio that induced seismicity in 2014 (Skoumal et al., 2015a). The only case to occur in West Virginia was a well that stimulated the Marcellus in July–August 2013 causing earthquakes up to 2.7 M_L. This case was exceptional in that it occurred along the eastern edge of the Rome Trough, where faults have offset strata above the basement (Skoumal, Brudzinski, & Currie, 2018).

The earliest reported case of HF-induced seismicity in Ohio occurred in Harrison County and this area has produced several other cases in which nearby well pads were stimulated (Figure 9b) (Friberg et al., 2014;

Kozłowska et al., 2018; Skoumal et al., 2016). In areas where HF has induced seismicity, the percentage of stimulated wells that produced detectable seismicity is approximately 10–33%. Detailed studies of induced seismicity via double difference relocation and focal mechanism analysis have revealed a series of linear strike-slip fault segments, none of which correspond to previously mapped faults. Yet the remarkable coherence in their orientation suggests these faults were preexisting, critically stressed, and optimally oriented in the regional stress field. The strongest HF-induced earthquakes appear to have occurred in the Precambrian basement, with several events reaching the ~3.0 M_L level and the largest (3.7 M_L) occurring on 3 June 2017 in Noble County, Ohio due to HF completions in the Utica Formation (Brudzinski & Kozłowska, 2019).

State regulations concerning seismic monitoring and traffic light protocol for HF wells operations were implemented by the Ohio Department of Natural Resources (ODNR) Division of Oil and Gas Resources in 2014 after the Poland Township sequence with seismicity up to 3.0 M_L (Skoumal et al., 2015a; ODNR 2017). HF operators are required to monitor potential seismicity if the permitted well is located within 3 miles (~4.8 km) from a known fault or previously cataloged seismicity. If a 1.5 M_L or higher earthquake occurs during HF, direct communication between the operator and ODNR is required. Modification of operation is required if 2.0–2.4 M_L occurs, a temporal halt of operation after a 2.5 M_L occurs, and suspension of the whole pad completion until an approved plan is submitted by operator if an event larger than 3.0 M_L occurs. These regulations have halted the whole pad in the Poland Township and Noble County cases and HF has not resumed.

2.7. The SCOOP and STACK Plays in the Anadarko and Arkoma Basins of Oklahoma, USA

In Oklahoma, there have been several areas of unconventional shale targets (e.g., Cardott, 2012). Vertical well stimulations intensified after 2006 and horizontal well drilling became more common by 2012. The STACK play is an area of the Anadarko Basin derived from "Sooner Trend (oil field), Anadarko (basin), Canadian and Kingfisher (counties)." The SCOOP play is immediately south of the STACK and is derived from "South Central Oklahoma Oil Province." It encompasses areas of the Anadarko, Ardmore, and Marietta Basins. Unlike other plays, these are not a specific geological formation but a geographic area. In contrast, the Arkoma Basin has been a long-standing target for dry gas but increased in activity with unconventional technologies. Although the organic, silica-rich Late Devonian Woodford Shale is a common target for HF in each of these plays, the wide range of basin depths has made a variety of formations economic targets. One example is the Mississippi Lime, a Mississippian-aged low-permeability carbonate limestone that is sourced by the Woodford Shale. There have been at least 12,000 HF wells completed in Oklahoma from 2013–2020 (www.fracfocus.org).

One of the most dramatic increases in seismicity in the Central and Eastern United States occurred in central and northern Oklahoma (e.g., Ellsworth, 2013). Historically, an average of approximately one to two earthquakes per year ($M_L \geq 3.0$) occurred in Oklahoma, but the number of earthquakes with $M_L \geq 3.0$ rose to over 900 earthquakes in 2015. While the seismicity rate began to decline in 2016, the yearly total seismic moment in Oklahoma remained high due to three $Mw \geq 5.0$ earthquakes, including the 3 September 2016 Pawnee earthquake (5.8 *Mw*), the largest earthquake ever recorded in Oklahoma. The seismicity rate increase has generally been interpreted to be due to the disposal of large volumes of produced water into the Arbuckle Group, a Cambrian-Ordovician formation composed primarily of dolomitized carbonates, which is proximal to the Precambrian basement (e.g., Haffener et al., 2018; Keranen et al., 2014; Walsh & Zoback, 2015). The disposal of produced water is likely associated with the 5.7 *Mw* 5 November 2011 Prague (Keranen et al., 2013; Sumy et al., 2014), 5.1 *Mw* 13 February 2016 Fairview (Goebel, Weingarten, et al., 2017; Yeck et al., 2016), 5.8 *Mw* 3 September 2016 Pawnee (Barbour et al., 2017; X. Chen et al., 2017), and 5.0 *Mw* 7 November 2016 Cushing earthquakes (McGarr & Barbour, 2017; McNamara, Hayes, et al., 2015). The increase in seismicity rate raised public concern due to the growing seismic risk to local populations and infrastructure (McNamara, Rubinstein, et al., 2015). During the peak seismicity rates, seismic hazard assessments of Oklahoma were comparable to those in California or New Madrid (Ellsworth et al., 2015; Petersen et al., 2017).

Initially, there were two individual reported cases of HF-induced seismicity in Oklahoma (Darold et al., 2014; Holland, 2011, 2013). These two documented examples occurred in southern Oklahoma and had seismicity with up to ~3.0 M_L. A recent Oklahoma study identified 274 HF wells correlated to seismicity over a broader spatial scale, with the largest event (3.5 M_L) occurring on 14 July 2015 (Figure 10) (Skoumal, Ries,

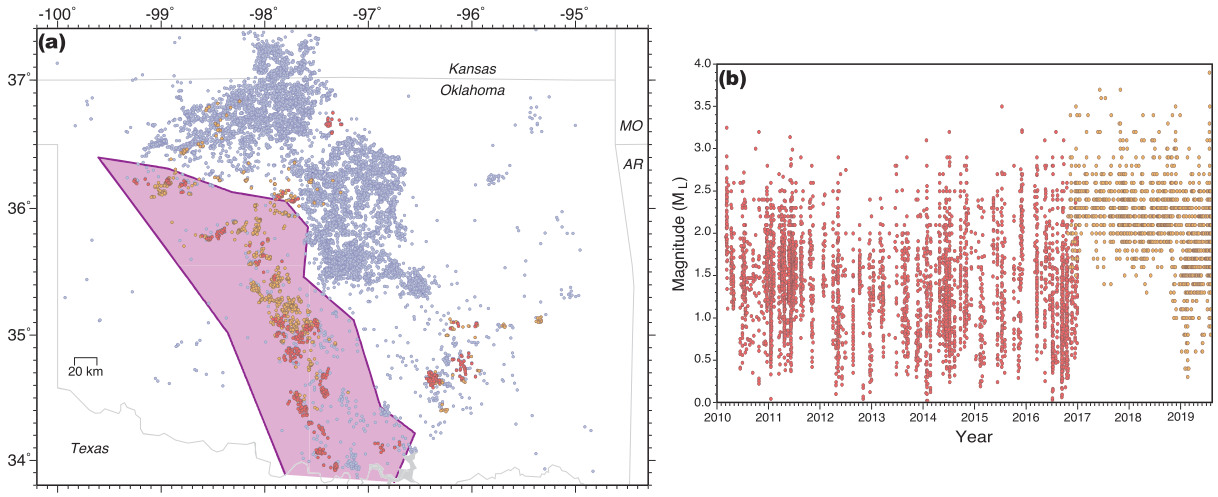

Figure 10. Locations and timings of central Oklahoma HF-induced events. (a) Map of seismicity catalog (blue circles) with HF-induced events from Skoumal, Ries, et al. (2018) (red circles) and Shemeta et al. (2019) (orange circles). The purple line outlines the SCOOP/STACK plays. (b) Magnitude versus time for earthquakes correlated with HF Skoumal, Ries, et al. (2018) (red circles) and Shemeta et al. (2019) (orange circles).

et al., 2018). This included ~130 HF wells within the SCOOP/STACK play between 2010 and 2016 that correlated with ~700 earthquakes of $M_L \geq 2$, which the state regulator (Oklahoma Corporation Commission, OCC) established as the magnitude threshold for an operator response in 2018 (OCC, 2018). In the 16 regions identified, ≥75% of the seismicity correlated with reported HF wells. In some regions, >95% of seismicity correlated with HF wells and >50% of the HF wells correlated with seismicity. The majority of HF-induced seismicity cases occurred in the SCOOP/STACK plays (within the Anadarko, Ardmore, and Marietta Basins), but there were also prominent cases in the Arkoma Basin. An additional 43 HF wells near the edge of the Anadarko Platform demonstrated evidence for both wastewater disposal and HF-induced seismicity.

In 2016, the OCC implemented mandatory submission of HF Notices and established operator protocols related to seismicity. Between 2016 and 2019, the OCC cross-referenced HF Notices with seismic events and identified when earthquakes occurred within 5 km of a well and between the start of HF and 7 days after flowback (Shemeta et al., 2019). This study identified 7.7% of HF wells had seismicity $M_L \geq 2$, but areas such as McClain county had 19.5% of HF wells with $M_L \geq 2$. There were 960 earthquakes with $M_L \geq 2$ and the largest HF-induced earthquake in this data set occurred on 25 July 2019 in Kingfisher County (3.9 M_L, 3.6 *Mw*). The rate of HF-induced seismicity has been relatively constant over both studies, but the number of $M_L \geq 3$ earthquakes jumped from 8 in 2010–2016 to 57 in 2016–2019.

There has been no detailed focal mechanisms study of HF-induced seismicity in Oklahoma, but studies of wastewater disposal-induced seismicity in central Oklahoma have shown coherent patterns of right-lateral and left-lateral strike slip faulting consistent with the regional stress field (McNamara, Benz, et al., 2015). The largest HF-induced earthquake on 25 July 2019 had a similar strike slip mechanism.

Starting in December 2016 and then updated in February 2018, the OCC issued seismicity guidelines for operators working in the SCOOP/STACK area of interest (Figure 10a) (OCC, 2018). Within this area of interest, any well that is associated with anomalous seismic activity within a 5 km radius of the wellbore is subject to a traffic light protocol. If a 2.0 M_L earthquake occurs, the operator is contacted by the OCC and implementation of a mitigation plan is commenced. At or above 2.5 M_L, the operator must pause completion operations for a minimum of 6 hr and must initiate a technical conference with the OCC to discuss mitigation procedures. At or above 3.0 M_L, the operator must follow the procedures of the previous level and receive permission from the OCC to resume HF. At or above 3.5 M_L, the operator must immediately suspend all HF and meet in person with OCC to determine under what circumstances the operator can safely resume. When a link between HF and seismicity is established, the mitigation strategies may include pausing HF, skipping stages in areas of concern, reducing the fluid injection rate and/or fluid volumes, changing fluid

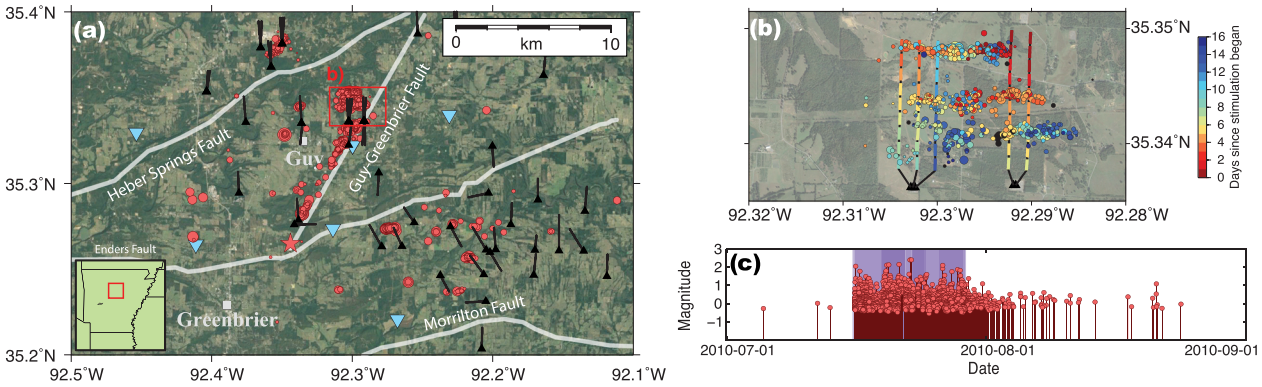

Figure 11. Locations and timings of Fayetteville HF-induced events. (a) Map showing seismicity (red circles), the 4.7 *M*, 27 February 2011 event (red star), HF pads (black triangles), HF laterals (black lines), and disposal wells (blue triangles) alongside municipalities (gray boxes) and known faults (gray lines) in the Guy-Greenbrier area in central Arkansas (inset box). (b) Back azimuth shifted locations of induced earthquakes (circles) near two HF pad completions; individual stages (colored lines) and earthquakes are colored according to time of occurrence. (c) Magnitudes of individual earthquakes (red circles) are shown as a function of time, alongside well completion schedules (purple areas). Figure modified from Yoon et al. (2017).

types, or modifying from multiwell zipper frack completions to single-well operations (Ground Water Protection Council and Interstate Oil and Gas Compact Commission [GWPC & IOGCC], 2017). Within the SCOOP/STACK area of interest, operators are required to disclose a seismic monitoring plan, whether they are deploying a private seismic array or utilizing publicly available stations. HF Notices also need to be filed 48 hr prior, providing the well surface and bottom-hole location, anticipated number of stages, average fluid volume per stage, scheduled start and end dates of operation, and initiation date of well flowback.

2.8. The Fayetteville Formation in the Arkoma Basin of Arkansas, USA

The Mississippian age Fayetteville Formation of Arkansas (Handford, 1986) became an early target for shale gas development following the successes in the Barnett Shale of the Fort Worth Basin, Texas. This unconventional play runs east-west across north central Arkansas for approximately 150 km (Browning et al., 2014) (Figure 11). By 2005, horizontal well completions in the middle to lower organic rich facies at depths typically between 1 and 2 km were coming online, and by 2009 0.5 trillion cubic feet (14×10^9 m^3) of gas was being produced per year (Browning et al., 2014; Harpel et al., 2012). To date, there have been more than 1,000 HF wells completed in Arkansas (www.fracfocus.org).

Within Arkansas, low-level seismicity occurs throughout with magnitudes approaching 5.0 *Mw*. The most intense activity in recent decades is in the New Madrid Seismic Zone of northeastern Arkansas. Within the footprint of the Fayetteville shale play, natural seismic swarms struck near the town of Enola in 1982 and 2001 with maximum magnitudes of 3.8 *Mw* and 4.4 *Mw*, respectively (Chiu et al., 1984; Rabak et al., 2010). Focal depths for well-located earthquakes ranged between 3 and 7 km, placing them in Cambrian carbonates and the Precambrian basement. Seismicity lingered for several years in the region, following the 2001 swarm. Scattered seismicity occurred during the development of the shale play, with magnitudes up to 2.8 M_L between 2004 and 2009 (Figure 11). Horton (2012) observed a spatial association between minor seismicity predominantly to a wastewater disposal well near the towns of Guy and Greenbrier.

On 23 September 2010 an intense seismic swarm began near Guy and continued until late 2010, with magnitudes approaching 5.0 *Mw*. Precise hypocenters determined by Horton (2012) showed that the activity was hosted by a basement strike-slip fault, now named the Guy-Greenbrier Fault (Figure 11). Activity jumped south in February 2011, enlarging the activated segment of the fault to 13 km. Following the largest earthquake (28 February 2011, 4.7 *Mw*), concerns about the potential for larger earthquakes led to an emergency shutdown order for injection by the Arkansas Oil and Gas Commission. Analysis of the seismicity, injection patterns and pore pressure diffusion built a strong case for the activation of the Guy-Greenbrier Fault by wastewater disposal (Horton, 2012; Ogwari et al., 2016; Ogwari & Horton, 2016; Park et al., 2020). In the neighboring states of Oklahoma and Texas, wastewater disposal by injection is understood to be the primary driver of induced seismicity (Ellsworth, 2013; Frohlich, 2012; Keranen et al., 2013). However, HF of the production wells can also induce earthquakes.

It is difficult to draw a simple conclusion about HF-induced seismicity within the entire Fayetteville shale play due to the sparse seismic station coverage during the development years of the field. However, installation of three stations near Guy and Greenbrier in May and June 2010 permitted a close examination of seismicity there in the three months leading up to the initiation of the intense swarm on the Guy-Greenbrier Fault in late September 2010. Yoon et al. (2017) use Fingerprinting and Similarity Thresholding (FAST) and template matching to detect over 14,000 earthquakes with magnitudes −1.5–2.9 M_L on a single station (Figure 11). The largest 1,740 of those were located and found to form 16 spatially compact clusters. Most of these clusters were temporally and spatially associated to public records of HF operations (Yoon et al., 2017), with about one third of the wells stimulated at this time being associated with seismicity. Significantly, seismicity continued for days and weeks following the completion of HF pads, with the largest magnitude event (2.9 M_L) occurring on June of 2010.

The detailed public records permitted Yoon et al. (2017) to separate events induced by HF from those induced by wastewater disposal. The presence of two industrial drivers—HF and wastewater disposal—and natural seismicity in the immediate vicinity of the shale play presented challenges for operational decision making. Given the limited technical resources available at the time as well as the undeveloped state of our understanding of the hazards posed by either HF or wastewater disposal, it is noteworthy that the regulator acted quickly to protect the public by halting wastewater injection into the wells most likely to be involved. In retrospect, the value of high-resolution seismic data affirms that decision while also revealing the ease with which HF operations also triggered seismicity. The possibility of enacting a traffic light protocol was considered during the peak induced seismicity in Arkansas but was postponed due to the decline in Fayetteville development.

2.9. The Eagle Ford Shale Play in the Western Gulf Basin of Texas, USA

South Texas has a history of active oil and gas production, HF, wastewater disposal, and seismicity, some of which occurs within or near areas of pervasive faulting (Figure 12a) (Ewing, 1990; Frohlich et al., 2016). With the advancements in horizontal drilling and HF, the Eagle Ford shale play has focused on hydrocarbon production of the Upper Cretaceous Eagle Ford Formation and the Austin Chalk Formation directly above since 2008 (Frohlich & Brunt, 2013; Martin et al., 2011; Pearson, 2012; Railroad Commission of Texas [RRC], 2019). Since 2012, the Eagle Ford has produced the second largest amount of oil in the United States, averaging 1.3 million barrels per day (0.2×10^6 m^3/day) (EIA, 2019a). To date, there have been more than 19,000 HF wells completed in the Eagle Ford Shale play (www.fracfocus.org).

Eagle Ford seismicity has been largely attributed to increases in hydrocarbon production with a few cases related to wastewater disposal since 1973 (Davis et al., 1995; Frohlich & Brunt, 2013; Frohlich & Davis, 2002; Olson & Frohlich, 1992; Pennington et al., 1986). The largest earthquake in south Texas (4.8 *Mw*) occurred in 2011 and has been interpreted to be induced by fluid extraction (Frohlich & Brunt, 2013).

In 2018, the rate of $M_L \geq 3.0$ earthquakes in the Eagle Ford grew to 33 times higher than background levels (3 per 10 years during 1980–2010, Figure 12b inset). Fasola et al. (2019) investigated seismicity since 2014 and identified how HF contributed to seismicity by comparing times and locations of HF with a catalog of seismicity extended with template matching. More than 85% of the seismicity was spatiotemporally correlated with HF, and there were 94 $M_L \geq 2.0$ earthquakes correlated to 211 HF well laterals. There was no spatiotemporal correlation between wastewater disposal and seismicity, with few wastewater disposal wells having injection rates more than 300,000 barrels per month (47,700 m^3/month) (Figure 12a). As of March 2020, the 4.0 *Mw* 1 May 2018 earthquake is the largest HF-induced earthquake documented in the United States (as opposed to other earthquakes mentioned above induced by the wastewater disposal process). It appeared to occur on a mapped Karnes Trough normal fault (Figure 12a), which also hosted the largest regional earthquake (4.8 *Mw*) in 2011 ~10 km away, indicating operational activities in this area are capable of producing felt and potentially damaging earthquakes. Considering all of the correlated cases, the effective injection rate (volume per day per area) had the strongest influence on the probability of seismicity (Fasola et al., 2019). Cases where multiple laterals were stimulated concurrently (e.g., alternating stages between laterals) tripled the probability of seismicity relative to a single lateral stimulated in isolation. No regulatory controls on HF-induced earthquakes have been implemented as of May 2020 in the Eagle Ford Shale play, or anywhere in Texas.

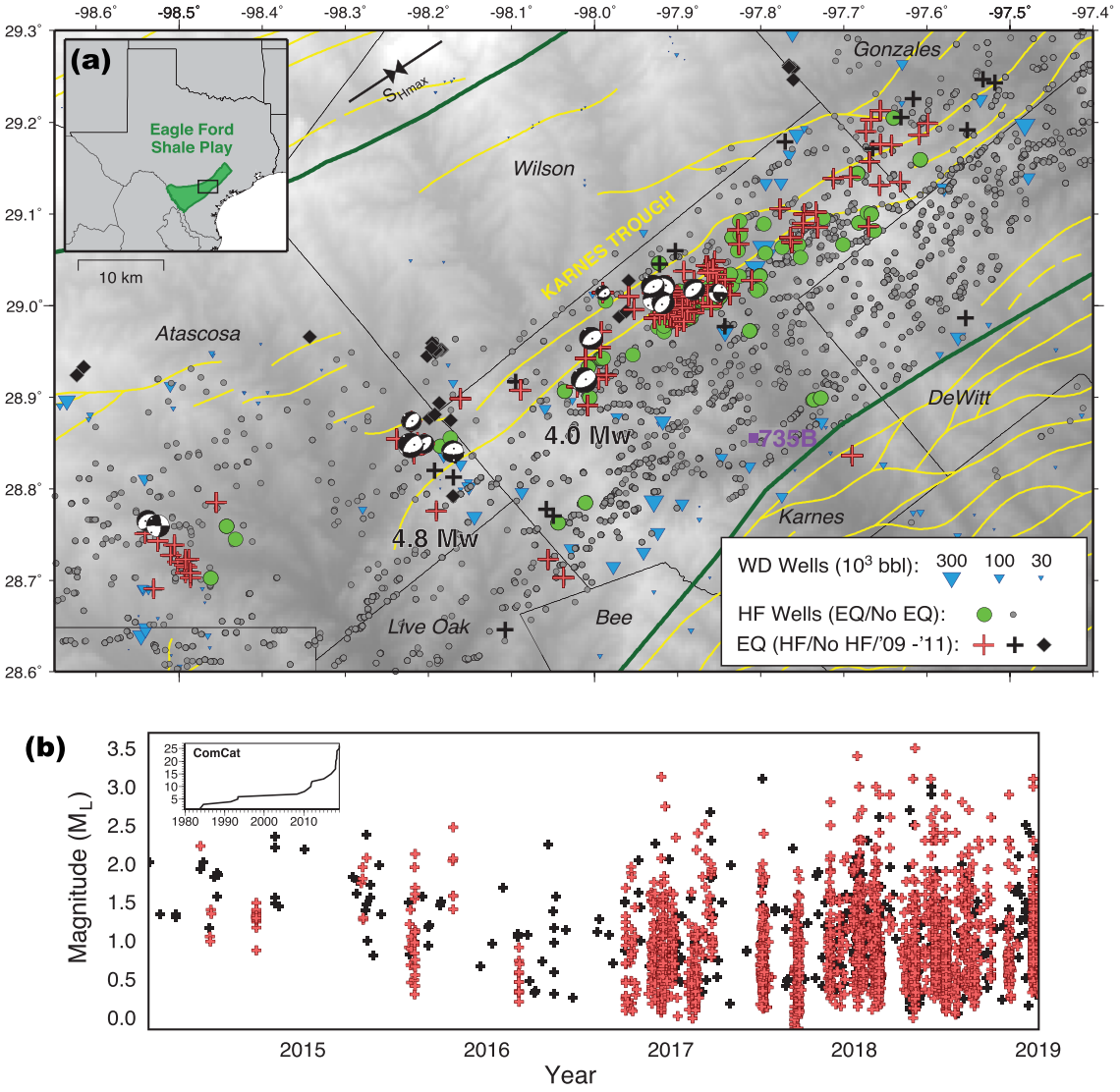

Figure 12. Locations and timings of Eagle Ford HF-induced events. (a) Map showing earthquakes (crosses) and focal mechanisms (beach balls) since 2017 from the Texas Seismological Network. HF wells are indicated by black circles (FracFocus). Correlated earthquakes and HF wells are red and green, respectively. Black diamonds show 2009–2011 earthquakes (Frohlich & Brunt, 2013). Purple square shows the seismic station (735B) used for template matching. Wastewater disposal wells are teal triangles sized by median monthly volumes. Arrows show regional S_{Hmax} orientation (Lund Snee & Zoback, 2016). Faults (Ewing, 1990) are in yellow. (b) Magnitude versus time for earthquakes (crosses) detected in the area shown in (a). Events are colored when correlated with HF. Inset shows cumulative number of earthquakes ($M \geq 3.0$) for this area from the USGS Comprehensive Catalog. Figure modified from Fasola et al. (2019).

2.10. The Wolfcamp and Bone Spring Formations in the Delaware Basin of Texas, USA

The Delaware Basin, a subbasin located in the western extent of the Permian Basin, is located in western Texas and southeastern New Mexico (Figure 13a). The Bone Spring Formation lies beneath the Delaware Mountain Group and is composed of calcareous, siliciclastic, and carbonaceous deposits (EIA, 2019b). Historically, the Bone Spring Formation was produced from conventional wells targeting sandy layers within the interval, but over the past decade it has been developed predominantly as an unconventional play. The Bone Spring Formation consists primarily of interbedded shale and carbonates. Beneath the Bone Spring Formation, the Wolfcamp Shale is a prolific tight oil and gas bearing formation. Together, the Bone Spring and Wolfcamp Formations are estimated to contain more than 33 billion barrels (5.2×10^9 m^3) of oil, 48 trillion cubic feet (1.4×10^{12} m^3) of natural gas, and 3.9 billion barrels (0.6×10^9 m^3) of natural gas liquids (Gaswirth et al., 2016, 2018). There have been at least 7,900 HF wells completed in the Texas portion of the Delaware Basin from 2011–2019.

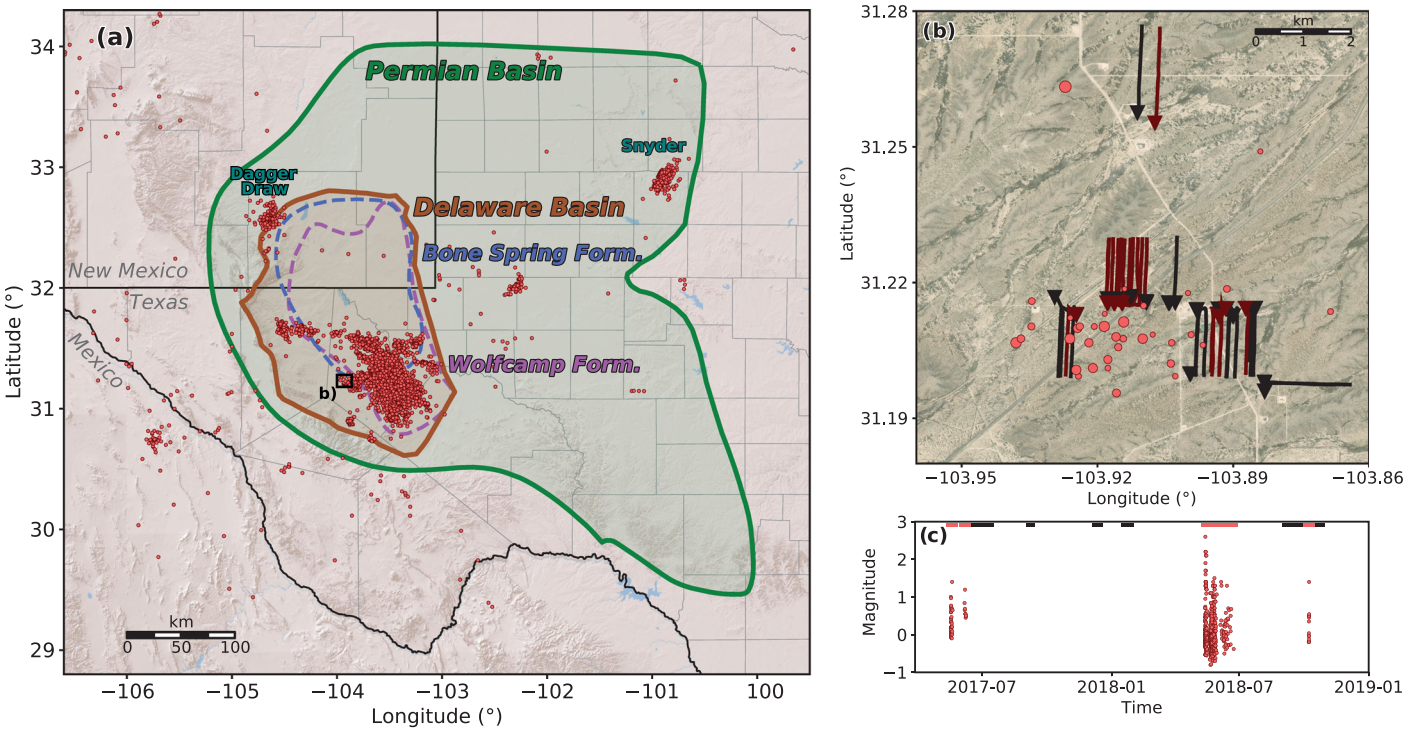

Figure 13. Locations and timings of Permian Basin earthquakes. (a) Map of seismicity (red circles) in the region near the Permian Basin (green polygon). The Delaware Basin (brown polygon) contains the Bone Spring and Wolfcamp Formations (blue and pink polygons, respectively; formation extents defined by EIA, 2019b). (b) Map of HF-induced seismicity examples with earthquakes (circles), well pads (triangles), and horizontal well laterals (lines). Colored wells are associated with induced earthquakes. Earthquake symbols are sized by the number of detected events (between 1 and 51 earthquakes), which template matching identified. (c) Time series of earthquakes (circles) and times of HF stimulations (bars) that are shown in (b). Figure modified from Skoumal et al. (2020).

Since hydrocarbon production began in the 1930s, the majority of earthquakes in the Permian Basin are interpreted to be induced (Frohlich et al., 2016). These induced earthquakes include events near the town of Snyder that were associated with secondary recovery during 1974–1982 (Davis & Pennington, 1989) and injection of supercritical CO_2 during 2006–2011 (Gan & Frohlich, 2013). Much of the recent seismicity has been located within the extent of the Delaware Basin (Figure 13a). The seismicity rate in the Delaware Basin has increased orders of magnitude over the past decade, particularly in the southern portion of the Basin (Frohlich et al., 2019; Skoumal et al., 2020). No earthquakes greater than 3.0 *M* had been detected in this area prior to 2015; during 2015–2020, more than 67 earthquakes ($M > 3$) occurred, with the largest event being a 5.0 *Mw*. The majority of the earthquakes have been suggested to be induced by wastewater disposal, with ~5% of seismicity (of 1,850 earthquakes) induced by HF (Skoumal et al., 2020), although another study has suggested HF as a primary factor for inducing many of these events (Lomax & Savvaidis, 2019). This discrepancy highlights potential difficulties of spatiotemporal association to HF stimulation, especially in areas with ongoing earthquakes. The most apparent cases of HF-induced seismicity is in the southwestern portion of the Basin (Lomax & Savvaidis, 2019; Skoumal et al., 2020), an area where limited wastewater disposal is occurring (Figures 13b and 13c). To date, the largest magnitude event (3.0 *M*) associated with HF in the Delaware Basin occurred in May 2018 (Skoumal et al., 2020). The true extent of HF-induced seismicity may be much larger, but confident assessments are limited by high seismicity rates (associated with wastewater disposal and/or hydrocarbon production) and the absence of HF stimulation details in public records documenting stimulation activities. To date, no regulatory controls on HF-induced earthquakes have been implemented in the Delaware Basin.

2.11. The Wufeng-Longmaxi Formation in the South Sichuan Basin, China

The Upper Ordovician Wufeng Formation and Lower Silurian Longmaxi Formation are interbedded, organic-rich mudstones/shales with a basal carbonaceous interval. Mineral composition is dominated by

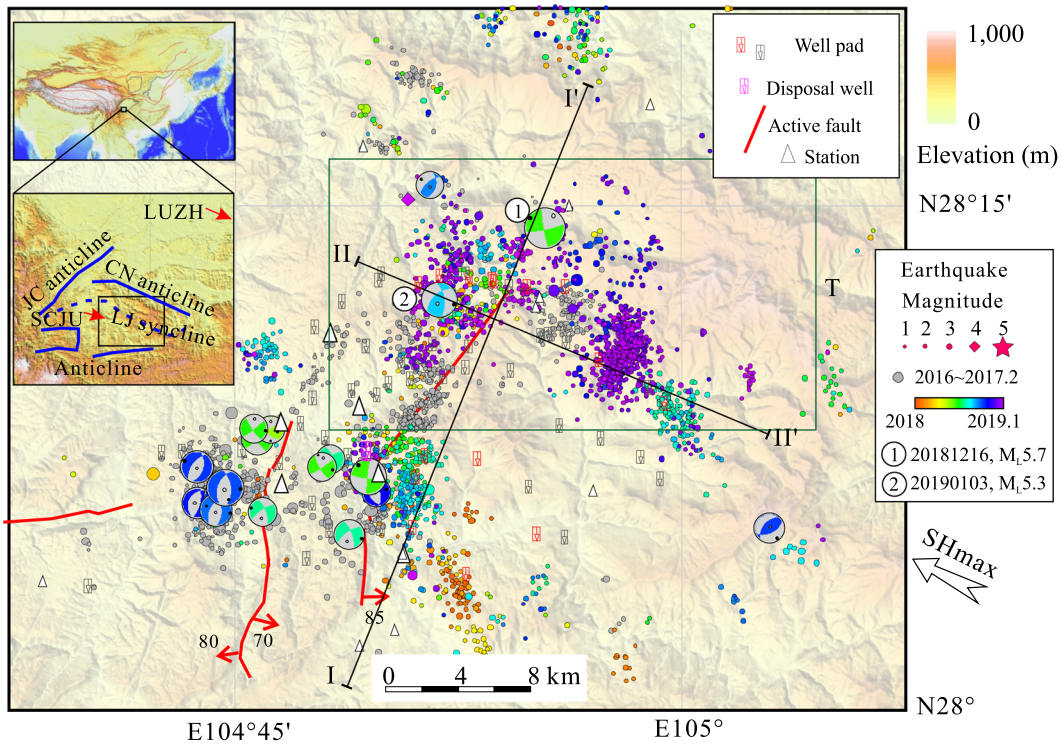

Figure 14. Map view of HF wells and earthquakes near Changning shale gas block in the Sichuan Basin, China. Earthquakes relocations (circles, colored by time) are shown alongside focal mechanisms of larger events (beach balls), stimulated HF pads (red polygons), producing HF wells (black polygons), disposal wells (pink polygons), known faults (red lines), and recording stations (triangles). Earthquake relocations are from two periods: 1 January 2016 through February 2017 (Lei et al., 2017) and 1 January 2018 through January 2019 (Lei et al., 2019). The inset maps provide geographical context with major fault systems. Figure reproduced from Lei et al. (2019).

clays, quartz, and feldspar (C. Liang et al., 2014). The fault-bounded Sichuan Basin covers an area of 260,000 km^2 in southern China, with tectonic controls from the Changning anticline creating a key area for shale gas development. In particular, these structural traps provide a means for overpressure accumulation—an important factor for increasing well productivity (Dong et al., 2018). Since 2008–2012, these formations have been the target of intensive shale gas development in the South Sichuan Basin of China, with HF stimulation beginning in 2014 (Dengfa et al., 2019). By 2017, there have been more than 500 Wufeng-Logmaxi HF wells drilled in the basin (Dong et al., 2018).

Following petroleum development of the Wufeng-Longmaxi Formations, exceptional increases in earthquake rates in the Zhaotong and Changning shale gas fields (Figure 14) have been noted (Lei et al., 2017; Meng et al., 2019). Seismicity in this region was relatively quiescent, with only ~60 earthquakes ($M_L > 2.5$) observed prior to HF development (1970 to October 2008) (Lei et al., 2017). The timing and proximity of these earthquake sequences with HF multiwell stimulation (coupled with the absence of nearby production and disposal operations) contributed to their interpretation as being induced by HF. More focused studies have linked induced events to pore pressure propagation from HF stimulation (Tan et al., 2020), with cumulative injected volume being particularly important for triggering events (F. Zhang, Yin, et al., 2019). One of the larger events (28 January 2017, 4.7 *Mw*) was noteworthy, as it occurred nine days after the completion of the HF pad. This event was superseded by a larger 5.7 M_L earthquake on 16 December 2018 near Xingwen County (Lei et al., 2019). All of these earthquakes had either reverse or strike-slip sense of motion on their faults and are predominantly located within the dolomitic strata, between the target formations and the crystalline basement (Lei et al., 2019; Tan et al., 2020). The HF-induced earthquakes in this basin are exceptional cases, as they have been the largest in the world to date and have caused ground motions intense enough to be felt, triggered landslides, caused ¥50 million ($7 million USD) in direct economic losses, injuries, and resulted in the first fatalities (Lei et al., 2019). The development of shale gas resources is expected to continue accelerating in the South Sichuan Basin (Dong et al., 2018). To date, there is no publicly reported regulation controlling HF-induced earthquakes in this play.

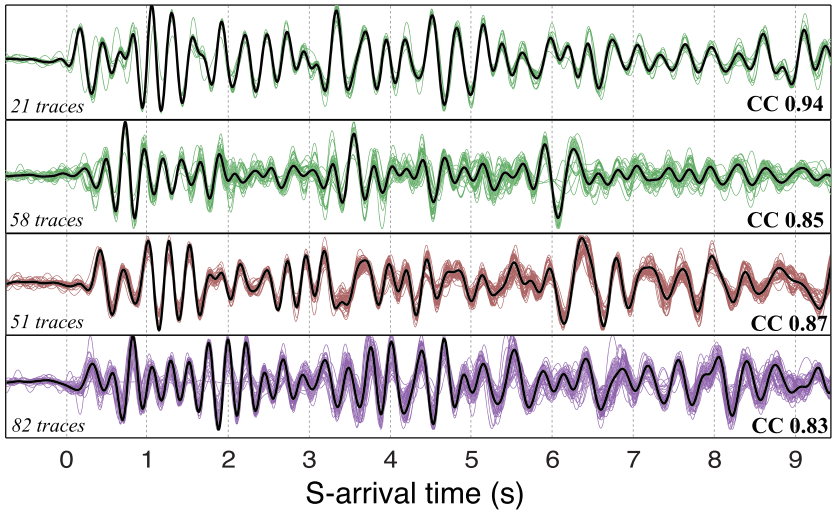

Figure 15. An example of similar earthquake waveforms caused by HF. Four clusters of earthquakes in the Duvernay Formation, aligned on their *S* arrival, are compared for waveform similarity in their beam average (black lines), and individual traces (colored lines). Counts of traces within the cluster and their cross-correlation coefficient are annotated. See also Schultz et al. (2017) for more details.

3. Common Themes

In this section, we identify themes and commonalities that are shared between most (or all) of the documented cases of HF-induced seismicity, to date. These common themes reflect both the uniqueness of the HF injection physics and the characteristics of the underlying geology for this category of earthquake. Interpretations of these common themes are then elaborated on in section 4.

3.1. Earthquake Similarity and Swarms

Common among the observed cases to date, HF-induced earthquakes are spatially clustered around their causal pad (Bao & Eaton, 2016; Meng et al., 2019; Schultz et al., 2017; Skoumal et al., 2015a; Tan et al., 2020). In cases where high-resolution locations have been determined, hypocenters tend to form clear fault plane delineations (Eaton et al., 2018; Eyre, Eaton, Zecevic, et al., 2019; Friberg et al., 2014; Yoon et al., 2017). Supporting this, HF-induced earthquakes within a cluster often show significant waveform similarity (Figure 15). Highly clustered earthquakes with the same focal mechanism will produce nearly identical seismograms when hypocentral distances are within a quarter wavelength of each other (Geller & Mueller, 1980; Poupinet et al., 1984). Consequently, waveform similarity only implies proximity, not repetition of the source, as is sometimes assumed. Indeed, similar earthquakes have been documented in many contexts (Ellsworth, 1995), including fluid-related volcanic processes (Uchida & Bürgmann, 2019) and enhanced geothermal systems (Majer et al., 2007). In the induced seismicity context, these similar events are often interpreted as resulting from the repeated stimulation of a fault to failure conditions (Goertz-Allmann & Wiemer, 2012). Due to this interpretation, waveform similarity is often leveraged for the identification of additional events during matched filtering analysis (Skoumal et al., 2016; B. Wang et al., 2015). Additional analysis on various HF cases would be helpful to better discern the role and importance of repeating events for this category of induced earthquake.

In addition to the observation of similar events, HF-induced clusters appear to have a consistently swarm-like nature (Kothari, 2019; Lei et al., 2017; Skoumal et al., 2015b). In this sense, the temporal evolution of earthquake swarms does not tend to follow traditional fore/main/aftershock patterns (Hill, 1977; Mogi, 1967). This swarm-like character is in accord with closer assessments of HF-induced earthquakes, where interevent times follow a nonhomogeneous Poisson distribution (Hajati et al., 2015) with smaller contributions from earthquake interactions (Catalli et al., 2016; Kettlety et al., 2019; Maghsoudi et al., 2018). This is not surprising, as stage-by-stage stimulation can sequentially illuminate faults. One example of this can be seen during HF in Guy, Arkansas (Yoon et al., 2017). Building on this observation, swarms of

earthquakes are often associated with specific geological conditions. For example, swarms are widely observed in volcanic environments (Roman & Cashman, 2006), along transform faults (Roland & McGuire, 2009), and within hydrothermal systems where pore pressure is elevated (Cox, 2016; Špičák, 2000). By both design and intent, the target formations for HF are highly impermeable and often overpressured (Eaton & Schultz, 2018).

3.2. Proximity to Well Bore and Basement

The majority of HF-induced earthquakes (with high-precision hypocenters) tend to locate within a few wellbore dimensions from their causal HF pad (Skoumal et al., 2020). In lower-resolution regional studies, nearly all of the clusters' error ellipsoids tend to encompass their causal pad location (Babaie Mahani et al., 2017; Lei et al., 2019; Schultz et al., 2017). In several higher-resolution examples, seismicity illuminates fault structures that intersect the target formation or are within a few hundreds of meters to the well bore laterals (Eaton et al., 2018; Eyre, Eaton, Zecevic, et al., 2019). These are plausible distances for stimulated fracture growth to hydraulically connect with the illuminated fault (R. J. Davies et al., 2012; Wilson et al., 2018) and to sufficiently increase fault pore pressure toward failure (Shen, Schmitt, & Schultz, 2019). This interpretation is consistent with the impermeable nature of HF target reservoirs impeding the diffusion of pore pressure through the matrix and the transient nature of HF pad completions (weeks to a month).

However, there are other cases with larger spatial separation between well and seismicity. For example, the Cardston, Alberta (Galloway et al., 2018; Schultz, Mei, et al., 2015) and Poland Township, Ohio cases (Kozłowska et al., 2018; Skoumal et al., 2015a) both situate earthquakes about 1 km deeper than the target formation, within the crystalline basement. As well, the Kaybob Duvernay observed induced seismicity up to a distance of more than 1 km from the HF stimulation (Bao & Eaton, 2016). We provide a cautionary reminder that event relocations tend to become shallower as receiver geometry becomes closer and velocity models are increasingly refined. Other examples from Red Deer, Alberta (Schultz & Wang, 2020) include earthquakes (~1.5 km) laterally offset from the nearest HF stage. In these cases, epicenters are well resolved and depth uncertainty plays no role in the apparent offset discrepancies. Such lateral offsets are well beyond the plausible extent of HF growth, rendering the earthquake triggering mechanism less obvious.

HF operations that induce earthquakes tend to be preferentially associated with deeper target formations (Pawley et al., 2018; Skoumal, Brudzinski, & Currie, 2018)—in many cases, Paleozoic formations that lie within hundreds of meters from crystalline basement. With respect to hypocenter depth, induced earthquakes range from just above the target formation (Eyre, Eaton, Zecevic, et al., 2019; Poulin et al., 2019) to well within the crystalline basement (Lei et al., 2017, 2019). Corroborating this observation, HF earthquakes have been interpreted by some as associated with basement rooted faults (Anderson & Underhill, 2020; Chopra et al., 2017; Corlett et al., 2018; Galloway et al., 2018; Kozłowska et al., 2018). In cases where earthquakes were located just above the target formation, there is a correspondence to the sedimentary termination of basement-rooted faults (Eaton et al., 2018). However, identification of basement-rooted faults, particularly those with steep dips, remains a daunting technical challenge.

3.3. Temporal Relationship to Stimulation and Delays in Occurrence

One criterion used to classify earthquakes as induced is a temporal correlation to the suspected anthropogenic activity (Davis & Frohlich, 1993; Schultz & Telesca, 2018). Due to the transient nature of HF completions (weeks to a month), HF-induced earthquakes are relatively straightforward to identify. In the majority of cases, earthquake rates peak during the stimulation of their associated HF pad (Lei et al., 2017; Schultz, Mei, et al., 2015; Yu et al., 2019). In many cases, ~90% of induced events occurred during the stimulation window (Figure 16) (e.g., Schultz et al., 2018). Usually, earthquake rates return to background within a few days. However, in other cases, the tapering of earthquake activity after HF completion can persist for months before returning to background levels (Atkinson et al., 2016; Ghofrani & Atkinson, 2020; Kozłowska et al., 2018). Furthermore, some of the largest magnitude events have occurred after completion of HF operations (Meng et al., 2019; Schultz et al., 2017).

In terms of rate-controlling factors, a study in the Duvernay play indicates that more than 96% of the variability in earthquake rate (in susceptible areas) is controlled by volume on a single pad (Schultz et al., 2018). Similar results have been found in a number of other basins (Fasola et al., 2019; Langenbruch & Zoback, 2019). Rarely, networked communication occurs between multiwell pads (i.e., multiple pads

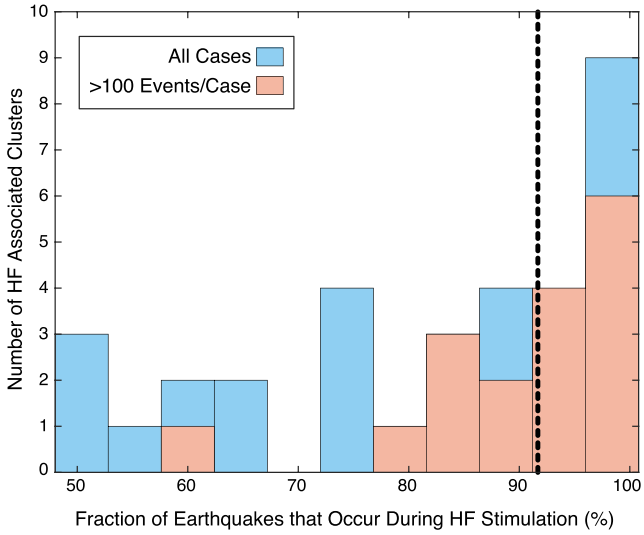

Figure 16. Histogram of earthquake percentages during stimulation. The fraction of earthquakes that occur before the HF pad was completed (bars) and the earthquake-count weighted average (dashed line) are depicted for clusters caused by mostly by Duvernay HF, with additions from the Exshaw, Arkansas, Ohio, and Oklahoma HF.

causing a single sequence of events). For example, in the Duvernay near Fox Creek only one nearby HF pad appears to have had some limited effect on a neighboring earthquake cluster (Bao & Eaton, 2016; Schultz et al., 2017). To a first order, controls on HF-induced earthquake cluster rates are isolated to just the completions of their associated pad.

Scaling down from the regional perspective to a multiwell pad level, similar observations are apparent. Admittedly, these observations are often obscured because of the narrowing gap in between stage simulations from increasingly fast completion pacing and styles (e.g., zipper fracks). However, there are noteworthy cases during the initial development of HF where simpler and slower completions caused earthquakes (Friberg et al., 2014; Kettlety et al., 2019). For example, in December of 2011 near Cardston, Alberta (Schultz, Mei, et al., 2015) a single-well pad was completed with ~24 hr between stages. In this case, earthquakes were more easily associated with discrete stages: where the first four were aseismic and the following six were seismogenic (Figure 6). Similar results can also be noted in more complex HF completions, where sufficiently close monitoring is available (Clarke et al., 2019; Eaton et al., 2018; Yu et al., 2019). In these cases, there tends to be clear and nearly immediate response (a few hours) between stage stimulation and resultant earthquakes (Kettlety et al., 2019; Kwiatek et al., 2019). As well, there is often a proximal association between these seismogenic stages and illuminated faults. Similar to what was discussed in section 3.2, there are also noteworthy cases where all stages appear to illuminate distant fault strands (up to a few km), regardless of proximity (H. Chen et al., 2018; Schultz & Wang, 2020; Yang & Zoback, 2014).

3.4. Paucity of Reported Cases

Many basins with unconventional petroleum resources have low to very low levels of historical seismicity. As a consequence, when HF induces earthquakes they dominate those of tectonic origin. Despite this, HF induces seismicity very rarely—approximately less than 1% of HF wells are associated with earthquakes (Atkinson et al., 2016; Ghofrani & Atkinson, 2020; Skoumal et al., 2015b). Some basins, such as the Williston Basin in north central United States, have no cases of induced seismicity despite similar amounts of HF activity (Figure 3). In basins with induced seismicity, HF wells that induce earthquakes tend to be spatially localized. Wells in areas more susceptible to inducing earthquakes exhibit association proportions around tens of percent, up to as large as 60% (Schultz et al., 2018; Skoumal, Ries, et al., 2018). This spatial localization persists, even after accounting for heterogeneities in regional detection capabilities. One of the factors best associated with this spatial localization appears to be depth of operation: deeper HF operations (i.e., closer to crystalline basement) are more likely to induce earthquakes (Pawley et al., 2018; Skoumal, Brudzinski, & Currie, 2018). In addition, areas where HF-induced earthquakes occur have been correlated with numerous geological factors such as proximity to carbonate reefs (Schultz et al., 2016), degree of target formation overpressure (Eaton & Schultz, 2018), or inferred ancient fluid flow along faults (Galloway et al., 2018). Even on a pad scale, localizations of seismicity are observed where induced events are asymmetrically distributed along only one side of the well laterals (Eyre, Eaton, Zecevic, et al., 2019). Interpreting this spatial bias in susceptibility as related to favorable subsurface conditions seems intuitive and similar to microseismic observations (Gale et al., 2014; Rutledge et al., 2004; Rutledge & Phillips, 2003). However, we defer our elaboration upon these ideas for the following section.

4. Interpretations and Research Questions

In summarizing the common themes observed among cases, questions come to light as to the physical processes controlling these commonalities. In this section, we discuss some interpretations of these commonalities, present competing models, and delineate unresolved research questions. Many of the subsections pull observations from prior subsections and overlap in presented ideas.

4.1. Challenges in Consistent Detection, Identification, and Reporting

Often HF-induced earthquakes have gone on unnoticed, taking years before being recognized in many cases. Here we discuss the merits and limitations of the techniques/data needed to detect, identify, and report cases of HF-induced seismicity. Ongoing research and improvements into these methods could help to better elucidate HF-induced earthquakes. This subsection discussion will pull in information from sections 3.1–3.4.

Since the initial hydraulic well stimulation test in Kansas in 1947 (Montgomery & Smith, 2010), the application of HF has grown considerably; there are now vastly more horizontally drilled HF wells being developed than conventional wells in the United States (Cook et al., 2018). Despite this proliferation, before 2012 only five basins were reported to have HF-induced seismicity worldwide (BC OGC, 2012; Clarke et al., 2014; Holland, 2013; Kanamori & Hauksson, 1992; Schultz, Mei, et al., 2015). To understand this discrepancy between pervasive HF stimulation and rarely reported induced earthquakes, it was initially suggested that the lower volumes of HF relative to wastewater disposal might be the cause (National Research Council (NRC), 2012; Rubinstein & Mahani, 2015). While volume does appear to influence the likelihood of earthquake occurrence (Schultz et al., 2018), we now know the dominant cause for this discrepancy was a combination of sparse seismic instrumentation, small induced magnitudes ($M < 3$) during HF stimulation, restricted access to stimulation records, and an underappreciated potential of this type of induced seismicity. For example, HF-induced events in Arkansas occurred in 2010 but were only disentangled from disposal related events by 2017 (Yoon et al., 2017). To determine the pervasiveness of HF-induced seismicity, large amounts of seismological and operational data had to be obtained and processed, with many such efforts only starting to become practical around 2015 (López-Comino et al., 2018). Recent advances in earthquake detection techniques have been instrumental in enriching catalogs and adaptation of clustering/association methods have helped to better identify the HF-induced cases.

4.1.1. Detection of Seismic Events

As fluid induced seismicity commonly occurs in a swarm-like manner (section 3.1), the similar nature of these sequences can be exploited to detect earthquakes commonly missed by traditional seismological processing methods. Given the sparse instrumentation and small magnitude events, several new approaches have proven to be effective for the investigation of HF-induced seismicity.

Template matching, also referred to as a matched filter detector, is an important technique for the characterization of similar seismic sources (Schaff & Waldhauser, 2010). A predetermined waveform (a template) is cross correlated against continuously recorded seismic data. In this process, previously undetected earthquakes similar to the template event can be detected. The results of template matching are dependent on many factors that include the nature of the source, network configuration, station quality, data bandwidth, and parameter selection. This technique commonly increases the number of detected earthquakes by roughly an order of magnitude (e.g., Schaff & Waldhauser, 2010). However, it is important to note that HF-induced seismicity sequences without a preidentified template event would go undetected. Because of this, template matching increases the number of detected earthquakes, but it does not improve the regional magnitude of completeness (Skoumal et al., 2020). Other, more general algorithms must be developed for this purpose. Despite this limitation, template matching has been successfully used to improve catalogs for individual HF-induced seismicity case sequences (Schultz, Mei, et al., 2015; Skoumal et al., 2015a) in addition to generating regional-scale catalogs to aid the identification of HF-induced seismicity across sedimentary basins (Schultz et al., 2017; Skoumal, Ries, et al., 2018).

Of these template matching approaches, the Repeating Signal Detector algorithm was created to detect similar earthquakes without the need for a starting earthquake catalog (Skoumal et al., 2016). By clustering signals of interest (most of which are expected to be noise) according to their frequency and time domain characteristics, families of repetitive events are identified. These families are stacked to improve the signal-to-noise ratio, and the resulting stacked signals are then used as templates in a template matching routing. Repeating Signal Detector has been used to detect HF-induced seismicity on both local (<5 km) and regional (~50 km) scales in the United States and Canada (Chiorini, 2019; Skoumal et al., 2016). Huang and Beroza (2015) used template matching to a single station to the Guy-Greenbrier, Arkansas earthquake sequence creating over 460,000 detections, more than 100 times the number of earthquakes in the ANSS catalog. However, the false positive rate was high (Yoon et al., 2017), which is a shortcoming of the template method as there is no fixed value for waveform similarity.

FAST generalizes this approach, by detecting earthquakes without a starting catalog or templates (C. E. Yoon, O'Reilly, et al., 2015). FAST conducts an unsupervised search using a highly efficient algorithm to identify similar waveforms in continuous data. FAST utilizes locality-sensitive hashing, and similar waveforms are grouped together in hash buckets based on the discriminative features of the signals. To date, FAST has only been applied to detect HF-induced seismicity at the Guy-Greenbrier Arkansas sequence using a single seismometer ~10 km away (Yoon et al., 2017), but it has been demonstrated to detect natural seismicity more than 500 km from a multistation network (Yoon et al., 2019). A direct comparison between template matching (Huang & Beroza, 2015) and FAST (Yoon et al., 2017) for the initial 3 months of the Guy-Greenbrier sequence achieved comparable results. FAST found 658 events missed by template matching while missing 1,578 that template matching found. Both methods result in superior catalogs to traditional network processing methods such as short-term average/long-term average (STA/LTA) detection.

Rapid progress in the application of machine learning methods to event detection, timing, association, and location is transforming the analysis of both natural and induced seismicity (Bergen et al., 2019; Mousavi et al., 2019). New machine learning algorithms for automatic detection and picking of *P* and *S* wave arrivals in continuous data are beginning to achieve results comparable to template matching and superior, in some cases, to traditional methods (Liu et al., 2020). For example, Park et al. (2020) applied the PhaseNet picker (Zhu & Beroza, 2018) to the entire Guy-Greenbrier, Arkansas, sequence to detect over 280,000 events (single station) and located almost 90,000 events, compared to fewer than 2000 reported by Horton (2012) using standard network procedures or 13,000 found by FAST. ConvNetQuake, a convolutional neural network, has been applied to detect induced seismicity in Oklahoma (Perol et al., 2018). Applications of these types of detection algorithms to HF-induced seismicity are just beginning (Dokht et al., 2019), with significant potential for these algorithms to improve the detection of HF-induced sequences. While we have focused on detection of events, we acknowledge that advancements in the earthquake location procedure have also been important for discerning cases of induced earthquakes (Cesca & Grigoli, 2015; Grigoli et al., 2017; Kwiatek et al., 2013; Li, et al., 2020; Niemz et al., 2020; Waldhauser & Ellsworth, 2000). As HF-induced seismicity frequently demonstrates strong spatiotemporal correlations with well operations, improving the seismic catalog can significantly increase the confidence in determining whether an earthquake sequence is associated with well operations.

4.1.2. Associating Earthquakes With HF

Several approaches have proposed to associate earthquakes with HF. Due to the aforementioned improvements in detection capabilities, many association approaches have focused on quantifying temporal and spatial relationships. For example, windowed spatiotemporal associations have been used to initially screen potential cases of HF-induced seismicity (Atkinson et al., 2016). Using simple space-time windows, HF wells are flagged if there is seismicity within a specified distance (e.g., 5 km) and time window during/after the stimulation interval (e.g., during stimulation and up to one month after). These screening criteria are often based on spatiotemporal associations noted in prior cases (sections 3.1 and 3.2). Using these flagged cases, further manual inspection remains the best current approach to identify cases of HF-induced seismicity. These spatiotemporal associations are a simple and effective approach to reduce the number of earthquakes and wells to inspect, but they provide limited statistical means to validate the strength of associations. Moreover, spatiotemporal associations are ineffective at distinguishing from natural seismicity or induced seismicity from other sources (e.g., wastewater disposal) which may occur in close proximity to HF operations. In these cases, additional criteria that account for the background seismicity and local geology are required to evaluate whether a sequence was induced by HF (Davis & Frohlich, 1993; Verdon et al., 2019).

Building on these windowing associations, the causal relationship of potential HF-induced seismicity cases has been investigated using a likelihood association between earthquakes and wells (Lomax & Savvaidis, 2019). Earthquake-well spatiotemporal window differences are weighted by a Gaussian taper. Earthquakes that exceed a cutoff threshold are relocated by constraining its hypocenter at a point along the HF well, and the phase residuals are used to determine ground truth station corrections. This has been applied to investigate HF-induced seismicity in the Permian Basin in West Texas (Lomax & Savvaidis, 2019).

Other measures have also been proposed for the identification of HF-induced seismicity. In the ΔEQ_{rate} approach, the earthquake rate during stimulation is compared to rates before and after the stimulation (Skoumal, Ries, et al., 2018; Skoumal et al., 2019). This approach provides a simple means to sort wells in a basin based on their degree of seismicity rate change. To determine a statistically significant ΔEQ_{rate}

threshold, earthquake origin times are randomly shuffled in a bootstrap process. This approach has been applied to identify HF-induced seismicity using large-scale template matching catalogs in both Oklahoma and Texas (Skoumal, Ries, et al., 2018; Skoumal et al., 2019).

Similarly, the robustness of the association between HF and seismicity has been determined using the algorithm ReshuffleCorr (Schultz & Telesca, 2018). With this approach, two time series (HF stimulation volume and binned earthquake counts within a cluster) are cross correlated to determine the strength of association and potential delays. Monte Carlo approaches randomly reshuffle the spectral phase information of cross-correlation functions to test for spurious correlations and statistical significance (Schultz & Telesca, 2018). ReshuffleCorr has been used in a number of induced earthquake cases to discern the statistical significance (e.g., >99.7%) of temporal associations (Schultz, Mei, et al., 2015; Schultz et al., 2014; Schultz, Stern, et al., 2015).

The four HF-induced seismicity association approaches listed above are intended to aid in identifying HF operations that caused earthquakes. In the majority of cases, spatiotemporal associations can be used to confidently identify which clusters of earthquakes were induced by HF (Davis & Frohlich, 1993; Verdon et al., 2019). On the other hand, many of these approaches struggle to confidently recognize HF cases when occurring contemporaneously to other sources of seismicity, either natural or induced. As well, poorer earthquake catalog resolutions can be detrimental to associating induced earthquakes with HF pads. Advances in the algorithms used to identify and associate earthquake sequences to HF completions would benefit from a focus on these drawbacks. While the listed approaches have varying degrees of sophistication and limitations, all of these approaches are similar in that they require detailed information of HF stimulation times and locations.

4.1.3. Limitations of HF Reporting

One of the greatest factors currently inhibiting the scientific investigation of HF-induced seismicity is the limited extent of public reporting of HF operations, specifically where and when individual stages are stimulated with how much fluid and pressure. In some jurisdictions, such as Canada and the state of Arkansas, the submission of HF stimulation reports is required by the regulators. However, in many required submission cases, these data are in inconvenient hardcopy formats, although third-party commercial vendors (e.g., AccuMap and GeoScout) have been providing increasingly convenient and complete digital formats with time. As well, recent developments in regulations in Alberta, Canada, have begun the mandated submission of seismological data collected as part of HF earthquake-related regulations. For example, the SCISMN is a repository on the Incorporated Research Institutions for Seismology (under the Network Code 2K_2014) that houses seismological data submitted to the regulator (Schultz, Yusifbayov, & Shipman, 2020). The traffic light protocol near Red Deer, Alberta, requires that industry submitted data are collected in real time and publicly released after a 1-year embargo (AER, 2019). In studies where stimulation reports have been supplemented with industry-derived seismological data, more confident assessments of the extent of HF-induced seismicity and the underlying mechanics have been made (Eaton et al., 2018; Eyre, Eaton, Zecevic, et al., 2019).

That said, the degree of access to this information can vary strongly by jurisdiction. For example, in the United States, most HF-induced seismicity research has relied on operators self-reporting to FracFocus (https://fracfocus.org/). While the investigation of HF-induced seismicity is not the intended purpose of FracFocus (a chemical composition repository), this is often the only publicly available source that includes an approximate spatiotemporal record of HF stimulations. Reported operational times are in the form of an approximate start and end date of stimulation activities at a well, with no information regarding the number, timing, or duration of individual stimulation stages disclosed. Several states began requiring reports to FracFocus beginning around 2012. However, even in states where reporting is mandatory, the accuracy and completeness are still suspect; in Oklahoma, ~8% of HF operations were not reported to FracFocus even after state reporting regulations went into effect (Skoumal, Ries, et al., 2018).

4.2. *b* Values Larger Than 1.5?

Many cases of HF-induced seismicity have encountered recurrence statistics that are atypical of natural earthquake sequences, especially near microseismic magnitudes ($Mw < 0$). This is intriguing from an energy release perspective, since *b* values larger than 1.5 predict a nonphysical infinite energy release. Here, we discuss some of the interpretations of these anomalous recurrence statistics. This subsection discussion will pull in information from sections 3.1 and 3.2.

The Gutenberg-Richter relationship provides a fundamental statistical description of seismicity within a given region (Gutenberg & Richter, 1944), which is critical for estimating the likelihood of larger earthquakes from an initial set of smaller events (Weichert, 1980). This relation defines the frequency-magnitude distribution as $log_{10} N_M = a - b$M, where N_M is the cumulative number of earthquakes larger than M, the a value characterizes the overall rate of seismicity, and the b value quantifies the proportion of large to small events. As in many self-similar distributions in nature, there is evidence for a long-term constant and universal b value of 1.0 (Burridge & Knopoff, 1967; Kagan, 1999). However, deviations from this value are thought to represent a wide range of physical phenomena (El-Isa & Eaton, 2014; Scholz, 1968; Schorlemmer et al., 2005). In particular, studies in areas where underground fluid injection is performed have associated changes in b value with changes of pressure gradient (Bachmann et al., 2012; Mousavi et al., 2017) or resolved shear stress (Dempsey et al., 2016). However, the ultimate importance of characterizing b values is that it is useful for forecasting the likelihood of larger events. For example, lower b values indicate more larger events relative to a typical population (i.e., 1.0) and hence a larger hazard.

Microseismicity studies have typically found that seismicity during injection is characterized by lower event magnitudes ($Mw < 0.0$) and higher b values (often ~2) but then can increase in magnitude or drop to b values that are more typical of natural seismicity (~1.0) between stages or after the end of pumping (Eaton et al., 2014; Maxwell et al., 2009; Wessels et al., 2011; Wolhart et al., 2006). Based on the locations and focal mechanisms of the different groups, a high b value seismicity is associated with activation of fracture networks while the low b value seismicity occurred on a preexisting fault outside the treatment zone. There are several potential explanations for why microseismic fracturing has a high b value; one hypothesis posits that, in the absence of activation of a large-scale fault system, the magnitude distribution of microseismicity is tapered at high magnitudes, following a form of the magnitude-frequency distribution such as described by Kagan (2010). A tapered magnitude distribution could result from the existence of an upper limit on source dimensions; this scenario is expected, for example, where microseismicity is linked to reactivation of a stratabound fracture network (Eaton et al., 2014). In the case of a tapered magnitude-frequency distribution, if the slope is measured within the tapered part of the distribution, it will always be greater than the slope of the main part of the distribution (Eaton & Maghsoudi, 2015). This scenario could occur if rupture dimensions of observed microseismicity approach the maximum fracture size (Eaton et al., 2014); in this case, only the tapered part of the distribution is observed, thus leading to an unusually high apparent b value.

Analysis of larger HF-induced seismicity in Ohio also found two groups of seismicity with higher (>1.5) and lower (<1.0) b values (Kozłowska et al., 2018). In this case, the depth distribution revealed the higher b value seismicity occurred within Paleozoic sedimentary rocks about 400 m below the target interval and lower b value seismicity occurred about 600 m deeper than the first group in the Precambrian basement. The seismicity appeared to occur on a single fault system originating in the Precambrian basement and continuing into Paleozoic strata. Subsurface stratigraphic mapping and seismic reflection data reveal basement-involved faults in eastern Ohio have experienced multiple periods of deformation throughout the Paleozoic, indicating fault zones would be more mature lower in the stratigraphic section, with the highest degree of maturity in the Precambrian basement (e.g., Baranoski & Riley, 2013). Recent lab and field results suggest fault maturity plays a key role in the frequency-magnitude distribution observed, with smoother faults allowing for larger events and lower b values (Goebel, Kwiatek, et al., 2017; Savage & Brodsky, 2011). This would suggest that the older, more mature Precambrian faults would have a smoother surface, which would promote larger slip and lower b values than younger, less mature, and thus more rough Paleozoic faults. This hypothesis is similar to the previous one, inasmuch as the magnitude distribution may exhibit a scale-dependent upper bound due to scale dependence of slip surfaces on immature faults.

Using a microseismicity data set from the Fox Creek area of Alberta, Igonin et al. (2018) also found significant spatial and temporal variability in b value within a single-well pad. The frequency-magnitude distribution showed a bilinear pattern with the intersection at $M \sim 1$, separating b values of 1.6 and 0.6 at small and large magnitudes, respectively. This was due to a superposition of clusters with b values close to 2.0 and other clusters with much lower b value. The event distribution further showed b value was influenced by the orientation and depth expression of the faults. In particular, seismicity clusters were associated with relatively low b values if they were characterized by narrow bands in focal depth and if they delineated fault planes that were well oriented for slip in the present-day stress field. Conversely, seismicity clusters that exhibited a

wider depth range and defined structures that were not well oriented for slip and appeared to be associated with higher *b* values.

In addition, several recent studies of HF-induced seismicity identified departures from the expected log linear power law relationship between frequency and magnitude. In some cases, the relationships appeared to taper with a curvature that produces fewer larger events relative to what is expected for a linear relationship (Eaton et al., 2014; Kozłowska et al., 2018). Similarly, tapered frequency-magnitude distributions have been found in disposal-induced seismicity (Huang & Beroza, 2015), and the cumulative injected volumes have provided a good constraint on the seismic moment, consistent with the idea that the finite size of the stimulated medium limited earthquake source volumes (Shapiro et al., 2011). For both HF and disposal events, the tapering tends to disappear after injection ends, suggesting that postinjection earthquakes reflect the activation of a larger fault system (see above) or are triggered by remaining stress concentrations away from the injection point (Segall & Lu, 2015).

The other cases of departure (from the expected log-log power law relationship) are distributions that follow a nonlinear trend with a curvature that produces more large events relative to what is expected for a linear frequency-magnitude relationship (Igonin et al., 2018; Kozłowska et al., 2018)—similar to some cases of disposal-induced seismicity (Skoumal et al., 2015c). These outliers have primarily occurred in the later stages, presumably when faults were being restimulated. This suggests that the activation of larger fault patches is influenced by the time and volume of fluid injected into the system and that the earlier, weaker seismicity occurred during fault loading. This pattern may be related to the characteristic earthquake model (Igonin et al., 2018), which hypothesizes that earthquake rupture occurs episodically on fault patches that are a large fraction of the total fault area, or the runaway rupture model (Galis et al., 2017), which hypothesizes that ruptures extend beyond the perturbed region of a fault (these two models are not mutually exclusive). For such systems, the larger characteristic earthquakes occur more frequently than would otherwise be predicted from frequency-magnitude distributions sampled during the interseismic time interval (Wesnousky, 1994).

4.3. Earthquake Triggering Mechanisms

One of the most important questions to discuss is the physical mechanism that allows earthquakes to nucleate in response to HF. In general, it is well established that induced earthquakes preferentially occur on faults that are close to failure in the prestimulation tectonic stress field; in other words, they occur on critically stressed/oriented faults. However, the means of perturbing stress on the fault is more contentious, as there are multiple proposed mechanisms to communicate stress changes (Figure 17). This subsection discussion will pull in information from sections 3.2 and 3.3.

The first proposed mechanism is also the oldest explanation for injection-induced seismicity (Hubbert & Rubey, 1959; Healy et al., 1968): Slip initiation is related to increased pore pressure within the fault, reducing the effective normal stress until reaching the point of failure. In the cases (section 3.2) where seismogenic faults are within proximity of stimulated fractures, pressure can plausibly migrate to the fault through conductive channels. HF stage stimulation propagates fractures that can intersect the hydraulically conductive damage zone of a fault (R. J. Davies et al., 2012; Wilson et al., 2018). Pore pressure propagates along this pathway, initiating slip on the weakest segment of the fault. In fact, cases that have accounted for the complete state of stress (Shen, Schmitt, & Haug, 2019) have found that slip initiation is guaranteed for most fault orientations under reasonable HF stimulation pressures (Shen, Schmitt, & Schultz, 2019; Lei et al., 2019), thus relaxing the requirement for a fault to be optimally oriented.

However, these arguments become less convincing (or more interesting) as we begin to consider cases with distant communication (Holland, 2013; Schultz & Wang, 2020). These distant but rapid earthquake responses would require preferential pathways for pressure migration to channel along. These ad hoc arguments are reinforced by the localization of HF-induced earthquakes (section 3.4) to geologically exceptional areas (Pawley et al., 2018). For example, many cases of HF-induced earthquakes are related to transtensional or transpressional flower structures (Chopra et al., 2017), a fault architecture especially conducive to fluid flow (Cox, 2016). Furthermore, inferential evidence of paleo fluid flow along a fault (resulting in karst collapse and brecciation) has also been associated with HF-induced earthquakes (Galloway et al., 2018). Cases have been observed where large changes in water production are observed after encountering

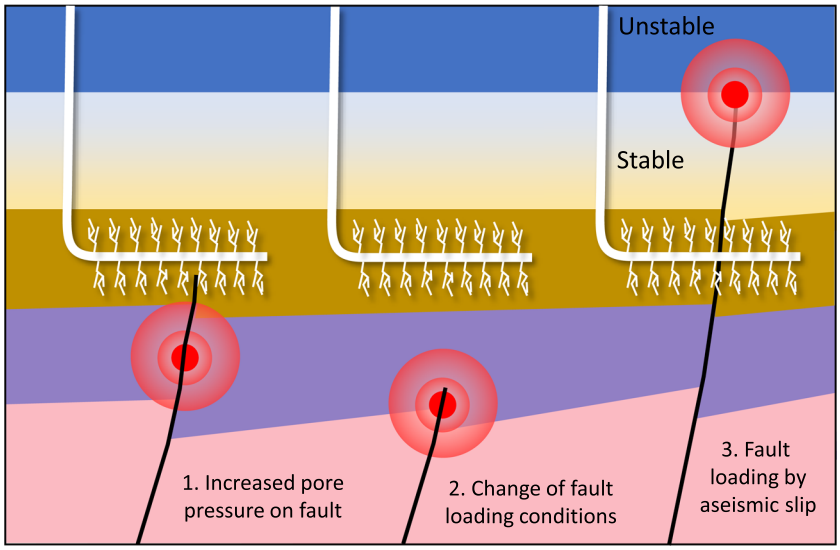

Figure 17. Conceptual diagram of HF earthquake triggering mechanisms. Three proposed mechanisms are displayed from left to right: direct pore pressure communication, poroelastic stress transmission, and pore pressure causing aseismic slip. Figure reproduced from Eyre, Eaton, Garagash, et al. (2019).

induced seismicity (Kozłowska et al., 2018). Supporting this, anecdotal stories of "frack hits" (cases where fluid/pressure communication is observed between wells) have been noted at distances of up to 1–2 km. Specifically, a comprehensive study of well pressures, radioactive tracers, and microseismic data during "frack hits" in the Horn River Basin suggested that fluid connectivity occurs along fault pathways at distances of up to 1.2 km (Fu & Dehghanpour, 2020). Based on these findings, it seems that the role of fluid flow along fault damage zones is an important aspect to better understanding HF-induced earthquakes (Guglielmi, Elsworth, et al., 2015; Shapiro & Dinske, 2009).

The second proposed mechanism introduces the concept of poroelastic stress transmission (Segall & Lu, 2015). In this constitutive framework, fluid pressure within pore space is coupled with elastic stresses of the rock frame. This concept provides a reasonable means to account for shut-in phenomenon such as increases in earthquake rate or the occurrence of the largest-magnitude event after HF completion. It can also help with cases where seismicity initiates ~1 km from injection within 2–3 hr, implying hydraulic diffusivities more than an order of magnitude larger than diffusion-triggered estimates (Kozłowska et al., 2018; Shapiro & Dinske, 2009). Furthermore, poroelasticity allows for distant communication, without any special considerations for fault architecture—this interpretation is especially enticing in cases where all stages appear in communication with the seismogenic fault (section 3.2). Poroelastic contributions have been proposed as the triggering mechanism at large distances from waste water disposal wells (Goebel & Brodsky, 2018; Shirzaei et al., 2016; Zbinden et al., 2019). Similarly, numerical simulations have suggested poroelastic effects are consistent with inferred values of stress changes needed to induce slip during HF (Deng et al., 2016). However, these models have also been criticized for their handling of how stimulated fracture propagation, fault slip, and fault architecture influence permeability and stress transmission (Lele et al., 2017). As well, poroelasticity is potentially problematic for explaining HF cases where only certain stages are seismogenic, since it is not generally clear how the poroelastic model could be stage selective, unless the stage locations relative to the fault vary enough for the orientation of stress applied to the fault to change substantially. Likely, disentangling the relative contributions of pore pressure and poroelasticity will require adequate modeling of how fracture propagation and fault architecture influence fluid and stress transmission (Faulkner et al., 2010; Gale et al., 2014; Haddad & Eichhubl, 2020; Ortiz et al., 2019; Zbinden et al., 2020). In this case, the application of expertise from disciplines outside of seismology, such as geomechanics and rock mechanics, may be useful to constrain the problem and models from a different perspective. As well, this area would likely benefit from contrasts against slower injection-induced seismicity, such as disposal-related cases.

A third possible mechanism is a hybrid model wherein fault loading occurs through a combined process of pore pressure change and aseismic slip. Here, fluid flow along fractures is still suggested to intersect faults; however, the slip at this portion of the fault is postulated to initiate aseismically, with creep along the fault outpacing the pore pressure migration front (Bhattacharya & Viesca, 2019; Guglielmi, Cappa, et al., 2015). This model is consistent with in situ and laboratory experiments, suggesting that fine-grained rocks that are clay rich and/or organic rich exhibit velocity-strengthening behavior, in accordance with rate-state friction theory (Cappa et al., 2019; Kohli & Zoback, 2013; Scuderi & Collettini, 2016, 2018). Heimisson et al. (2019) found theoretical evidence for the generation of slow slip pulses on mildly rate-strengthening faults in response to pressure perturbation through poroelastic effects. The existence of aseismic fault slip during injection has support in the observation that moment released from the injection process is aseismic deformation and strain, with only minor proportions from seismic sources (De Barros et al., 2018; Goodfellow et al., 2015; Kwiatek et al., 2018). In this model, dynamic rupture may then initiate after creep propagates along a stable (velocity-strengthening) segment of a fault. Hydraulic communication could be slightly restricted in extent, only causing nearby aseismic slip that subsequently triggers more distant seismic slip (Eyre, Eaton, Garagash, et al., 2019). Anecdotal evidence of well bore shearing and deformation could be related to this mechanism (Mohammed et al., 2019). However, asserting or refuting this conjecture will require pad-scale in situ measurements of strain and displacement, complemented by lab experiments using pressures above the fracture gradient (Gischig et al., 2019). Overall, scrutinizing the unique high-pressure stimulation operations causing HF-induced earthquakes could help yield a better understanding of the processes responsible for earthquake nucleation and the dynamics of slip behavior.

4.4. Geological Susceptibility to HF-Induced Earthquakes

In this section, we introduce the concept of geological susceptibility: an interpretation suggesting that subsurface conditions control the likelihood of where HF-induced earthquakes are observed (or not). This subsection discussion pulls in information from sections 3.2 and 3.4.

Cases of HF stimulation-inducing earthquakes are typically rare, less than 1% at a basin scale (Atkinson et al., 2016; Ghofrani & Atkinson, 2020; Skoumal et al., 2015b). In smaller regions, this proportion increases (section 3.4) to upward of tens of percent (Schultz et al., 2018; Skoumal, Ries, et al., 2018). One of the clearer factors associated with this localization appears to be depth of the HF operation; deeper stimulations are significantly more likely to encounter HF earthquakes (Pawley et al., 2018; Skoumal, Brudzinski, & Currie, 2018). Often, the association made here is that proximity to crystalline basement increases the likelihood of encountering basement-rooted faults with depth (Anderson & Underhill, 2020; Chopra et al., 2017; Corlett et al., 2018). In this sense, depth is utilized as a proxy for a geological factor that is conducive to induced seismicity. As well, the depositional history of basins has been inferred as a proxy for fault structure (Corlett et al., 2018; Schultz et al., 2016) and fluid flow along wrench faults (Cox, 2016; G. R. Davies & Smith, 2006). Again, tectonic and hydrological proxies are noted in cases where karst collapse (related to fluid flow along faults) is another proxy for susceptible regions (Galloway et al., 2018), similar to microseismic studies noting prevalence of stimulated events coincident with low-impedance flow paths (Rutledge & Phillips, 2003).

Geomechanical factors such as target formation overpressure have been statistically linked to HF-induced earthquake locations (Eaton & Schultz, 2018) and interpreted as a proxy for slip potential and fault-valve processes (Sibson, 2020). Certainly, the state of in situ stress has a strong influence on which faults can host slip (Shen, Schmitt, & Haug, 2019; Shen, Schmitt, & Schultz, 2019; Zoback & Lund Snee, 2018). In many basins, the regional state of stress has been quantified (Lund Snee & Zoback, 2016, 2018), allowing for an indication of which faults may potentially host slip (Hennings et al., 2019). A tectonic factor controlling HF-induced earthquakes locations has been proposed in Alberta and BC based on the correlation between regions of higher tectonic strain rate and the intensity of HF-induced seismicity (Kao, Hyndman, et al., 2018). However, HF seismicity is also abundant in the central United States where the tectonic strain rates are much lower than the low strain rate and relatively aseismic areas in Canada (Calais et al., 2016; Ellsworth et al., 2015). Release of stored tectonic strain on favorably oriented and critically stressed faults would appear to be the critical factor in areas such as Oklahoma.

Overall, interpreting this spatial localization of susceptibility as related to proxies for favorable subsurface conditions seems intuitive. Based on this success with proxies, a machine learning approach was

developed that systematically ranked the importance of all (publicly available) proxies and simultaneously estimated the geological susceptibility (Pawley et al., 2018; Schultz & Pawley, 2019). This ranking of proxy importance allows for prioritizing areas of further research or identifying new factors that were previously overlooked. Similar statistical approaches have been taken in other plays, like the South Sichuan Basin (Hu et al., 2018). Similar localizations of disposal-related earthquakes have been observed in Oklahoma (Langenbruch et al., 2018).

Much of the previous discussion has revolved around the use of statistical methods and proxies for tectonic, geomechanical, hydrological, or geological conditions to infer susceptible regions. Understandably, much of this impetus has been related to practical difficulties in reliably imaging subtle (often strike-slip) fault structures on the order of 1 km (or less) a priori. In addition to this, HF pads are almost always new stimulations in new locations, so characterizing undiscovered fault systems is usually an ongoing challenge. Even in cases where 3-D reflection seismic data are available, difficulties arise in both identifying the existence of all faults and then correctly assigning which are likely to be seismogenic (Eaton et al., 2018). Unfortunately, it would seem that fluid injection (coupled with monitoring of earthquakes) is one of the best techniques for locating seismogenic faults. That said, there is likely room to integrate more physics-based approaches (Maxwell et al., 2015; Rutqvist et al., 2015; Walsh & Zoback, 2016; J. S. Yoon, Zimmermann, et al., 2015) into understanding geological susceptibility.

4.5. Operational Controls, Forecasting Methods, and Mitigation

The imposition of regulations and traffic light protocols around HF-induced earthquakes has driven recent research toward forecasting and mitigation of induced earthquakes. Important to answering this question is better understanding the controls that HF operators have at their command. This subsection discussion will pull in information from sections 3.1 and 3.3.

Given HF stimulation in a susceptible area, observations of HF-induced earthquakes have suggested that their sequences are dominantly swarm like with limited amounts of aftershock productivity (section 3.1). Thus, volume-based metrics are anticipated to control earthquake rates, especially considering their success in modeling other induced seismicity cases (Shapiro & Dinske, 2010). Accordingly, completion volume has been shown as one of the most significant operational controls on HF-induced seismicity (F. Zhang, Yin, et al., 2019; Fasola et al., 2019; Langenbruch & Zoback, 2019; Schultz et al., 2018). Based on these concepts, statistical volume-based forecasting approaches have been developed (Karimi & Baturan, 2018; Mignan et al., 2017). For example, the case at Preston New Road (PNR-1Z), the United Kingdom implemented a real-time forecasting approach to keep HF seismicity within levels deemed acceptable by the local regulator (Clarke et al., 2019). However, Clarke et al. (2019) had to retrospectively alter the approach to account for a previously unidentified fracture zone and the method did not perform well for the second operation (PNR-2). The post mortem analysis of the Pohang enhanced geothermal system successfully determined risk-informed shut-in thresholds (Langenbruch et al., 2020). Moreover, epidemic-type aftershock sequence (ETAS) approaches have been applied to model seismicity rates, as a function of injection rates (Bachmann et al., 2011; Lei et al., 2017). Likely, forecasting approaches developed for enhanced geothermal systems could be easily adapted here as well (Gaucher et al., 2015).

On the other hand, there has been mounting evidence that volume does not entirely control the maximum magnitude of HF-induced earthquakes (Atkinson et al., 2016). In particular, the 5.5 M_W Pohang, South Korea, earthquake injected only 1/500 of the volume expected for an earthquake of this magnitude, according to some models (Ellsworth et al., 2019; Woo et al., 2019). Instead, tectonic factors such as fault length and slip area ultimately constrain the maximum magnitude earthquake any given fault can host (Aki & Richards, 2002; Zoback & Kohli, 2019). With these tectonic considerations, the statistical nature of seismicity can be factored into the temporal evolution of maximum magnitude (van der Elst et al., 2016).

Despite these understandings, the decision-making process and quantification of effective mitigation have been sparsely published (CAPP, 2019). Likely, much of this information is kept proprietary by the operators. As well, the complexities of disentangling geologically susceptible conditions from operational response remains very challenging (section 3.3). On the other hand, there are general mitigation approaches that can be grouped into two categories: reactionary mitigation strategies and longer-term planning/avoidance strategies. For the reactionary mitigation strategies, there is a general suite of approaches that are often

applied (CAPP, 2019): rate/pressure/volume reduction, stage pausing, stage skipping, and as a last resort well/pad abandonment. For example, reductions in stage rate/pressure/volume in response to earthquakes during geothermal stimulation were employed to mitigate against a disruptive red light event (Kwiatek et al., 2019). For the longer-term planning and avoidance strategies, there is also a general suite of approaches (CAPP, 2019): these include earthquake monitoring, stress measurement, geophysical hazard preassessments, stimulation fluid design, well/pad orientation, stage spacing, and completion schemas (e.g., single wells and zipper fracks). Here, learnings from these data sets inform longer-term HF completion planning. For example, both quicker HF completion schemas and multiwell pads have been found as more likely to encounter induced earthquakes (Fasola et al., 2019). As well, unique stage completion strategies could be tailored to minimize induced earthquakes while simultaneously allowing for permeability enhancement (Zang et al., 2013). There are currently no guarantees; however, as a similar cyclic pumping strategy employed during long-term injection in the Paradox Valley Project in Colorado (King et al., 2016) did not prevent a 4.5 *Mw* earthquake in 2019. Further discoveries on the conditions that trigger HF earthquakes would be invaluable to developing more effective mitigation strategies. Verification of these results from hydrogeomechanical modeling studies (Jeanne et al., 2014; Maxwell et al., 2015; Rutqvist et al., 2015) will also be invaluable to ascertain the physical mechanisms involved in mitigation. These types of studies have been sparse in the HF earthquake literature; however, the modeling approaches from enhanced geothermal systems will likely be portable to HF-induced earthquakes (Rathnaweera et al., 2020).

4.6. Effective Regulation and Traffic Light Protocols

With these HF-induced earthquakes comes a need to manage their hazards, risks, and nuisances. Here, regulatory agencies are responsible for designing a rule set that enforces a tolerable amount of risk to the public and industry—these rules are then imposed on operators, who must mitigate to stay within the prescribed boundaries. This subsection discussion pulls in information from sections 3.2–3.4.

Traffic light protocols are the de facto rule set choice used to manage induced earthquakes (Baisch et al., 2019; Kao et al., 2016; Wong et al., 2015; Walters, et al., 2012). Within most traffic light protocols, an operator is allowed to complete their wells unrestricted during a green light, must begin reactionary mitigation strategies after the yellow light, and must suspend operations after a red light. Traffic light protocols have been implemented in many of the basins that have encountered HF-induced seismicity: including in the United Kingdom (Clarke et al., 2019), Alberta (AER, 2015; 2019), BC (Kao et al., 2016), Ohio (Wong et al., 2015), and Oklahoma (OCC, 2016). We note, however, that not all jurisdictions have subscribed to the same philosophy of traffic light management. For example, the red light threshold (0.5 M_L) in the United Kingdom only requires that operators temporarily suspend their operations. Mixing prescribed mitigation into a regulation carries some burden, as it stymies the development of more effective mitigation strategies. On the other hand, some jurisdictions encountering HF-induced earthquakes have neglected regulatory controls. Scientific developments and risk-based recommendations on traffic light protocol design will be required to bring greater credibility and transparency to these rule sets (Schultz, Beroza, et al., 2020).

From a regulatory perspective, traffic light protocols must encourage simple and robust risk-reducing decisions with limited information (Kao et al., 2016; Schultz, Beroza, et al., 2020; Shipman et al., 2018). For example, local magnitude-based thresholds (M_L) have been implemented to delineate traffic light thresholds in virtually all jurisdictions, likely due to its simplicity in computation—although there are considerations to make here about suitable magnitude calibrations. Because M_L does not have physical units and depends on local wave propagation characteristics, it is important to set the scale in a consistent manner, typically by reference to *Mw*. This requires calibration, which can be done empirically once activity is detected (Babaie Mahani & Kao, 2019; Butcher et al., 2017; Yenier, 2017) but may also be done using knowledge of crustal structure before seismicity occurs (Al-Ismail et al., 2020). Along the lines of emphasizing simplicity, spatiotemporal relationships (e.g., all contemporaneous earthquakes within 5 km) are used to rapidly evaluate if a HF pad stimulation induced an earthquake (Davis & Frohlich, 1993; Skoumal et al., 2019). Due to prior observations of earthquakes in spatiotemporal association with the HF pad (sections 3.2 and 3.3), this approach works reasonably well. As well, the spatial localization of HF-induced seismicity susceptibility (section 3.4) has often been utilized to restrict traffic light protocols to just the seismogenic formations and regions. Recently, efforts have been made in Alberta to begin collecting industry seismological data in

real time and release it publicly after a 1-year embargo (AER, 2019; Schultz, Yusifbayov, & Shipman, 2020). Despite these understandings, little work has been done to rigorously quantify the impacts of traffic light protocols designs and effective performance management (Kao, Visser, et al., 2018; Schultz, Beroza, et al., 2020; Shipman et al., 2018). Likely, findings from other induced earthquake cases, such as enhanced geothermal systems, could be adapted to HF-induced earthquakes (Baisch et al., 2019; Mignan et al., 2015). For example, by utilizing ground motion thresholds and distance-magnitude scaling relationships to inform better magnitude threshold choices (Bommer et al., 2006; Rodríguez-Pradilla & Eaton, 2019). To date, the only HF-oriented studies on this subject has been directed toward the impacts/risks on critical infrastructure (Atkinson, 2017) and developing risk-informed choices on nuisance and damage for choosing magnitude thresholds (Schultz, Beroza, et al., 2020).

5. Summary

Induced seismicity caused by HF has grown in recognition in recent years. In this paper, we have reviewed of all the currently documented cases of HF-induced earthquakes worldwide: within Canada, the United Kingdom, the United States, and China. We have noted cases where HF has induced events as large as 5.7 M_L, earthquakes are triggered up to 1.5 km away from their causal pad, and red light thresholds that have been set as low as 0.5 M_L. In examining these disparate cases, we also identified themes in common: similarity of waveforms, swarm-like clustering, proximity to causal pad, temporal relationship to stimulation, and rarity of occurrence. We expanded upon these commonalities by presenting the previously established interpretations. For example, in discussing the possible triggering mechanisms, the factors control the localization of HF-induced earthquakes, the operational controls influencing the rate of events, and effective management via traffic light protocols. Ultimately, a better understanding of these key features of HF-induced earthquakes will facilitate informed management of their associated risks.

Glossary

Breccia	A rock composed of other broken rock fragments, often cemented together.
b value	A metric used to measure the relative proportion of small to large earthquakes.
Completion	In industry jargon, completion is the series of processes after drilling to bring a well into production. HF is a part of completion in many unconventional wells.
Critically stressed	A description of the state of stress on a fault, where it is nearly ready to produce earthquake slip. To be critically stressed, a fault has to have the proper orientation in the present-day stress field.
Damage zone	A region around a fault core that is intensely fractured and therefore permeable, allowing for fluid flow.
Enhanced geothermal system	A system process designed to extract heat energy from the subsurface. Wells are drilled and HF stages stimulation is used to enhance the permeability of hot and deep rocks. Due to the use of HF in this process, enhanced geothermal systems often encounter induced earthquakes similar to petroleum development HF cases.
Epicenter	The location of the point of initiation of an earthquake, projected to the Earth's surface.
Fractures	A planar discontinuity in a medium. Fractures that lack shear offset are called joints. Fractures can accommodate fluid flow along the spaces between the rocks.
Fault	Similar to a fracture, but larger. A discontinuity in a rock that has hosted earthquake slip in the past. In the context of HF-induced seismicity, this is often distinguished from fractures that are intentionally stimulated for resource production and faults that are accidentally reactivated to cause earthquakes.

Flowback	The process of flowing stimulation fluids back to the surface after HF completion.
Frack hits	Adjacent wells may encounter circumstances where fluid/pressure communication is established between two or more wells during completion. Typically, this is not intended and has detrimental consequences for productivity. Synonymously, it is also called well interference.
Heel	The horizontal section of a well just after it deviates from vertical into horizontal.
Horizontal well	A well that is drilled vertically, until reaching the target formation where it is deviated into a horizontal orientation. The section where the transition from vertical to horizontal occurs is called the "heel" and the end of the horizontal portion is called the "toe" (Figure 1). Typically, horizontal sections are up to 2 km in length.
Hydraulic fracturing (HF)	A technique in which fluid is pumped into the ground at pressures higher than the smallest principal stress. Doing so causes fractures to slip, open, and propagate. These stimulated fractures enhance the permeability of the target formation. See King (2010) for a history of HF completion technologies, from a petroleum operator's perspective.
Hypocenter	The location (in the subsurface) where an earthquake initiates rupture.
Induced seismicity	A type of earthquake activity that is caused or accelerated by human activities. Sometimes, these earthquakes are distinguished into either triggered or induced, depending on the degree of human influence. In this paper we make no distinction and refer to both types as induced.
Karst	A sinkhole caused by the dissolution of soluble rocks, such as limestone, dolomite, or anhydrites.
Microseismicity	Stimulation of fractures during HF causes earthquake-like shear/tensile slip called microseismicity. Some authors ascribe this term to events below a specific magnitude level (Eaton, 2018).
Minifrack	Adiagnostic injection test performed in well bores to determine information about the state of in situ stress and permeability by performing a small HF stimulation. This can be used to determine the magnitude of the least principal stress. Synonymously, it is called diagnostic fracture injection tests.
Mitigation	Procedures enacted by the HF operator to reduce the likelihood and severity of induced seismicity.
Pad	A surface location where horizontal well(s) are drilled by an operator. Pads may have a single well or multiple wells, sometimes as many as 10 at a single location (Figure 1).
Perforation	One of the initial steps in a single stage completion is to perforate the nearby well bore and formation, often using shaped explosive charges.
Permeability	The capacity for rocks to allow or resist fluid flow. A measure of the ease with which a fluid can pass through a porous medium.
Play	A term used to denote the extent of a target formation (or a package of formations) exploited by HF. For example, the Duvernay play in Alberta is HF completions targeting the Duvernay Formation.
Porosity	The proportion of filled space to empty space in a rock.
Operator	The company who owns the HF pad and is responsible for completion.
Regulator	The institution responsible for the oversight of responsible operator development.
Secondary recovery	A hydrocarbon recovery technique that uses the injection of fluids (e.g., water or CO_2) into a formation, with the intent to maintain or enhance reservoir pressure.

Shale	A term often used loosely in association with HF, sometimes as a synonym for play. Technically, shales are fine-grained sedimentary rocks deposited in laminations; often, they are highly impermeable. Shales may contain organic matter, which matured into petroleum, and are thus a primary target for HF.
Stage	HF wells are completed in multiple stages, with up to many tens of stages per well (Figure 1). Stages are an isolated potion of the well, where HF stimulation occurs. Multiple stages along a well are completed sequentially.
Stimulation	A term used to describe fluid pumping to enhance permeability via HF. Stimulated fractures enhance the permeability of a target formation.
Toe	The horizontal section of a well furthest from the vertical section.
Traffic light protocol	A regulatory framework intended to reduce the hazards and risks of induced seismicity. Often, magnitude values are chosen at green, yellow, and red thresholds, respectively, marking points to proceed, mitigate, and stop.
Vendor	Companies hired by operators to provide services, in aid of HF completion.
Zipper frack	A completion schema used by HF operators in which stages are completed alternatingly between multiple wells, forming a zipper-like pattern (Figure 1).

Data Availability Statement

Data were not used nor created for most of this research. Case study figures use data from prior works (Brudzinski & Kozłowska, 2019; Clarke et al., 2014; Farahbod, Kao, Cassidy, & Walker, 2015; Farahbod, Kao, Walker, & Cassidy, 2015; Fasola et al., 2019; Kozłowska et al., 2018; Lei et al., 2017, 2019; Schultz et al., 2017, 2018; Schultz, Mei, et al., 2015; Schultz, Stern, et al., 2015; Schultz & Wang, 2020; Shemeta et al., 2019; Skoumal et al., 2015b, 2020; Yoon et al., 2017) and are also cited in their respective figure captions. HF well counts in Figure 2b were obtained from FracFocus (www.fracfocus.org).

Acknowledgments

We would like to thank Shawn Maxwell for his comments and edits in drafting this manuscript. We would also like the thank Justin Rubinstein and Art McGarr for their U.S. Geological Survey (USGS) internal reviews, which helped improve this manuscript. We would also like to thank Gail Atkinson, Cristiano Collettini, and an anonymous reviewer for their critiques during the paper submission process.

References

AER, Alberta Energy Regulator (2015). *Subsurface order no. 2: Monitoring and reporting of seismicity in the vicinity of hydraulic fracturing operations in the Duvernay zone, Fox Creek, Alberta* (pp. 3). Calgary, Canada: AER Bulletin 2015–07.

AER, Alberta Energy Regulator (2019). *Subsurface order no. 7: Monitoring and reporting of seismicity in the vicinity of hydraulic fracturing operations in the Duvernay zone, Red Deer, Alberta* (4 pp.). Calgary, Canada: AER Bulletin 2019–07. https://www.aer.ca/documents/orders/subsurface-orders/SO7.pdf

Aki, K., & Richards, P. G. (2002). *Quantitative seismology* (p. 700). University Science Books.

Al-Ismail, F., Ellsworth, W. L., & Beroza, G. C. (2020). Empirical and synthetic approaches to the calibration of the local magnitude scale, M_L, in southern Kansas. *Bulletin of the Seismological Society of America*, *110*(2), 689–697. https://doi.org/10.1785/0120190189

Anderson, I., & Underhill, J. R. (2020). Structural constraints on Lower Carboniferous shale gas exploration in the Craven Basin, NW England. *Petroleum Geoscience*, *26*(2), 303–324. https://doi.org/10.1144/petgeo2019-125

Andrews, I. J. (2013). *The Carboniferous Bowland Shale gas study: Geology and resource estimation* (p. 64). London, UK: British Geological Survey Report for Department of Energy and Climate Change.

Assatourians, K., & Atkinson, G. M. (2020). Processed ground-motion records from induced earthquakes for use in engineering applications. *Canadian Journal of Civil Engineering*, *47*(1), 96–108. https://doi.org/10.1139/cjce-2018-0222

Atkinson, G. M. (2017). Strategies to prevent damage to critical infrastructure due to induced seismicity. *FACETS*, *2*, 374–394. https://doi.org/10.1139/facets-2017-0013

Atkinson, G. M., & Assatourians, K. (2017). Are ground-motion models derived from natural events applicable to the estimation of expected motions for induced earthquakes? *Seismological Research Letters*, *88*(2A), 430–441. https://doi.org/10.1785/0220160153

Atkinson, G. M., Eaton, D. W., Ghofrani, H., Walker, D., Cheadle, B., Schultz, R., et al. (2016). Hydraulic fracturing and seismicity in the Western Canada Sedimentary Basin. *Seismological Research Letters*, *87*(3), 631–647. https://doi.org/10.1785/0220150263

Atkinson, G. M., Eaton, D. W., & Igonin, N. (2020). Developments in understanding seismicity triggered by hydraulic fracturing. *Nature Reviews Earth & Environment*, 1–14. https://doi.org/10.1038/s43017-020-0049-7

Babaie Mahani, A., Esfahani, F., Kao, H., Gaucher, M., Hayes, M., Visser, R., & Venables, S. (2020). A systematic study of earthquake source mechanism and regional stress field in the southern Montney unconventional play of Northeast British Columbia, Canada. *Seismological Research Letters*, *91*(1), 195–206. https://doi.org/10.1785/0220190230

Babaie Mahani, A., & Kao, H. (2018). Ground motion from M 1.5 to 3.8 induced earthquakes at hypocentral distance <45 km in the Montney play of northeast British Columbia, Canada. *Seismological Research Letters*, *89*(1), 22–34. https://doi.org/10.1785/0220170119

Babaie Mahani, A., & Kao, H. (2019). Accurate determination of local magnitude for earthquakes in the western Canada sedimentary basin. *Seismological Research Letters*, *90*(1), 203–211. https://doi.org/10.1785/0220180264

Babaie Mahani, A., Kao, H., Atkinson, G. M., Assatourians, K., Addo, K., & Liu, Y. (2019). Ground motion characteristics of the 30 November 2018 injection-induced earthquake sequence in northeast British Columbia, Canada. *Seismological Research Letters*, *90*(4), 1457–1467. https://doi.org/10.1785/0220190127

Babaie Mahani, A., Schultz, R., Kao, H., Walker, D., Johnson, J., & Salas, C. (2017). Fluid injection and seismic activity in the northern Montney Play, British Columbia, Canada, with special reference to the 17 August 2015 *Mw* 4.6 induced earthquake. *Bulletin of the Seismological Society of America*, *107*. https://doi.org/10.1785/0120160175

Bachmann, C. E., Wiemer, S., Goertz-Allmann, B. P., & Woessner, J. (2012). Influence of pore pressure on the event-size distribution of induced earthquakes. *Geophysical Research Letters*, *39*. https://doi.org/10.1029/2012GL051480

Bachmann, C. E., Wiemer, S., Woessner, J., & Hainzl, S. (2011). Statistical analysis of the induced Basel 2006 earthquake sequence: Introducing a probability-based monitoring approach for Enhanced Geothermal Systems. *Geophysical Journal International*, *186*(2), 793–807. https://doi.org/10.1111/j.1365-246X.2011.05068.x

Baisch, S., Koch, C., & Muntendam-Bos, A. (2019). Traffic light systems: To what extent can induced seismicity be controlled? *Seismological Research Letters*, *90*(3), 1145–1154. https://doi.org/10.1785/0220180337

Bao, X., & Eaton, D. W. (2016). Fault activation by hydraulic fracturing in western Canada. *Science*, *354*, 1406–1409. https://doi.org/10.1126/science.aag2583

Baptie, B. (2010). Seismogenesis and state of stress in the UK. *Tectonophysics*, *482*(1-4), 150–159. https://doi.org/10.1016/j.tecto.2009.10.006

Baranoski, M. T., & Riley, R. A. (2013). *Analysis of stratigraphic, structural, and production relationships of Devonian shale gas reservoirs in Meigs County, Ohio*, Columbus, OH: Ohio Department of Natural Resources Division of Geological Survey Open File Report.

Baranova, V., Mustaqeem, A., & Bell, S. (1999). A model for induced seismicity caused by hydrocarbon production in the Western Canada Sedimentary Basin. *Canadian Journal of Earth Sciences*, *36*(1), 47–64. https://doi.org/10.1139/e98-080

Barbour, A. J., Norbeck, J. H., & Rubinstein, J. L. (2017). The effects of varying injection rates in Osage County, Oklahoma, on the 2016 *Mw* 5.8 Pawnee earthquake. *Seismological Research Letters*, *88*(5). https://doi.org/10.1785/0220170003

BC Oil & Gas Commission (2014a). *Montney Formation Play Atlas NEBC* (p. 36). Victoria, Canada: BC Oil and Gas Commission Publications. https://www.bcogc.ca/node/8131/download

BC Oil & Gas Commission (2014b). *Investigation of observed seismicity in the Montney trend* (p. 32). Victoria, Canada: BC Oil and Gas Commission Publications. https://www.bcogc.ca/node/12291/download

BC Oil and Gas Commission (2012). *Investigation of observed seismicity in the Horn River Basin* (p. 29). Victoria, Canada: BC Oil and Gas Commission Publications. https://www.bcogc.ca/node/8046/download

Bergen, K. J., Johnson, P. A., Maarten, V., & Beroza, G. C. (2019). Machine learning for data-driven discovery in solid Earth geoscience. *Science*, *363*(6433). https://doi.org/10.1126/science.aau0323

Bhattacharya, P., & Viesca, R. C. (2019). Fluid-induced aseismic fault slip outpaces pore-fluid migration. *Science*, *364*(6439), 464–468. https://doi.org/10.1126/science.aaw7354

Bommer, J. J., Oates, S., Cepeda, J. M., Lindholm, C., Bird, J., Torres, R., et al. (2006). Control of hazard due to seismicity induced by a hot fractured rock geothermal project. *Engineering Geology*, *83*(4), 287–306. https://doi.org/10.1016/j.enggeo.2005.11.002

Browning, J., Tinker, S. W., Ikonnikova, S., Gülen, G., Potter, E., Fu, Q., et al. (2014). Study develops Fayetteville Shale reserves, production forecast. *Oil & Gas Journal*, *112*(1), 64–73.

Brudzinski, M. R., & Kozłowska, M. (2019). Seismicity induced by hydraulic fracturing and wastewater disposal in the Appalachian Basin, USA: A review. *Acta Geophysica*, *67*(1), 351–364. https://doi.org/10.1007/s11600-019-00249-7

Burridge, R., & Knopoff, L. (1967). Model and theoretical seismicity. *Bulletin of the seismological society of america*, *57*(3), 341–371.

Butcher, A., Luckett, R., Verdon, J. P., Kendall, J. M., Baptie, B., & Wookey, J. (2017). Local magnitude discrepancies for near-event receivers: Implications for the UK traffic-light scheme. *Bulletin of the Seismological Society of America*, *107*(2), 532–541. https://doi.org/10.1785/0120160225

Calais, E., Camelbeeck, T., Stein, S., Liu, M., & Craig, T. J. (2016). A new paradigm for large earthquakes in stable continental plate interiors. *Geophysical Research Letters*, *43*, 10,621–10,637. https://doi.org/10.1002/2016GL070815

Campbell, N. M., Leon-Corwin, M., Ritchie, L. A., & Vickery, J. (2020). Human-induced seismicity: Risk perceptions in the State of Oklahoma. *The Extractive Industries and Society*.

CAPP, Canadian Association of Petroleum Producers (2019). Anomalous induced seismicity: Assessment, monitoring, mitigations, and response. In *Hydraulic fracturing guiding principles and operating practices* (pp. 4). Calgary, Canada: CAPP, Canadian Association of Petroleum Producers.

Cappa, F., Scuderi, M. M., Collettini, C., Guglielmi, Y., & Avouac, J. P. (2019). Stabilization of fault slip by fluid injection in the laboratory and in situ. *Science Advances*, *5*(3). https://doi.org/10.1126/sciadv.aau4065

Cardott, B. J. (2012). Thermal maturity of Woodford Shale gas and oil plays, Oklahoma, USA. *International Journal of Coal Geology*, *103*, 109–119. https://doi.org/10.1016/j.coal.2012.06.004

Carr, T. R., Wang, G., & McClain, T. (2013). Petrophysical analysis and sequence stratigraphy of the Utica shale and Marcellus shale, Appalachian Basin, USA. In *IPTC 2013: International Petroleum Technology Conference* (p. 350). Beijing, China: European Association of Geoscientists & Engineers.

Catalli, F., Rinaldi, A. P., Gischig, V., Nespoli, M., & Wiemer, S. (2016). The importance of earthquake interactions for injection-induced seismicity: Retrospective modeling of the Basel Enhanced Geothermal System. *Geophysical Research Letters*, *43*, 4992–4999. https://doi.org/10.1002/2016GL068932

Cesca, S., & Grigoli, F. (2015). Full waveform seismological advances for microseismic monitoring. *Advances in Geophysics*, *56*, 169–228. https://doi.org/10.1016/bs.agph.2014.12.002

Chen, H., & Carter, K. E. (2016). Water usage for natural gas production through hydraulic fracturing in the United States from 2008 to 2014. *Journal of Environmental Management*, *170*, 152–159. https://doi.org/10.1016/j.jenvman.2016.01.023

Chen, H., Meng, X., Niu, F., Tang, Y., Yin, C., & Wu, F. (2018). Microseismic monitoring of stimulating shale gas reservoir in SW China: 2. Spatial clustering controlled by the preexisting faults and fractures. *Journal of Geophysical Research: Solid Earth*, *123*, 1659–1672. https://doi.org/10.1002/2017JB014491

Chen, X., Nakata, N., Pennington, C., Haffener, J., Chang, J. C., He, X., et al. (2017). The Pawnee earthquake as a result of the interplay among injection, faults and foreshocks. *Scientific Reports*, *7*(1), 4945. https://doi.org/10.1038/s41598-017-04992-z

Chiorini, C. C. (2019). *Strategies for discriminating earthquakes using a Repeating Signal Detector to investigate induced seismicity in eastern Ohio (Master's thesis)*. Miami University, Ohio: Oxford, OH. Available at http://rave.ohiolink.edu/etdc/view?acc_num=miami1575050124689057, (last accessed January 2020)

Chiu, J. M., Johnston, A. C., Metzger, A. G., Haar, L., & Fletcher, J. (1984). Analysis of analog and digital records of the 1982 Arkansas earthquake swarm. *Bulletin of the Seismological Society of America*, *74*(5), 1721–1742.

Chopra, S., Sharma, R. K., Ray, A. K., Nemati, H., Morin, R., Schulte, B., & D'Amico, D. (2017). Seismic reservoir characterization of Duvernay shale with quantitative interpretation and induced seismicity considerations—A case study. *Interpretation*, *5*(2), T185–T197. https://doi.org/10.1190/INT-2016-0130.1

Clarke, H., Eisner, L., Styles, P., & Turner, P. (2014). Felt seismicity associated with shale gas hydraulic fracturing: The first documented example in Europe. *Geophysical Research Letters*, *41*, 8308–8314. https://doi.org/10.1002/2014GL062047

Clarke, H., Verdon, J. P., Kettlety, T., Baird, A. F., & Kendall, J. M. (2019). Real-time imaging, forecasting, and management of human-induced seismicity at Preston New Road, Lancashire, England. *Seismological Research Letters*, *90*(5), 1902–1915. https://doi.org/10.1785/0220190110

Clerc, F., Harrington, R. M., Liu, Y., & Gu, Y. J. (2016). Stress drop estimates and hypocenter relocations of induced seismicity near Crooked Lake, Alberta. *Geophysical Research Letters*, *43*, 6942–6951. https://doi.org/10.1002/2016GL069800

Cook, T., Perrin, J., & Van Wagener, D. (2018). Hydraulically fractured horizontal wells account for most new oil and natural gas wells. In *U.S. Energy Information Administration: Today in Energy* (pp. 2). Washington, DC: U.S. Energy Information Administration. Retreived from https://www.eia.gov/todayinenergy/detail.php?id=34732 (last accessed January 2020).

Corlett, H., Schultz, R., Branscombe, P., Hauck, T., Haug, K., MacCormack, K., & Shipman, T. (2018). Subsurface faults inferred from reflection seismic, earthquakes, and sedimentological relationships: Implications for induced seismicity in Alberta, Canada. *Marine and Petroleum Geology*, *93*, 135–144. https://doi.org/10.1016/j.marpetgeo.2018.03.008

Cox, S. F. (2016). Injection-driven swarm seismicity and permeability enhancement: Implications for the dynamics of hydrothermal ore systems in high fluid-flux, overpressured faulting regimes—An invited paper. *Economic Geology*, *111*(3), 559–587. https://doi.org/10.2113/econgeo.111.3.559

Darold, A., Holland, A. A., Chen, C., & Youngblood, A. (2014). Preliminary analysis of seismicity near Eagleton 1–29. In *Oklahoma Geological Survey Open File Report* (pp. 17). Carter County. OF2-2014 Oklahoma Geological Survey.

Davies, G. R., & Smith, L. B. Jr. (2006). Structurally controlled hydrothermal dolomite reservoir facies: An overview. *AAPG Bulletin*, *90*(11), 1641–1690. https://doi.org/10.1306/05220605164

Davies, R., Foulger, G., Bindley, A., & Styles, P. (2013). Induced seismicity and hydraulic fracturing for the recovery of hydrocarbons. *Marine and Petroleum Geology*, *45*, 171–185. https://doi.org/10.1016/j.marpetgeo.2013.03.016

Davies, R. J., Mathias, S. A., Moss, J., Hustoft, S., & Newport, L. (2012). Hydraulic fractures: How far can they go? *Marine and Petroleum Geology*, *37*(1), 1–6. https://doi.org/10.1016/j.marpetgeo.2012.04.001

Davis, S. D., & Frohlich, C. (1993). Did (or will) fluid injection cause earthquakes?—Criteria for a rational assessment. *Seismological Research Letters*, *64*(3-4), 207–224. https://doi.org/10.1785/gssrl.64.3-4.207

Davis, S. D., Nyffenegger, P. A., & Frohlich, C. (1995). The 9 April 1993 earthquake in south-central Texas: Was it induced by fluid withdrawal? *Bulletin of the Seismological Society of America*, *85*(6), 1888–1895.

Davis, S. D., & Pennington, W. D. (1989). Induced seismic deformation in the Cogdell oil field of west Texas. *Bulletin of the Seismological Society of America*, *79*, 1477–1495.

De Barros, L., Guglielmi, Y., Rivet, D., Cappa, F., & Duboeuf, L. (2018). Seismicity and fault aseismic deformation caused by fluid injection in decametric in-situ experiments. *Comptes Rendus Geoscience*, *350*(8), 464–475. https://doi.org/10.1016/j.crte.2018.08.002

Dempsey, D., Suckale, J., & Huang, Y. (2016). Collective properties of injection-induced earthquake sequences: 2. Spatiotemporal evolution and magnitude frequency distributions. *Journal of Geophysical Research: Solid Earth*, *121*, 3638–3665. https://doi.org/10.1002/2015JB012551

Deng, K., Liu, Y., & Harrington, R. M. (2016). Poroelastic stress triggering of the December 2013 Crooked Lake, Alberta, induced seismicity sequence. *Geophysical Research Letters*, *43*, 8482–8491. https://doi.org/10.1002/2016GL070421

Dengfa, H. E., Renqi, L. U., Huang, H., Xiaoshan, W., Jiang, H., & Zhang, W. (2019). Tectonic and geological setting of the earthquake hazards in the Changning shale gas development zone, Sichuan Basin, SW China. *Petroleum Exploration and Development*, *46*(5), 1051–1064. https://doi.org/10.1016/S1876-3804(19)60262-4

Department of Energy and Climate Change of the United Kingdom (DECC) (2013). Traffic light monitoring system (shale gas and fracking). https://www.gov.uk/government/publications/traffic-light-monitoring-system-shale-gas-and-fracking

Detournay, E. (2016). Mechanics of hydraulic fractures. *Annual Review of Fluid Mechanics*, *48*, 311–339. https://doi.org/10.1146/annurev-fluid-010814-014736

Dokht, R. M., Kao, H., Visser, R., & Smith, B. (2019). Seismic event and phase detection using time-frequency representation and convolutional neural networks. *Seismological Research Letters*, *90*(2A), 481–490. https://doi.org/10.1785/0220180308

Dong, D., Shi, Z., Guan, Q., Jiang, S., Zhang, M., Zhang, C., et al. (2018). Progress, challenges and prospects of shale gas exploration in the Wufeng-Longmaxi reservoirs in the Sichuan Basin. *Natural Gas Industry B*, *5*(5), 415–424. https://doi.org/10.1016/j.ngib.2018.04.011

Eaton, D., Davidsen, J., Pedersen, P., & Boroumand, N. (2014). Breakdown of the Gutenberg-Richter relation for microearthquakes induced by hydraulic fracturing: Influence of stratabound fractures. *Geophysical Prospecting*, *62*(4), 806–818. https://doi.org/10.1111/1365-2478.12128

Eaton, D. W., Igonin, N., Poulin, A., Weir, R., Zhang, H., Pellegrino, S., & Rodriguez, G. (2018). Induced seismicity characterization during hydraulic-fracture monitoring with a shallow-wellbore geophone array and broadband sensors. *Seismological Research Letters*, *89*(5), 1641–1651. https://doi.org/10.1785/0220180055

Eaton, D. W., & Maghsoudi, S. (2015). 2b or not 2b? Interpreting magnitude distributions from microseismic catalogs. *First Break*, *33*(10), 79–86. https://doi.org/10.3997/1365-2397.33.10.83159

Eaton, D. W., Milkereit, B., Ross, G. M., Kanasewich, E. R., Geis, W., Edwards, D. J., et al. (1995). Lithoprobe basin-scale seismic profiling in central Alberta: Influence of basement on the sedimentary cover. *Bulletin of Canadian Petroleum Geology*, *43*, 65–77.

Eaton, D. W., & Schultz, R. (2018). Increased likelihood of induced seismicity in highly overpressured shale formations. *Geophysical Journal International*, *214*(1), 751–757. https://doi.org/10.1093/gji/ggy167

Edwards, D. E., Barclay, J., Gibson, D., Kvill, G., & Halton, E. (1994). Triassic strata of the Western Canada Sedimentary Basin. In G. D. Mossop, & I. Shetsen (Eds.), *Geological Atlas of the Western Canada Sedimentary Basin*, Edmonton, Canada: Canadian Society of Petroleum Geologists and Alberta Research Council. https://ags.aer.ca/document/Atlas/chapter_16.pdf (2020.01.28)

El-Isa, Z., & Eaton, D. W. (2014). Spatiotemporal variations in the *b*-value of earthquake magnitude-frequency distributions: Classification and causes. *Tectonophysics*, *615*, 1–11. https://doi.org/10.1016/j.tecto.2013.12.001

Ellsworth, W. L. (1995). Characteristic earthquakes and long-term earthquake forecasts: Implications of central California seismicity. In *Urban disaster mitigation: The role of engineering and technology* (pp. 1–14). Pergamon.

Ellsworth, W. L. (2013). Injection-induced earthquakes. *Science*, *341*(6142), 1225942. https://doi.org/10.1126/science.1225942

Ellsworth, W. L., Giardini, D., Townend, J., Ge, S., & Shimamoto, T. (2019). Triggering of the Pohang, Korea, earthquake (*Mw* 5.5) by enhanced geothermal system stimulation. *Seismological Research Letters*, *90*(5), 1844–1858. https://doi.org/10.1785/0220190102

Ellsworth, W. L., Llenos, A. L., McGarr, A. F., Michael, A. J., Rubinstein, J. L., Mueller, C. S., et al. (2015). Increasing seismicity in the US midcontinent: Implications for earthquake hazard. *The Leading Edge*, *34*(6), 618–626. https://doi.org/10.1190/tle34060618.1

Energy Information Administration, EIA (2019a). *Drilling productivity report: For key tight oil and shale gas regions*. Washington, DC: US Energy Information Administration, EIA. https://www.eia.gov/petroleum/drilling/

Energy Information Administration, EIA (2019b). *Permian Basin: Wolfcamp and Bone Spring Shale Plays. U.S. Energy Information Administration report*. Washington, DC: US Energy Information Administration, EIA. Retrived from https://www.eia.gov/maps/pdf/Wolfcamp_BoneSpring_EIA_Report_July2019_v2.pdf (last accessed January 2020)

Energy Information Administration, EIA (2019c). *U.S. Crude Oil and Natural Gas Proved Reserves*, Washington, DC: US Energy Information Administration, EIA. https://www.eia.gov/naturalgas/crudeoilreserves/, Last accessed February 2020

Ewing, T. E. (1990). *Tectonic map of Texas (scale 1: 750,000)*. Austin, Tex: University of Texas Bureau of Economic Geology.

Eyre, T. S., Eaton, D. W., Garagash, D. I., Zecevic, M., Venieri, M., Weir, R., & Lawton, D. C. (2019). The role of aseismic slip in hydraulic fracturing-induced seismicity. *Science Advances*, *5*(8). https://doi.org/10.1126/sciadv.aav7172

Eyre, T. S., Eaton, D. W., Zecevic, M., D'Amico, D., & Kolos, D. (2019). Microseismicity reveals fault activation before *Mw* 4.1 hydraulic-fracturing induced earthquake. *Geophysical Journal International*, *218*(1), 534–546. https://doi.org/10.1093/gji/ggz168

Farahbod, A. M., Kao, H., Cassidy, J. F., & Walker, D. (2015). How did hydraulic-fracturing operations in the Horn River Basin change seismicity patterns in northeastern British Columbia, Canada? *The Leading Edge*, *34*(6), 658–663. https://doi.org/10.1190/tle34060658.1

Farahbod, A. M., Kao, H., Walker, D. M., & Cassidy, J. F. (2015). Investigation of regional seismicity before and after hydraulic fracturing in the Horn River Basin, northeast British Columbia. *Canadian Journal of Earth Sciences*, *52*(2), 112–122. https://doi.org/10.1139/cjes-2014-0162

Farrugia, J. J., Atkinson, G. M., & Molnar, S. (2018). Validation of 1D earthquake site characterization methods with observed earthquake site amplification. *Bulletin of the Seismological Society of America*, *108*(1), 291–308. https://doi.org/10.1785/0120170148

Farrugia, J. J., Molnar, S., & Atkinson, G. M. (2017). Noninvasive techniques for site characterization of Alberta seismic stations based on shear-wave velocity. *Bulletin of the Seismological Society of America*, *107*(6), 2885–2902. https://doi.org/10.1785/0120170086

Fasola, S. L., Brudzinski, M. R., Skoumal, R. J., Langenkamp, T., Currie, B. S., & Smart, K. J. (2019). Hydraulic fracture injection strategy influences the probability of earthquakes in the Eagle Ford shale play of South Texas. *Geophysical Research Letters*, *46*, 12,958–12,967. https://doi.org/10.1029/2019GL085167

Faulkner, D. R., Jackson, C. A. L., Lunn, R. J., Schlische, R. W., Shipton, Z. K., Wibberley, C. A. J., & Withjack, M. O. (2010). A review of recent developments concerning the structure, mechanics and fluid flow properties of fault zones. *Journal of Structural Geology*, *32*(11), 1557–1575. https://doi.org/10.1016/j.jsg.2010.06.009

Foulger, G. R., Wilson, M., Gluyas, J., Julian, B. R., & Davies, R. (2017). Global review of human-induced earthquakes. *Earth-Science Reviews*, *178*. https://doi.org/10.1016/j.earscirev.2017.07.008

Friberg, P. A., Besana-Ostman, G. M., & Dricker, I. (2014). Characterization of an earthquake sequence triggered by hydraulic fracturing in Harrison County, Ohio. *Seismological Research Letters*, *85*(6), 1295–1307. https://doi.org/10.1785/0220140127

Frohlich, C. (2012). Two-year survey comparing earthquake activity and injection-well locations in the Barnett Shale, Texas. *Proceedings of the National Academy of Sciences*, *109*(35), 13,934–13,938. https://doi.org/10.1073/pnas.1207728109

Frohlich, C., & Brunt, M. (2013). Two-year survey of earthquakes and injection/production wells in the Eagle Ford Shale, Texas, prior to the *MW* 4.8 20 October 2011 earthquake. *Earth and Planetary Science Letters*, *379*, 56–63. https://doi.org/10.1016/j.epsl.2013.07.025

Frohlich, C., & Davis, S. D. (2002). *Texas earthquakes*, (Vol. 2, p. 275). Austin, Tex: University of Texas Press.

Frohlich, C., DeShon, H., Stump, B., Hayward, C., Hornbach, M., & Walter, J. I. (2016). A historical review of induced earthquakes in Texas. *Seismological Research Letters*, *87*(4), 1022–1038. https://doi.org/10.1785/0220160016

Frohlich, C., Hayward, C., Rosenblit, J., Aiken, C., Hennings, P., Savvaidis, A., et al. (2019). Onset and cause of increased seismic activity near Pecos, West Texas, USA from observations at the Lajitas TXAR Seismic Array. *Journal of Geophysical Research: Solid Earth*, *125*. https://doi.org/10.1029/2019JB017737

Fu, Y., & Dehghanpour, H. (2020). How far can hydraulic fractures go: A comparative analysis of water flowback, tracer, and microseismic data from the Horn River Basin. *Marine and Petroleum Geology*, 104259. https://doi.org/10.1016/j.marpetgeo.2020.104259

Gale, J. F., Laubach, S. E., Olson, J. E., Eichhubl, P., & Fall, A. (2014). Natural fractures in shale: A review and new observations. *AAPG Bulletin*, *98*(11), 2165–2216. https://doi.org/10.1306/08121413151

Galis, M., Ampuero, J. P., Mai, P. M., & Cappa, F. (2017). Induced seismicity provides insight into why earthquake ruptures stop. *Science Advances*, *3*(12). https://doi.org/10.1126/sciadv.aap7528

Galloway, E., Hauck, T., Corlett, H., Pană, D., & Schultz, R. (2018). Faults and associated karst collapse suggest conduits for fluid flow that influence hydraulic fracturing-induced seismicity. *Proceedings of the National Academy of Sciences*, *115*(43), E10003–E10012. https://doi.org/10.1073/pnas.1807549115

Gan, W., & Frohlich, C. (2013). Gas injection may have triggered earthquakes in the Cogdell oil field, Texas. *Proceedings of the National Academy of Sciences*, *110*(47), 18,786–18,791. https://doi.org/10.1073/pnas.1311316110

Gaswirth, S. B., French, K. L., Pitman, J. K., Marra, K. R., Mercier, T. J., Leathers-Miller, H. M., et al. (2018). Assessment of undiscovered continuous oil and gas resources in the Wolfcamp Shale and Bone Spring Formation of the Delaware Basin, Permian Basin Province, New Mexico and Texas, 2018. In *U.S. Geological Survey Fact Sheet 2018–3073*. Denver, CO: US Geological Survey.

Gaswirth, S. B., Marra, K. R., Lillis, P. G., Mercier, T. J., Leathers-Miller, H. M., Schenk, C. J., et al. (2016). Assessment of undiscovered continuous oil resources in the Wolfcamp shale of the Midland basin, Permian basin Province, Texas, 2016. In *U.S. Geological Survey Fact Sheet 2016–3092* (pp. 4). Denver, CO: US Geological Survey.

Gaucher, E., Schoenball, M., Heidbach, O., Zang, A., Fokker, P. A., van Wees, J. D., & Kohl, T. (2015). Induced seismicity in geothermal reservoirs: A review of forecasting approaches. *Renewable and Sustainable Energy Reviews*, *52*, 1473–1490. https://doi.org/10.1016/j.rser.2015.08.026

Geller, R. J., & Mueller, C. S. (1980). Four similar earthquakes in central California. *Geophysical Research Letters*, *7*(10), 821–824. https://doi.org/10.1029/GL007i010p00821

Ghofrani, H., & Atkinson, G. M. (2016). A preliminary statistical model for hydraulic fracture-induced seismicity in the Western Canada Sedimentary basin. *Geophysical Research Letters*, *43*, 10,164–10,172. https://doi.org/10.1002/2016GL070042

Ghofrani, H., & Atkinson, G. M. (2020). Activation rate of seismicity for hydraulic fracture wells in the Western Canada Sedimentary Basin. *Bulletin of the Seismological Society of America*. https://doi.org/10.1785/0120200002

Ghofrani, H., Atkinson, G. M., Schultz, R., & Assatourians, K. (2019). Short-term hindcasts of seismic hazard in the Western Canada Sedimentary Basin caused by induced and natural earthquakes. *Seismological Research Letters*, *90*(3), 1420–1435. https://doi.org/10.1785/0220180285

Gischig, V. S., Giardini, D., Amann, F., Hertrich, M., Krietsch, H., Loew, S., et al. (2019). Hydraulic stimulation and fluid circulation experiments in underground laboratories: Stepping up the scale towards engineered geothermal systems. *Geomechanics for Energy and the Environment*, 100175. https://doi.org/10.1016/j.gete.2019.100175

Goebel, T. H., & Brodsky, E. E. (2018). The spatial footprint of injection wells in a global compilation of induced earthquake sequences. *Science*, *361*(6405), 899–904. https://doi.org/10.1126/science.aat5449

Goebel, T. H. W., Kwiatek, G., Becker, T. W., Brodsky, E. E., & Dresen, G. (2017). What allows seismic events to grow big?: Insights from *b*-value and fault roughness analysis in laboratory stick-slip experiments. *Geology*, *45*. https://doi.org/10.1130/G39147.1

Goebel, T. H. W., Weingarten, M., Chen, X., Haffener, J., & Brodsky, E. E. (2017). The 2016 *Mw* 5. 1 Fairview, Oklahoma earthquakes: Evidence for long-range poroelastic triggering at >40 km from fluid disposal wells. *Earth and Planetary Science Letters*, *472*, 50–61. https://doi.org/10.1016/j.epsl.2017.05.011

Goertz-Allmann, B. P., & Wiemer, S. (2012). Geomechanical modeling of induced seismicity source parameters and implications for seismic hazard assessment. *Geophysics*, *78*(1), KS25–KS39. https://doi.org/10.1190/geo2012-0102.1

Goodfellow, S. D., Nasseri, M. H. B., Maxwell, S. C., & Young, R. P. (2015). Hydraulic fracture energy budget: Insights from the laboratory. *Geophysical Research Letters*, *42*, 3179–3187. https://doi.org/10.1002/2015GL063093

Gregory, K. B., Vidic, R. D., & Dzombak, D. A. (2011). Water management challenges associated with the production of shale gas by hydraulic fracturing. *Elements*, *7*(3), 181–186. https://doi.org/10.2113/gselements.7.3.181

Grigoli, F., Cesca, S., Priolo, E., Rinaldi, A. P., Clinton, J. F., Stabile, T. A., et al. (2017). Current challenges in monitoring, discrimination, and management of induced seismicity related to underground industrial activities: A European perspective. *Reviews of Geophysics*, *55*, 310–340. https://doi.org/10.1002/2016RG000542

Ground Water Protection Council and Interstate Oil and Gas Compact Commission, GWPC & IOGCC (2017). *Potential injection-induced seismicity associated with oil & gas development: A primer on technical and regulatory considerations informing risk management and mitigation* (Second ed. pp. 181). Oklahoma City, OK: Ground Water Protection Council.

Grünthal, G. (Ed) (1998). European Macroseismic Scale 1998. In *Cahiers du Centre European de Geodynamique et de Seismologie* (Vol. 15). European Centre for Geodynamics and Seismology: Luxembourg City, Luxembourg.

Guglielmi, Y., Cappa, F., Avouac, J. P., Henry, P., & Elsworth, D. (2015). Seismicity triggered by fluid injection-induced aseismic slip. *Science*, *348*(6240), 1224–1226. https://doi.org/10.1126/science.aab0476

Guglielmi, Y., Elsworth, D., Cappa, F., Henry, P., Gout, C., Dick, P., & Durand, J. (2015). In situ observations on the coupling between hydraulic diffusivity and displacements during fault reactivation in shales. *Journal of Geophysical Research: Solid Earth*, *120*, 7729–7748. https://doi.org/10.1002/2015JB012158

Gutenberg, B., & Richter, C. F. (1944). Frequency of earthquakes in California. *Bulletin of the Seismological Society of America*, *34*, 185–118.

Haddad, M., & Eichhubl, P. (2020). Poroelastic models for fault reactivation in response to concurrent injection and production in stacked reservoirs. *Geomechanics for Energy and the Environment*, 100181. https://doi.org/10.1016/j.gete.2020.100181

Haffener, J., Chen, X., & Murray, K. (2018). Multiscale analysis of spatiotemporal relationship between injection and seismicity in Oklahoma. *Journal of Geophysical Research: Solid Earth*, *123*, 8711–8731. https://doi.org/10.1029/2018JB015512

Hajati, T., Langenbruch, C., & Shapiro, S. A. (2015). A statistical model for seismic hazard assessment of hydraulic-fracturing-induced seismicity. *Geophysical Research Letters*, *42*, 10,601–10,606. https://doi.org/10.1002/2015GL066652

Handford, C. R. (1986). Facies and beddding sequences in shelf-storm-deposited carbonates; Fayetteville Shale and Pitkin Limestone (Mississippian), Arkansas. *Journal of Sedimentary Research*, *56*(1), 123–137. https://doi.org/10.1306/212F88A0-2B24-11D7-8648000102C1865D

Harpel, J. M., Barker, L. B., Fontenot, J. M., Carroll, C. L., Thomson, S. L., & Olson, K. E. (2012). Case history of the Fayetteville shale completions. In *SPE hydraulic fracturing technology conference*, Woodlands, TX: Society of Petroleum Engineers.

Healy, J. H., Rubey, W. W., Griggs, D. T., & Raleigh, C. B. (1968). The Denver earthquakes. *Science*, *161*(3848), 1301–1310. https://doi.org/10.1126/science.161.3848.1301

Heimisson, E. R., Dunham, E. M., & Almquist, M. (2019). Poroelastic effects destabilize mildly rate-strengthening friction to generate stable slow slip pulses. *Journal of the Mechanics and Physics of Solids*, *130*, 262–279. https://doi.org/10.1016/j.jmps.2019.06.007

Hennings, P. H., Lund Snee, J. E., Osmond, J. L., DeShon, H. R., Dommisse, R., Horne, E., et al. (2019). Injection-induced seismicity and fault-slip potential in the Fort Worth Basin, Texas. *Bulletin of the Seismological Society of America*, *109*(5), 1615–1634. https://doi.org/10.1785/0120190017

Hill, D. P. (1977). A model for earthquake swarms. *Journal of Geophysical Research*, *82*(8), 1347–1352. https://doi.org/10.1029/JB082i008p01347

Holland, A. (2011). Examination of possibly induced seismicity from hydraulic fracturing in the Eola Field, Garvin County, Oklahoma. In *Oklahoma Geological Survey, Open-File Report* (pp. 31). OF1-2011, Norman, OK: Oklahoma Geological Survey.

Holland, A. A. (2013). Earthquakes triggered by hydraulic fracturing in south-central Oklahoma. *Bulletin of the Seismological Society of America*, *103*(3), 1784–1792. https://doi.org/10.1785/0120120109

Holmgren, J. M., Atkinson, G. M., & Ghofrani, H. (2019). Stress drops and directivity of induced earthquakes in the Western Canada Sedimentary Basin. *Bulletin of the Seismological Society of America*, *109*(5), 1635–1652. https://doi.org/10.1785/0120190035

Holmgren, J. M., Atkinson, G. M., & Ghofrani, H. (2020). Reconciling ground motions and stress drops for induced earthquakes in the western Canada sedimentary Basin. *Bulletin of the Seismological Society of America*. https://doi.org/10.1785/0120190308

Homman, K. A. (2015). *Seismicity in Pennsylvania (M.S. thesis)*. University Park: Pennsylvania State University. p. 128.

Horton, S. (2012). Disposal of hydrofracking waste fluid by injection into subsurface aquifers triggers earthquake swarm in central Arkansas with potential for damaging earthquake. *Seismological Research Letters*, *83*(2), 250–260. https://doi.org/10.1785/gssrl.83.2.250

Hu, J., Chen, J., Chen, Z., Cao, J., Wang, Q., Zhao, L., et al. (2018). Risk assessment of seismic hazards in hydraulic fracturing areas based on fuzzy comprehensive evaluation and AHP method (FAHP): A case analysis of Shangluo area in Yibin City, Sichuan Province, China. *Journal of Petroleum Science and Engineering*, *170*, 797–812. https://doi.org/10.1016/j.petrol.2018.06.066

Huang, Y., & Beroza, G. C. (2015). Temporal variation in the magnitude-frequency distribution during the Guy-Greenbrier earthquake sequence. *Geophysical Research Letters*, *42*, 6639–6646. https://doi.org/10.1002/2015GL065170

Hubbert, M. K., & Willis, D. G. (1972). Mechanics of hydraulic fracturing. *Transactions of Society of Petroleum Engineers of AIME*, *210*, 153–163. https://doi.org/10.2118/686-g

Igonin, N., Zecevic, M., & Eaton, D. W. (2018). Bilinear magnitude-frequency distributions and characteristic earthquakes during hydraulic fracturing. *Geophysical Research Letters*, *45*, 12–866. https://doi.org/10.1029/2018GL079746

Jeanne, P., Rutqvist, J., Vasco, D., Garcia, J., Dobson, P. F., Walters, M., et al. (2014). A 3D hydrogeological and geomechanical model of an Enhanced Geothermal System at The Geysers, California. *Geothermics*, *51*, 240–252. https://doi.org/10.1016/j.geothermics.2014.01.013

Johnson, M. F., Walsh, W., Budgell, P. A., & Davidson, J. A. (2011). The ultimate potential for unconventional gas in the Horn River basin: integrating geological mapping with Monte Carlo simulations. In *Canadian Unconventional Resources Conference. Society of Petroleum Engineers* (pp. 17). Calgary, Canada: Canadian Society for Unconventional Resources.

Kagan, Y. Y. (1999). Universality of the seismic moment-frequency relation. *Pure and Applied Geophysics*, *155*, 537–574. https://doi.org/10.1007/978-3-0348-8677-2_16

Kagan, Y. Y. (2010). Earthquake size distribution: Power-law with exponent $\beta \equiv 12$? *Tectonophysics*, *490*(1-2), 103–114. https://doi.org/10.1016/j.tecto.2010.04.034

Kanamori, H., & Hauksson, E. (1992). A slow earthquake in the Santa Maria Basin, California. *Bulletin of the Seismological Society of America*, *82*(5), 2087–2096.

Kao, H., Eaton, D. W., Atkinson, G. M., Maxwell, S., & Mahani, A. B. (2016). Technical meeting on the traffic light protocols (TLP) for induced seismicity: summary and recommendations. In *Geological Survey of Canada, Open File, 8075*. Victoria, Canada: Geological Survey of Canada.

Kao, H., Hyndman, R., Jiang, Y., Visser, R., Smith, B., Babaie Mahani, A., et al. (2018). Induced seismicity in western Canada linked to tectonic strain rate: Implications for regional seismic hazard. *Geophysical Research Letters*, *45*, 11–104. https://doi.org/10.1029/2018GL079288

Kao, H., Visser, R., Smith, B., & Venables, S. (2018). Performance assessment of the induced seismicity traffic light protocol for northeastern British Columbia and western Alberta. *The Leading Edge*, *37*(2), 117–126. https://doi.org/10.1190/tle37020117.1

Karimi, S., & Baturan, D. (2018). Real-time induced seismicity forecasting and risk management utilizing research-grade seismic catalogs. *CSEG Recorder*, *43*.

Kaski, K. M., & Atkinson, G. M. (2017). A comparison of ground-motion characteristics from induced seismic events in Alberta with those in Oklahoma. *Seismological Research Letters*, *88*(6), 1570–1585. https://doi.org/10.1785/0220170064

Keranen, K. M., Savage, H. M., Abers, G. A., & Cochran, E. S. (2013). Potentially induced earthquakes in Oklahoma, USA: Links between wastewater injection and the 2011 *Mw* 5.7 earthquake sequence. *Geology*, *41*(6), 699–702. https://doi.org/10.1130/G34045.1

Keranen, K. M., & Weingarten, M. (2018). Induced seismicity. *Annual Review of Earth and Planetary Sciences*, *46*, 149–174. https://doi.org/10.1146/annurev-earth-082517-010054

Keranen, K. M., Weingarten, M., Abers, G. A., Bekins, B. A., & Ge, S. (2014). Sharp increase in central Oklahoma seismicity since 2008 induced by massive wastewater injection. *Science*, *345*, 448–451. https://doi.org/10.1126/science.1255802

Kettlety, T., Verdon, J. P., Werner, M. J., & Kendall, J. M. (2019). Stress transfer from opening hydraulic fractures controls the distribution of induced seismicity. *Journal of Geophysical Research: Solid Earth*, *125*, e2019JB018794. https://doi.org/10.1029/2019JB018794

Kim, W. Y. (2013). Induced seismicity associated with fluid injection into a deep well in Youngstown, Ohio. *Journal of Geophysical Research: Solid Earth*, *118*, 3506–3518. https://doi.org/10.1002/jgrb.50247

King, G. E. (2010). Thirty years of gas shale fracturing: What have we learned? In *SPE Annual Technical Conference and Exhibition* (pp. 50). Florence, Italy: Society of Petroleum Engineers.

Hubbert, M. K., & Rubey, W. W. (1959). Role of fluid pressure in mechanics of overthrust faulting: I. Mechanics of fluid-filled porous solids and its application to overthrust faulting. *Geological Society of America Bulletin*, *70*(2), 115–166. https://doi.org/10.1130/0016-7606(1959)70(115:ROFPIM)2.0.CO;2

King, V. M., Block, L. V., & Wood, C. K. (2016). Pressure/flow modeling and induced seismicity resulting from two decades of high-pressure deep-well brine injection, Paradox Valley, Colorado. *Geophysics*, *81*(5), B119–B134. https://doi.org/10.1190/geo2015-0414.1

Kohli, A. H., & Zoback, M. D. (2013). Frictional properties of shale reservoir rocks. *Journal of Geophysical Research: Solid Earth*, *118*, 5109–5125. https://doi.org/10.1002/jgrb.50346

Kothari, S. (2019). Statistical modeling and characterization of induced seismicity within the Western Canada Sedimentary Basin. In *Electronic Thesis and Dissertation Repository. 6638*, London, Canada: Western University. https://ir.lib.uwo.ca/etd/6638

Kozłowska, M., Brudzinski, M. R., Friberg, P., Skoumal, R. J., Baxter, N. D., & Currie, B. S. (2018). Maturity of nearby faults influences seismic hazard from hydraulic fracturing. *Proceedings of the National Academy of Sciences*, *115*(8), E1720–E1729. https://doi.org/10.1073/pnas.1715284115

Kwiatek, G., Bohnhoff, M., Martínez-Garzón, P., Bulut, F., & Dresen, G. (2013). High resolution reservoir characterization using induced seismicity and state of the art waveform processing techniques. *First Break*, *31*(7), 81–88. https://doi.org/10.3997/1365-2397.31.7.70359

Kwiatek, G., Martínez-Garzón, P., Plenkers, K., Leonhardt, M., Zang, A., von Specht, S., et al. (2018). Insights into complex subdecimeter fracturing processes occurring during a water injection experiment at depth in Äspö Hard Rock Laboratory, Sweden. *Journal of Geophysical Research: Solid Earth*, *123*, 6616–6635. https://doi.org/10.1029/2017JB014715

Kwiatek, G., Saarno, T., Ader, T., Bluemle, F., Bohnhoff, M., Chendorain, M., et al. (2019). Controlling fluid-induced seismicity during a 6.1-km-deep geothermal stimulation in Finland. *Science Advances*, *5*(5). https://doi.org/10.1126/sciadv.aav7224

Langenbruch, C., Ellsworth, W. L., Woo, J. U., & Wald, D. J. (2020). Value at induced risk: Injection-induced seismic risk from low-probability, high-impact events. *Geophysical Research Letters*, *47*, e2019GL085878. https://doi.org/10.1029/2019GL085878

Langenbruch, C., Weingarten, M., & Zoback, M. D. (2018). Physics-based forecasting of man-made earthquake hazards in Oklahoma and Kansas. *Nature Communications*, *9*(1), 3946. https://doi.org/10.1038/s41467-018-06167-4

Langenbruch, C., & Zoback, M. D. (2019). Assessing and managing seismic hazards in Oklahoma associated with hydraulic fracturing. In *AGU Fall Meeting 2019*, San Francisco, CA: . AGU.

Lecampion, B., Desroches, J., Weng, X., Burghardt, J., & Brown, J. E. (2015). Can we engineer better multistage horizontal completions? Evidence of the importance of near-wellbore fracture geometry from theory, lab and field experiments. In *SPE Hydraulic Fracturing Technology Conference* (pp. 19). Woodlands, TX: Society of Petroleum Engineers.

Lei, X., Huang, D., Su, J., Jiang, G., Wang, X., Wang, H., et al. (2017). Fault reactivation and earthquakes with magnitudes of up to *Mw*4. 7 induced by shale-gas hydraulic fracturing in Sichuan Basin, China. *Scientific Reports*, *7*(1), 7971. https://doi.org/10.1038/s41598-017-08557-y

Lei, X., Wang, Z., & Su, J. (2019). The December 2018 M_L 5.7 and January 2019 M_L 5.3 earthquakes in South Sichuan Basin induced by shale gas hydraulic fracturing. *Seismological Research Letters*, *90*(3), 1099–1110. https://doi.org/10.1785/0220190029

Lele, S. P., Tyrrell, T., Dasari, G. R., & Symington, W. A. (2017). Geomechanical analysis of hydraulic fracturing induced seismicity at Duvernay field in western Canadian sedimentary basin. In *GeoConvention 2017* (p. 5). Calgary: Canadian Society of Petroleum Geologists.

Li, L., Tan, J., Schwarz, B., Staněk, F., Poiata, N., Shi, P., et al. (2020). Recent advances and challenges of waveform-based seismic location methods at multiple scales. *Reviews of Geophysics*, *58*, e2019RG000667. https://doi.org/10.1029/2019RG000667

Li, L., Tan, J., Wood, D. A., Zhao, Z., Becker, D., Lyu, Q., et al. (2019). A review of the current status of induced seismicity monitoring for hydraulic fracturing in unconventional tight oil and gas reservoirs. *Fuel*, *242*, 195–210. https://doi.org/10.1016/j.fuel.2019.01.026

Li, T., Gu, Y. J., Wang, Z., Wang, R., Chen, Y., Song, T. R. A., & Wang, R. (2019). Spatiotemporal variations in crustal seismic anisotropy surrounding induced earthquakes near Fox Creek, Alberta. *Geophysical Research Letters*, *46*, 5180–5189. https://doi.org/10.1029/2018GL081766

Liang, C., Jiang, Z., Zhang, C., Guo, L., Yang, Y., & Li, J. (2014). The shale characteristics and shale gas exploration prospects of the Lower Silurian Longmaxi shale, Sichuan Basin, South China. *Journal of Natural Gas Science and Engineering*, *21*, 636–648. https://doi.org/10.1016/j.jngse.2014.09.034

Liang, F., Sayed, M., Al-Muntasheri, G. A., Chang, F. F., & Li, L. (2016). A comprehensive review on proppant technologies. *Petroleum*, *2*(1), 26–39. https://doi.org/10.1016/j.petlm.2015.11.001

Liu, M., Zhang, M., Zhu, W., Ellsworth, W. L., & Li, H. (2020). Rapid characterization of the July 2019 Ridgecrest, California earthquake sequence from raw seismic data using machine learning phase picker. *Geophysical Research Letters*, *47*, e2019GL086189. https://doi.org/10.1029/2019GL086189

Lomax, A., & Savvaidis, A. (2019). Improving absolute earthquake location in west Texas using probabilistic, proxy ground-truth station corrections. *Journal of Geophysical Research: Solid Earth*, *124*, 11,447–11,465. https://doi.org/10.1029/2019JB017727

López-Comino, J. A., Cesca, S., Jarosławski, J., Montcoudiol, N., Heimann, S., Dahm, T., et al. (2018). Induced seismicity response of hydraulic fracturing: Results of a multidisciplinary monitoring at the Wysin site, Poland. *Scientific Reports*, *8*(1), 8653. https://doi.org/10.1038/s41598-018-26970-9

Lund Snee, J. E., & Zoback, M. D. (2016). State of stress in Texas: Implications for induced seismicity. *Geophysical Research Letters*, *43*, 10208–10214. https://doi.org/10.1002/2016GL070974

MacLean, B. C., & Morrow, D. W. (2004). Bovie structure: Its evolution and regional context. *Bulletin of Canadian Petroleum Geology*, *52*(4), 302–324. https://doi.org/10.2113/52.4.302

Maghsoudi, S., Baró, J., Kent, A., Eaton, D., & Davidsen, J. (2018). Interevent triggering in microseismicity induced by hydraulic fracturing. *Bulletin of the Seismological Society of America*, *108*(3A), 1133–1146. https://doi.org/10.1785/0120170368

Majer, E. L., Baria, R., Stark, M., Oates, S., Bommer, J., Smith, B., & Asanuma, H. (2007). Induced seismicity associated with enhanced geothermal systems. *Geothermics*, *36*(3), 185–222. https://doi.org/10.1016/j.geothermics.2007.03.003

Martin, R., Baihly, J. D., Malpani, R., Lindsay, G. J., & Atwood, W. K. (2011). Understanding production from Eagle Ford-Austin chalk system. In *Paper presented at SPE Annual Technical Conference and Exhibition*. Denver, Colorado: Society of Petroleum Engineers.

Maxwell, S. C., Jones, M., Parker, R., Miong, S., Leaney, S., Dorval, D., et al. (2009). Fault activation during hydraulic fracturing. In *SEG Technical Program Expanded Abstracts 2009*, (pp. 1552–1556). Society of Exploration Geophysicists.

Maxwell, S. C., Zhang, F., & Damjanac, B. (2015). Geomechanical modeling of induced seismicity resulting from hydraulic fracturing. *The Leading Edge*, *34*(6), 678–683. https://doi.org/10.1190/tle34060678.1

McGarr, A., & Barbour, A. J. (2017). Wastewater disposal and the earthquake sequences during 2016 near Fairview, Pawnee, and Cushing, Oklahoma. *Geophysical Research Letters*, *44*, 9330–9336. https://doi.org/10.1002/2017GL075258

McGarr, A., Simpson, D., Seeber, L., & Lee, W. (2002). Case histories of induced and triggered seismicity. *International Geophysics Series*, *81*(A), 647–664.

McNamara, D. E., Benz, H. M., Herrmann, R. B., Bergman, E. A., Earle, P., Holland, A., et al. (2015). Earthquake hypocenters and focal mechanisms in central Oklahoma reveal a complex system of reactivated subsurface strike-slip faulting. *Geophysical Research Letters*, *42*, 2742–2749. https://doi.org/10.1002/2014GL062730

McNamara, D. E., Hayes, G. P., Benz, H. M., Williams, R. A., McMahon, N. D., Aster, R. C., et al. (2015). Reactivated faulting near Cushing, Oklahoma: Increased potential for a triggered earthquake in an area of United States strategic infrastructure. *Geophysical Research Letters*, *42*, 8328–8332. https://doi.org/10.1002/2015GL064669

McNamara, D. E., Rubinstein, J. L., Myers, E., Smoczyk, G., Benz, H. M., Williams, R. A., et al. (2015). Efforts to monitor and characterize the recent increasing seismicity in central Oklahoma. *The Leading Edge*, *34*(6), 628–639. https://doi.org/10.1190/tle34060628.1

Meng, L., McGarr, A., Zhou, L., & Zang, Y. (2019). An investigation of seismicity induced by hydraulic fracturing in the Sichuan basin of China based on data from a temporary seismic network. *Bulletin of the Seismological Society of America*, *109*(1), 348–357. https://doi.org/10.1785/0120180310

Mignan, A., Broccardo, M., Wiemer, S., & Giardini, D. (2017). Induced seismicity closed-form traffic light system for actuarial decision-making during deep fluid injections. *Scientific Reports*, *7*(1), 13607. https://doi.org/10.1038/s41598-017-13585-9

Mignan, A., Landtwing, D., Kästli, P., Mena, B., & Wiemer, S. (2015). Induced seismicity risk analysis of the 2006 Basel, Switzerland, Enhanced Geothermal System project: Influence of uncertainties on risk mitigation. *Geothermics*, *53*, 133–146. https://doi.org/10.1016/j.geothermics.2014.05.007

Mogi, K. (1967). Earthquakes and fractures. *Tectonophysics*, *5*(1), 35–55. https://doi.org/10.1016/0040-1951(67)90043-1

Mohammed, A. I., Oyeneyin, B., Atchison, B., & Njuguna, J. (2019). Casing structural integrity and failure modes in a range of well types—A review. *Journal of Natural Gas Science and Engineering*, *68*. https://doi.org/10.1016/j.jngse.2019.05.011

Montgomery, C. T., & Smith, M. B. (2010). Hydraulic fracturing: History of an enduring technology. *Journal of Petroleum Technology*, *62*(12), 26–40. https://doi.org/10.2118/1210-0026-JPT

Mousavi, S. M., Ogwari, P. O., Horton, S. P., & Langston, C. A. (2017). Spatio-temporal evolution of frequency-magnitude distribution and seismogenic index during initiation of induced seismicity at Guy-Greenbrier, Arkansas. *Physics of the Earth and Planetary Interiors*, *267*, 53–66. https://doi.org/10.1016/j.pepi.2017.04.005

Mousavi, S. M., Zhu, W., Sheng, Y., & Beroza, G. C. (2019). CRED: A deep residual network of convolutional and recurrent units for earthquake signal detection. *Scientific Reports*, *9*(1), 1–14. https://doi.org/10.1038/s41598-019-45748-1

Musson, R. M. W. (1996). The seismicity of the British Isles. *Annali di Geofisica*, *39*, 463–469. https://doi.org/10.4401/ag-3982

Myers, T. (2012). Potential contaminant pathways from hydraulically fractured shale to aquifers. *Groundwater*, *50*(6), 872–882. https://doi.org/10.1111/j.1745-6584.2012.00933.x

National Energy Board (2013). *Energy Briefing Note: The Ultimate Potential for Unconventional Petroleum from the Montney Formation of British Columbia and Alberta* (pp. 17). Canada Energy Regulator: Calgary, Canada.

National Research Council (NRC) (2012) *Induced seismicity potential in energy technologies*, Washington, DC: The National Academies Press.

Nicholson, C., & Wesson, R. L. (1990). *Earthquake hazard associated with deep well injection: A report to the U.S. Environmental Protection Agency* (pp. 86). Reston, VA: U.S. Geological Survey Bulletin. 1951.

Nicholson, C., & Wesson, R. L. (1992). Triggered earthquakes and deep well activities. *Pure and Applied Geophysics*, *139*(3-4), 561–578. https://doi.org/10.1007/BF00879951

Niemz, P., Cesca, S., Heimann, S., Grigoli, F., von Specht, S., Hammer, C., et al. (2020). Full-waveform-based characterization of acoustic emission activity in a mine-scale experiment: A comparison of conventional and advanced hydraulic fracturing schemes. *Geophysical Journal International*, *222*(1), 189–206. https://doi.org/10.1093/gji/ggaa127

OCC, Oklahoma Corporation Commission (2016). *New year, new plays, new plans* (pp 4). Oklahoma City, OK: OCC News Release. https://www.occeweb.com/News/2016/12-20-16SCOOP-STACK.pdf

Ogwari, P. O., & Horton, S. P. (2016). Numerical model of pore-pressure diffusion associated with the initiation of the 2010–2011 Guy-Greenbrier, Arkansas earthquakes. *Geofluids*, *16*(5), 954–970. https://doi.org/10.1111/gfl.12198

Ogwari, P. O., Horton, S. P., & Ausbrooks, S. (2016). Characteristics of induced/triggered earthquakes during the startup phase of the Guy-Greenbrier earthquake sequence in north-central Arkansas. *Seismological Research Letters*, *87*(3), 620–630. https://doi.org/10.1785/0220150252

Ohio Department of Natural Resources, ODNR (2017). Ohio Department of Natural Resources: Division of Oil & Gas Resources Management. In *AGI Policy & Critical Issues Webinar: OhioNET*, Columbus, OH: State of Ohio's Response to Induced Seismicity.

Oklahoma Corporation Commission, OCC (2018). *Moving forward: New protocol to further address seismicity in state's largest oil and gas play (Press release)*. Oklahoma Corporation Commission: Oklahoma City, OK. https://www.occeweb.com/og/02-27-18PROTOCOL.pdf

Olson, D. R., & Frohlich, C. (1992). Research note: Felt reports from the 20 July 1991 Falls City earthquake, Karnes County, Texas. *Seismological Research Letters*, *63*(4), 603–604. https://doi.org/10.1785/gssrl.63.4.603

Ortiz, J. P., Person, M. A., Mozley, P. S., Evans, J. P., & Bilek, S. L. (2019). The role of fault-zone architectural elements on pore pressure propagation and induced seismicity. *Groundwater*, *57*(3), 465–478. https://doi.org/10.1111/gwat.12818

Palisch, T. T., Vincent, M., & Handren, P. J. (2010). Slickwater fracturing: Food for thought. *SPE Production & Operations*, *25*(03), 327–344. https://doi.org/10.2118/115766-PA

Park, Y., Mousavi, S. M., Zhu, W., Ellsworth, W. L., & Beroza, G. C. (2020). Machine-learning-based analysis of the Guy-Greenbrier, Arkansas earthquakes: A tale of two sequences. *Geophysical Research Letters*, *47*, e2020GL087032. https://doi.org/10.1029/2020GL087032

de Pater, H., & Baisch, S. (2011). Geomechanical study of Bowland Shale seismicity. In *Synthesis Report*(pp. 71). Cuadrilla Resources Ltd.

Pawley, S., Schultz, R., Playter, T., Corlett, H., Shipman, T., Lyster, S., & Hauck, T. (2018). The geological susceptibility of induced earthquakes in the Duvernay play. *Geophysical Research Letters*, *45*, 1786–1793. https://doi.org/10.1002/2017GL076100

Pearson, K. (2012). Geologic models and evaluation of undiscovered conventional and continuous oil and gas resources—Upper Cretaceous Austin Chalk. U.S. Gulf Coast. In *U.S. Geological Survey Scientific Investigations Report 2012-5159* (Vol. 26). Denver, CO: US Geological Survey.

Pennington, W. D., Davis, S. D., Carlson, S. M., DuPree, J., & Ewing, T. E. (1986). The evolution of seismic barriers and asperities caused by the depressuring of fault planes in oil and gas fields of south Texas. *Bulletin of the Seismological Society of America*, *76*(4), 939–948.

Perol, T., Gharbi, M., & Denolle, M. (2018). Convolutional neural network for earthquake detection and location. *Science Advances*, *4*(2). https://doi.org/10.1126/sciadv.1700578

Petersen, M. D., Mueller, C. S., Moschetti, M. P., Hoover, S. M., Shumway, A. M., McNamara, D. E., et al. (2017). 2017 one-year seismic-hazard forecast for the central and eastern United States from induced and natural earthquakes. *Seismological Research Letters*, *88*(3), 772–783. https://doi.org/10.1785/0220170005

Poulin, A., Weir, R., Eaton, D., Igonin, N., Chen, Y., Lines, L., & Lawton, D. (2019). Focal-time analysis: A new method for stratigraphic depth control of microseismicity and induced seismic events. *Geophysics*, *84*(6), KS173–KS182. https://doi.org/10.1190/geo2019-0046.1

Poupinet, G., Ellsworth, W. L., & Frechet, J. (1984). Monitoring velocity variations in the crust using earthquake doublets: An application to the Calaveras Fault, California. *Journal of Geophysical Research*, *89*(B7), 5719–5731. https://doi.org/10.1029/JB089iB07p05719

Rabak, I., Langston, C., Bodin, P., Horton, S., Withers, M., & Powell, C. (2010). The Enola, Arkansas, intraplate swarm of 2001. *Seismological Research Letters*, *81*(3), 549–559. https://doi.org/10.1785/gssrl.81.3.549

Rafiee, M., Soliman, M. Y., & Pirayesh, E. (2012). Hydraulic fracturing design and optimization: A modification to zipper frac. In *SPE Annual Technical Conference and Exhibition*, San Antonio, TX: Society of Petroleum Engineers.

Railroad Commission of Texas (RRC) (2019). *Texas Eagle Ford Shale Oil Production 2008 through March 2019*, Railroad Commission of Texas: Austin, TX. https://www.rrc.state.tx.us/media/52456/eagle-ford-oil.pdf

Rathnaweera, T. D., Wu, W., Ji, Y., & Gamage, R. P. (2020). Understanding injection-induced seismicity in enhanced geothermal systems: From the coupled thermo-hydro-mechanical-chemical process to anthropogenic earthquake prediction. *Earth-Science Reviews*, *205*. https://doi.org/10.1016/j.earscirev.2020.103182

Rinaldi, A. P., & Rutqvist, J. (2019). Joint opening or hydroshearing? Analyzing a fracture zone stimulation at Fenton Hill. *Geothermics*, *77*, 83–98. https://doi.org/10.1016/j.geothermics.2018.08.006

Rodríguez-Pradilla, G., & Eaton, D. W. (2019). Ground-motion analysis of hydraulic-fracturing induced seismicity at close epicentral distance. *Bulletin of the Seismological Society of America*, *110*. https://doi.org/10.1785/0120190103

Rokosh, C. D., Lyster, S., Anderson, S. D. A., Beaton, A. P., Berhane, H., Brazzoni, T., et al. (2012). Summary of Alberta's shale-and siltstone-hosted hydrocarbon resource potential. In *Energy Resources Conservation Board, ERCB/AGS Open File Report* (pp. 327). Edmonton, Canada: Alberta Geological Survey/Alberta Energy Regulator.

Roland, E., & McGuire, J. J. (2009). Earthquake swarms on transform faults. *Geophysical Journal International*, *178*(3), 1677–1690. https://doi.org/10.1111/j.1365-246X.2009.04214.x

Roman, D. C., & Cashman, K. V. (2006). The origin of volcano-tectonic earthquake swarms. *Geology*, *34*(6), 457–460. https://doi.org/10.1130/G22269.1

Royal Society and Royal Academy of Engineering (2012). *Shale gas extraction in the UK: A review of hydraulic fracturing*. London: Royal Society and Royal Academy of Engineering. 76 pp

Rubinstein, J. L., & Mahani, A. B. (2015). Myths and facts on wastewater injection, hydraulic fracturing, enhanced oil recovery, and induced seismicity. *Seismological Research Letters*, *86*(4), 1060–1067. https://doi.org/10.1785/0220150067

Rutledge, J. T., & Phillips, W. S. (2003). Hydraulic stimulation of natural fractures as revealed by induced microearthquakes, Carthage Cotton Valley gas field, east Texas. *Geophysics*, *68*(2), 441–452. https://doi.org/10.1190/1.1567214

Rutledge, J. T., Phillips, W. S., & Mayerhofer, M. J. (2004). Faulting induced by forced fluid injection and fluid flow forced by faulting: An interpretation of hydraulic-fracture microseismicity, Carthage Cotton Valley gas field, Texas. *Bulletin of the Seismological Society of America*, *94*(5), 1817–1830. https://doi.org/10.1785/012003257

Rutqvist, J., Rinaldi, A. P., Cappa, F., & Moridis, G. J. (2015). Modeling of fault activation and seismicity by injection directly into a fault zone associated with hydraulic fracturing of shale-gas reservoirs. *Journal of Petroleum Science and Engineering*, *127*, 377–386. https://doi.org/10.1016/j.petrol.2015.01.019

Savage, H. M., & Brodsky, E. E. (2011). Collateral damage: Evolution with displacement of fracture distribution and secondary fault strands in fault damage zones. *Journal of Geophysical Research*, *116*, B03405. https://doi.org/10.1029/2010JB007665

Schaff, D. P., & Waldhauser, F. (2010). One magnitude unit reduction in detection thresh-old by cross correlation applied to Parkfield (California) and China seismicity. *Bulletin of the Seismological Society of America*, *100*, 3224–3238. https://doi.org/10.1785/0120100042

Scholz, C. H. (1968). The frequency-magnitude relation of microfracturing in rock and its relation to earthquakes. *Bulletin of the Seismological Society of America*, *58*(1), 399–415.

Schorlemmer, D., Wiemer, S., & Wyss, M. (2005). Variations in earthquake-size distribution across different stress regimes. *Nature*, *437*, 539–542. https://doi.org/10.1038/nature04094

Schultz, R., Atkinson, G., Eaton, D. W., Gu, Y. J., & Kao, H. (2018). Hydraulic fracturing volume is associated with induced earthquake productivity in the Duvernay play. *Science*, *359*(6373), 304–308. https://doi.org/10.1126/science.aao0159

Schultz, R., Beroza, G., Ellsworth, W., & Baker, J. (2020). Risk-informed recommendations for managing hydraulic fracturing induced seismicity via traffic light protocols. *Bulletin of the Seismological Society of America*. https://doi.org/10.1785/0120200016

Schultz, R., Corlett, H., Haug, K., Kocon, K., MacCormack, K., Stern, V., & Shipman, T. (2016). Linking fossil reefs with earthquakes: Geologic insight to where induced seismicity occurs in Alberta. *Geophysical Research Letters*, *43*, 2534–2542. https://doi.org/10.1002/2015GL067514

Schultz, R., Mei, S., Pană, D., Stern, V., Gu, Y. J., Kim, A., & Eaton, D. (2015). The Cardston earthquake swarm and hydraulic fracturing of the Exshaw Formation (Alberta Bakken play). *Bulletin of the Seismological Society of America*, *105*(6), 2871–2884. https://doi.org/10.1785/0120150131

Schultz, R., & Nanometrics (2019). Initial seismic hazard assessment for the 2016 induced earthquakes near Fox Creek, Alberta (between January 2013 and January 2016). In *AER/AGS Special Report 104* (pp. 115). Edmonton, Canada: Alberta Geological Survey/Alberta Energy Regulator.

Schultz, R., & Pawley, S. (2019). Induced earthquakes geological susceptibility model for the Duvernay Formation, central Alberta—Version 2. In *AER/AGS Open File Report 2019-02* (8 p). Edmonton, Canada: Alberta Geological Survey / Alberta Energy Regulator.

Schultz, R., Stern, V., & Gu, Y. J. (2014). An investigation of seismicity clustered near the Cordel Field, west central Alberta, and its relation to a nearby disposal well. *Journal of Geophysical Research: Solid Earth*, *119*, 3410–3423. https://doi.org/10.1002/2013JB010836

Schultz, R., Stern, V., Novakovic, M., Atkinson, G., & Gu, Y. J. (2015). Hydraulic fracturing and the Crooked Lake Sequences: Insights gleaned from regional seismic networks. *Geophysical Research Letters*, *42*, 2750–2758. https://doi.org/10.1002/2015GL063455

Schultz, R., & Telesca, L. (2018). The cross-correlation and reshuffling tests in discerning induced seismicity. *Pure and Applied Geophysics*, *175*. https://doi.org/10.1007/s00024-018-1890-1

Schultz, R., & Wang, R. (2020). A newly emerging case of hydraulic fracturing induced seismicity in the Duvernay East Shale Basin. *Tectonophysics*, *779*. https://doi.org/10.1016/j.tecto.2020.228393

Schultz, R., Wang, R., Gu, Y. J., Haug, K., & Atkinson, G. (2017). A seismological overview of the induced earthquakes in the Duvernay play near Fox Creek, Alberta. *Journal of Geophysical Research: Solid Earth*, *122*, 492–505. https://doi.org/10.1002/2016JB013570

Schultz, R., Yusifbayov, J., & Shipman, T. (2020). The Scientific Induced Seismicity Monitoring Network (SCISMN). In *AER/AGS Open File Report 2019-09* (16 p). Edmonton, Canada: Alberta Geological Survey/Alberta Energy Regulator.

Scuderi, M. M., & Collettini, C. (2016). The role of fluid pressure in induced vs. triggered seismicity: Insights from rock deformation experiments on carbonates. *Scientific Reports*, *6*, 24852. https://doi.org/10.1038/srep24852

Scuderi, M. M., & Collettini, C. (2018). Fluid injection and the mechanics of frictional stability of shale-bearing faults. *Journal of Geophysical Research: Solid Earth*, *123*, 8364–8384. https://doi.org/10.1029/2018JB016084

Segall, P., & Lu, S. (2015). Injection-induced seismicity: Poroelastic and earthquake nucleation effects. *Journal of Geophysical Research: Solid Earth*, *120*, 5082–5103. https://doi.org/10.1002/2015JB012060

Shapiro, S. A., & Dinske, C. (2009). Fluid-induced seismicity: Pressure diffusion and hydraulic fracturing. *Geophysical Prospecting*, *57*(2), 301–310. https://doi.org/10.1111/j.1365-2478.2008.00770.x

Shapiro, S. A., Dinske, C., Langenbruch, C., & Wenzel, F. (2010). Seismogenic index and magnitude probability of earthquakes induced during reservoir fluid stimulations. *The Leading Edge*, *29*(3), 304–309. https://doi.org/10.1190/1.3353727

Shapiro, S. A., Krüger, O. S., Dinske, C., & Langenbruch, C. (2011). Magnitudes of induced earthquakes and geometric scales of fluid-stimulated rock volume. *Geophysics*, *76*(6), 55–63. https://doi.org/10.1190/geo2010-0349.1

Shelly, D. R., Hill, D. P., Massin, F., Farrell, J., Smith, R. B., & Taira, T. (2013). A fluid-driven earthquake swarm on the margin of the Yellowstone caldera. *Journal of Geophysical Research: Solid Earth*, *118*, 4872–4886. https://doi.org/10.1002/jgrb.50362

Shemeta, J. E., Brooks, C. E., & Lord, C. C. (2019). Well stimulation seismicity in Oklahoma: Cataloging earthquakes related to hydraulic fracturing. In *Unconventional Resources Technology Conference (URTEC)*, (95–106). Brisbane, Australia: Society for Exploration Geophysicists.

Shen, L. W., Schmitt, D. R., & Haug, K. (2019). Quantitative constraints to the complete state of stress from the combined borehole and focal mechanism inversions: Fox Creek, Alberta. *Tectonophysics*, *764*, 110–123. https://doi.org/10.1016/j.tecto.2019.04.023

Shen, L. W., Schmitt, D. R., & Schultz, R. (2019). Frictional stabilities on induced earthquake fault planes at Fox Creek, Alberta: A pore fluid pressure dilemma. *Geophysical Research Letters*, *46*, 8753–8762. https://doi.org/10.1029/2019GL083566

Shipman, T., MacDonald, R., & Byrnes, T. (2018). Experiences and learnings from induced seismicity regulation in Alberta. *Interpretation*, *6*(2), SE15–SE21. https://doi.org/10.1190/INT-2017-0164.1

Shirzaei, M., Ellsworth, W. L., Tiampo, K. F., González, P. J., & Manga, M. (2016). Surface uplift and time-dependent seismic hazard due to fluid injection in eastern Texas. *Science*, *353*(6306), 1416–1419. https://doi.org/10.1126/science.aag0262

Sibson, R. H. (2020). Dual-driven fault failure in the lower seismogenic zone. *Bulletin of the Seismological Society of America*, *110*. https://doi.org/10.1785/0120190190

Skoumal, R. J., Barbour, A. J., Brudzinski, M. R., Langenkamp, T., & Kaven, J. O. (2020). Induced seismicity in the Delaware Basin, Texas. *Journal of Geophysical Research: Solid Earth*, *125*, e2019JB018558. https://doi.org/10.1029/2019JB018558

Skoumal, R. J., Brudzinski, M. R., & Currie, B. S. (2015a). Earthquakes induced by hydraulic fracturing in Poland Township, Ohio. *Bulletin of the Seismological Society of America*, *105*(1), 189–197. https://doi.org/10.1785/0120140168

Skoumal, R. J., Brudzinski, M. R., & Currie, B. S. (2015b). Distinguishing induced seismicity from natural seismicity in Ohio: Demonstrating the utility of waveform template matching. *Journal of Geophysical Research: Solid Earth*, *120*, 6284–6296. https://doi.org/10.1002/2015JB012265

Skoumal, R. J., Brudzinski, M. R., & Currie, B. S. (2015c). Microseismicity induced by deep wastewater injection in Southern Trumbull County, Ohio. *Seismological Research Letters*, *86*(5). https://doi.org/10.1785/0220150055

Skoumal, R. J., Brudzinski, M. R., & Currie, B. S. (2016). An efficient repeating signal detector to investigate earthquake swarms. *Journal of Geophysical Research: Solid Earth*, *121*, 5880–5897. https://doi.org/10.1002/2016JB012981

Skoumal, R. J., Brudzinski, M. R., & Currie, B. S. (2018). Proximity of Precambrian basement affects the likelihood of induced seismicity in the Appalachian, Illinois, and Williston Basins, central and eastern United States. *Geosphere*, *14*(3), 1365–1379. https://doi.org/10.1130/GES01542.1

Skoumal, R. J., Brudzinski, M. R., Currie, B. S., & Levy, J. (2014). Optimizing multi-station earthquake template matching through re-examination of the Youngstown, Ohio, sequence. *Earth and Planetary Science Letters*, *405*, 274–280. https://doi.org/10.1016/j.epsl.2014.08.033

Skoumal, R. J., Ries, R., Brudzinski, M. R., Barbour, A. J., & Currie, B. S. (2018). Earthquakes induced by hydraulic fracturing are pervasive in Oklahoma. *Journal of Geophysical Research: Solid Earth*, *123*, 10,918–10,935. https://doi.org/10.1029/2018JB016790

Skoumal, R. J., Brudzinski M. R., Currie B. S., Ries R. (2019). Temporal patterns of induced seismicity in Oklahoma revealed from multi-station template matching. *Journal of Seismology*, https://doi.org/10.1007/s10950-019-09864-9

Snee, J. E. L., & Zoback, M. D. (2018). State of stress in the Permian Basin, Texas and New Mexico: Implications for induced seismicity. *The Leading Edge*, *37*(2), 127–134. https://doi.org/10.1190/tle37020127.1

Špičák, A. (2000). Earthquake swarms and accompanying phenomena in intraplate regions: A review. *Studia Geophysica et Geodaetica*, *44*(2), 89–106. https://doi.org/10.1023/A:1022146422444

Stern, V. H., Schultz, R. J., Shen, L., Gu, Y. J., & Eaton, D. W. (2013). Alberta earthquake catalogue, version 1.0: September 2006 through December 2010. In *Alberta Geological Survey Open-File Report* (Vol. 15, p. 36). Edmonton, Canada: Alberta Geological Survey/Alberta Energy Regulator.

Stoakes, F. A. (1980). Nature and control of shale basin fill and its effect on reef growth and termination: Upper Devonian Duvernay and Ireton formations of Alberta, Canada. *Bulletin of Canadian Petroleum Geology*, *28*, 345–410.

Sumy, D. F., Cochran, E. S., Keranen, K. M., Wei, M., & Abers, G. A. (2014). Observations of static Coulomb stress triggering of the November 2011 *M*5. 7 Oklahoma earthquake sequence. *Journal of Geophysical Research: Solid Earth*, *119*, 1904–1923. https://doi.org/10.1002/2013JB010612

Switzer, S. B., Holland, W. G., Christie, D. S., Graf, G. C., Hedinger, A. S., McAuley, R. J., et al. (1994). The Woodbend-Winterburn strata of the Western Canada Sedimentary Basin. In G. D. Mossop, & I. Shetsen (Eds.), *Geological Atlas of the Western Canada Sedimentary Basin*, *Geological Survey of Canada* (Chap. 12). Geological Survey of Canada.

Tan, Y., Hu, J., Zhang, H., Chen, Y., Qian, J., Wang, Q., et al. (2020). Hydraulic fracturing induced seismicity in the Southern Sichuan Basin due to fluid diffusions inferred from seismic and injection data analysis. *Geophysical Research Letters*, *47*, e2019GL084885. https://doi.org/10.1029/2019GL084885

Uchida, N., & Bürgmann, R. (2019). Repeating earthquakes. *Annual Review of Earth and Planetary Sciences*, *47*, 305–332. https://doi.org/10.1146/annurev-earth-053018-060119

U.S. Energy Information Administration (2013). *Technically recoverable shale oil and shale gas resources: An assessment of 137 shale formations in 41 countries outside the United States*. Washington, DC: U.S. Department of Energy/ Energy Information Administration (EIA). http://www.eia.gov/analysis/studies/worldshalegas

Van der Elst, N. J., Page, M. T., Weiser, D. A., Goebel, T. H., & Hosseini, S. M. (2016). Induced earthquake magnitudes are as large as (statistically) expected. *Journal of Geophysical Research: Solid Earth*, *121*, 4575–4590. https://doi.org/10.1002/2016JB012818

Verdon, J. P., Baptie, B. J., & Bommer, J. J. (2019). An improved framework for discriminating seismicity induced by industrial activities from natural earthquakes. *Seismological Research Letters*, *90*(4), 1592–1611. https://doi.org/10.1785/0220190030

Visser, R., Smith, B., Kao, H., Babaie Mahani, A., Hutchinson, J., & McKay, J. (2017). A comprehensive earthquake catalogue for northeastern British Columbia and western Alberta, 2014–2016. In *Geological Survey of Canada Open File* (Vol. 8335, pp. 28). Victoria, Canada: Geological Survey of Canada.

Waldhauser, F., & Ellsworth, W. L. (2000). A double-difference earthquake location algorithm: Method and application to the northern Hayward fault, California. *Bulletin of the Seismological Society of America*, *90*(6), 1353–1368. https://doi.org/10.1785/0120000006

Walsh, F. R., & Zoback, M. D. (2015). Oklahoma's recent earthquakes and saltwater disposal. *Science Advances*, *1*(5), e1500195. https://doi.org/10.1126/sciadv.1500195

Walsh, F. R. III, & Zoback, M. D. (2016). Probabilistic assessment of potential fault slip related to injection-induced earthquakes: Application to north-central Oklahoma, USA. *Geology*, *44*(12), 991–994. https://doi.org/10.1130/G38275.1

Walters, R. J., Zoback, M. D., Baker, J. W., & Beroza, G. C. (2015). Characterizing and responding to seismic risk associated with earthquakes potentially triggered by fluid disposal and hydraulic fracturing. *Seismological Research Letters*, *86*(4), 1110–1118. https://doi.org/10.1785/0220150048

Wang, B., Harrington, R. M., Liu, Y., Kao, H., & Yu, H. (2019). Remote dynamic triggering of earthquakes in three unconventional Canadian hydrocarbon regions based on a multiple-station matched-filter approach. *Bulletin of the Seismological Society of America*, *109*(1), 372–386. https://doi.org/10.1785/0120180164

Wang, B., Harrington, R. M., Liu, Y., Yu, H., Carey, A., & van der Elst, N. J. (2015). Isolated cases of remote dynamic triggering in Canada detected using cataloged earthquakes combined with a matched-filter approach. *Geophysical Research Letters*, *42*, 5187–5196. https://doi.org/10.1002/2015GL064377

Wang, R., Gu, Y. J., Schultz, R., & Chen, Y. (2018). Faults and non-double-couple components for induced earthquakes. *Geophysical Research Letters*, *45*, 8966–8975. https://doi.org/10.1029/2018GL079027

Wang, R., Gu, Y. J., Schultz, R., Kim, A., & Atkinson, G. (2016). Source analysis of a potential hydraulic-fracturing-induced earthquake near Fox Creek, Alberta. *Geophysical Research Letters*, *43*, 564–573. https://doi.org/10.1002/2015GL066917

Wang, R., Gu, Y. J., Schultz, R., Zhang, M., & Kim, A. (2017). Source characteristics and geological implications of the January 2016 induced earthquake swarm near Crooked Lake, Alberta. *Geophysical Journal International*, *210*(2), 979–988. https://doi.org/10.1093/gji/ggx204

Warpinski, N. R., Du, J., & Zimmer, U. (2012). Measurements of hydraulic-fracture-induced seismicity in gas shales. *SPE Production & Operations*, *27*(03), 240–252. https://doi.org/10.2118/151597-PA

Weichert, D. H. (1980). Estimation of the earthquake recurrence parameters for unequal observation periods for different magnitudes. *Bulletin of the Seismological Society of America*, *70*, 1337–1346.

Weng, X., Kresse, O., Cohen, C. E., Wu, R., & Gu, H. (2011). Modeling of hydraulic fracture network propagation in a naturally fractured formation. In *SPE Hydraulic Fracturing Technology Conference* (pp. 18). Woodlands, TX: Society of Petroleum Engineers.

Wesnousky, S. G. (1994). The Gutenberg-Richter or characteristic earthquake distribution, which is it? *Bulletin of the Seismological Society of America*, *84*(6), 1940–1959.

Wessels, S. A., De La Peña, A., Kratz, M., Williams-Stroud, S., & Jbeili, T. (2011). Identifying faults and fractures in unconventional reservoirs through microseismic monitoring. *First Break*, *29*(7), 99–104.

Wetmiller, R. J. (1986). Earthquakes near Rocky Mountain House, Alberta, and their relationship to gas production facilities. *Canadian Journal of Earth Sciences*, *23*(2), 172–181. https://doi.org/10.1139/e86-020

Wilson, M. P., Worrall, F., Davies, R. J., & Almond, S. (2018). Fracking: How far from faults? *Geomechanics and Geophysics for Geo-Energy and Geo-Resources*, *4*(2), 193–199. https://doi.org/10.1007/s40948-018-0081-y

Wolhart, S. L., Harting, T. A., Dahlem, J. E., Young, T., Mayerhofer, M. J., & Lolon, E. P. (2006). Hydraulic fracture diagnostics used to optimize development in the Jonah field. In *SPE Annual Technical Conference and Exhibition*, San Antonio, TX: Society of Petroleum Engineers. https://doi.org/10.2118/102528-MS

Wong, I., Nemser, E., Bott, J., & Dober, M. (2015). *White paper on induced seismicity and traffic light systems as related to hydraulic fracturing in Ohio*, Columbus, OH: Ohio Oil and Gas Association. http://www.ooga.org/resource/resmgr/Files/OOGA_IS_TLS_White_Paper_fina.pdf

Woo, J. U., Kim, M., Sheen, D. H., Kang, T. S., Rhie, J., Grigoli, F., & WL Ellsworth Giardini, D. (2019). An in-depth seismological analysis revealing a causal link between the 2017 *MW* 5.5 Pohang earthquake and EGS project. *Journal of Geophysical Research: Solid Earth*, *124*, 13060–13078. https://doi.org/10.1029/2019JB018368

Yang, Y., & Zoback, M. D. (2014). The role of preexisting fractures and faults during multistage hydraulic fracturing in the Bakken Formation. *Interpretation*, *2*(3), SG25–SG39. https://doi.org/10.1190/INT-2013-0158.1

Yeck, W. L., Weingarten, M., Benz, H. M., McNamara, D. E., Bergman, E. A., Herrmann, R. B., & Rubinstein Earle, P. S. (2016). Far-field pressurization likely caused one of the largest injection induced earthquakes by reactivating a large preexisting basement fault structure. *Geophysical Research Letters*, *43*, 10,198–10,207. https://doi.org/10.1002/2016GL070861

Yenier, E. (2017). A local magnitude relation for earthquakes in the Western Canada Sedimentary Basin. *Bulletin of the Seismological Society of America*, *107*(3), 1421–1431. https://doi.org/10.1785/0120160275

Yoon, C. E., Bergen, K. J., Rong, K., Elezabi, H., Ellsworth, W. L., Beroza, G. C., et al. (2019). Unsupervised large-scale search for similar earthquake signals. *Bulletin of the Seismological Society of America*, *109*(4), 1451–1468. https://doi.org/10.1785/0120190006

Yoon, C. E., Huang, Y., Ellsworth, W. L., & Beroza, G. C. (2017). Seismicity during the initial stages of the Guy-Greenbrier, Arkansas, earthquake sequence. *Journal of Geophysical Research: Solid Earth*, *122*, 9253–9274. https://doi.org/10.1002/2017JB014946

Yoon, C. E., O'Reilly, O., Bergen, K. J., & Beroza, G. C. (2015). Earthquake detection through computationally efficient similarity search. *Science Advances*, *1*(11). https://doi.org/10.1126/sciadv.1501057

Yoon, J. S., Zimmermann, G., Zang, A., & Stephansson, O. (2015). Discrete element modeling of fluid injection-induced seismicity and activation of nearby fault. *Canadian Geotechnical Journal*, *52*(10), 1457–1465. https://doi.org/10.1139/cgj-2014-0435

Yu, H., Harrington, R. M., Liu, Y., & Wang, B. (2019). Induced seismicity driven by fluid diffusion revealed by a near-field hydraulic stimulation monitoring array in the Montney Basin, British Columbia. *Journal of Geophysical Research: Solid Earth*, *124*, 4694–4709. https://doi.org/10.1029/2018JB017039

Zaitlin, B. A., Kennedy, J., & Kehoe, S. (2010). The Alberta Bakken: A new, unconventional tight oil resource play. In *BMO Capital Markets Oil and Gas Report* (pp. 21). Calgary, Canada: Bank of Montreal.

Zang, A., Yoon, J. S., Stephansson, O., & Heidbach, O. (2013). Fatigue hydraulic fracturing by cyclic reservoir treatment enhances permeability and reduces induced seismicity. *Geophysical Journal International*, *195*(2), 1282–1287. https://doi.org/10.1093/gji/ggt301

Zbinden, D., Rinaldi, A. P., Diehl, T., & Wiemer, S. (2019). Pore-pressure diffusion, enhanced by poroelastic stresses, controls induced seismicity in Oklahoma. *Proceedings of the National Academy of Sciences*, *116*(33), 16228–16233. https://doi.org/10.1073/pnas.1819225116

Zbinden, D., Rinaldi, A. P., Diehl, T., & Wiemer, S. (2020). Hydromechanical modeling of fault reactivation in the St. Gallen Deep Geothermal Project (Switzerland): Poroelasticity or hydraulic connection? *Geophysical Research Letters*, *47*, e2019GL085201. https://doi.org/10.1029/2019GL085201

Zhang, F., Yin, Z., Chen, Z., Maxwell, S., Zhang, L., & Wu, Y. (2019). Fault reactivation and induced seismicity during multistage hydraulic fracturing: Microseismic analysis and geomechanical modeling. *SPE Journal*, *25*, SPE-199883-PA. https://doi.org/10.2118/199883-PA

Zhang, H., Eaton D. W., Li G., Liu Y., & Harrington R. M. (2016). Discriminating induced seismicity from natural earthquakes using moment tensors and source spectra. *Journal of Geophysical Research: Solid Earth*, *121*, 972–993. https://doi.org/10.1002/2015jb012603

Zhang, H., Eaton, D. W., Rodriguez, G., & Jia, S. Q. (2019). Source-mechanism analysis and stress inversion for hydraulic-fracturing-induced event sequences near Fox Creek, Alberta. *Bulletin of the Seismological Society of America*, *109*(2), 636–651. https://doi.org/10.1785/0120180275

Zhu, W., & Beroza G. C. (2018). PhaseNet: A deep-neural-network-based seismic arrival time picking method. *Geophysical Journal International*, https://doi.org/10.1093/gji/ggy423

Zoback, M. D., & Kohli, A. H. (2019). *Unconventional reservoir geomechanics*. Cambridge: Cambridge University Press. 492 p

Zoback, M. D., & Lund Snee, J. E. (2018). Predicted and observed shear on pre-existing faults during hydraulic fracture stimulation. In *SEG Technical Program Expanded Abstracts 2018* (pp. 3588–3592). Society of Exploration Geophysicists. https://doi.org/10.1190/segam2018-2991018.1